CLOSED-LOOP CONTROL OF FORMING STABILITY DURING METAL STAMPING

by

RALPH CHRISTIAN FENN

M.S., Mechanical Engineering
Stanford University
(1981)

B.S., Animal Physiology
University of California, Davis
(1976)

Submitted to the Department of Mechanical Engineering
in partial fulfillment of
the requirements for the degree of

DOCTOR OF PHILOSOPHY

at the

August 1989

Signature of Author _____
Department of Mechanical Engineering
August 24, 1989

Certified by_____
David E. Hardt
Thesis Supervisor

Accepted by_____
Ain A. Sonin
Chairman, Departmental Committee on Graduate Studies

CLOSED-LOOP CONTROL OF FORMING STABILITY DURING METAL STAMPING

by

RALPH CHRISTIAN FENN

Submitted to the Department of Mechanical Engineering
on August 24, 1989 in partial fulfillment of the
requirements for the degree of Doctor of Philosophy
in Mechanical Engineering

ABSTRACT

Changes in process conditions during deep drawing of sheet metal parts often cause failure due to fracture or buckling. A constant blank holder force will no longer be optimal when frictional, geometric or material variations occur. Predictive methods based on applied mechanics provide one technique to adjust blank holder force for varying conditions. However this approach can not compensate for process variations over small numbers of parts due to the time requirements of measurement and computation. Closed-loop feedback control techniques provide an alternative method of blank holder force calculation and are the theme of this thesis. Rather than modeling from initial conditions, in-process measurements are used for real-time calculation of stress-strain correlate values. Control of these correlate variables to desired levels results in blank holder force changes. Experiments with non-axisymmetric geometries show that these modified blank holder force trajectories give near-optimal failure height irrespective of process conditions.

Thesis Supervisor: Dr. David E. Hardt
Title: Associate Professor of Mechanical Engineering
Director, Laboratory for Manufacturing and Productivity

Acknowledgements

Many people have helped to make this work possible. People on the faculty and staff, other students, family and friends have all provided much appreciated support and encouragement. Foremost among the few that I can mention here is my adviser, Professor Hardt. Over the course of this work he provided critical support and guidance when required. At other times he encouraged me to pursue my own ideas and develop my professional independence. Another member of my doctoral committee, Professor Mary Boyce, helped to relate this work to the principles underlying the broader field of deformation processing. As a member of my committee, Dr. Robin Stevenson provided the benefits of extensive experience in metal forming research. As the representative of the sponsoring organization, General Motors Corporation, he was instrumental to arrangement of the financial support for this thesis. In addition, he arranged the supply of critical tooling and materials which would have been extremely difficult to purchase locally.

Several other students in Professor Hardt's research group, Mike Hale, Karl Ousterhout, Robert Farra, and Joe Knapke, supported me with much appreciated technical assistance and the comradery that comes especially from others in the same program.

My mother and father provided the original encouragement to rejoin the academic world to pursue further education. Their support and concern has been a continuous source of strength.

A more recent entrant into my life, Irene, has been a continuous reminder of the best things in life. She has provided the day to day support and encouragement that was so important to completion of this work.

Financial support for this research was provided by the General Motors Corporation.

Table of Contents

List of Figures

Chapter 1 INTRODUCTION

American industry is today facing unprecedented pressure from overseas. Intense competition based on cost, quality, and product variety is occurring in most major business segments including the automotive industry. In automotive companies there is a new emphasis on manufacturing research in order to accelerate progress in these areas of competition. Because sheet metal stampings comprise a significant portion of total auto production costs, special emphasis is being given to improving the manufacture of these parts.

The difficulty of producing high quality parts with minimal scrap has recently been exacerbated by the use of thinner steel sheet in auto body panels. This trend was initiated by the need for lighter, more fuel efficient cars. The thinner materials have significantly different properties which reduce their stamping performance. For a given part shape, the new materials have a smaller safety margin that exaggerates the adverse effects of unavoidable process variations. Product introduction may be delayed because more die adjustments are needed before production begins. Today there is a particular need for reduction of tryout time and scrap costs while improving quality. This thesis addresses these requirements. Computer control techniques are proposed and tested that reduce the deleterious effects of process variations on stamped sheet metal parts.

The Drawing Process

The drawing method of stamping is chosen for study because of its

industrial importance. Drawing is widely used to manufacture a variety of products including auto body panels. More complex shapes can often be made using this process because additional material is pulled into the die cavity as the punch advances (Fig. 1-1). This additional material often reduces radial tensile stresses during forming and allows production of deeper stampings. However, unlike stretch forming where no draw-in occurs, the drawing process produces compressive circumferential (hoop) stresses. If too much material is draw-in during forming, large hoop stresses develop and buckling occurs. Because both tensile and compressive stresses are generated during drawing, failure can occur by either tearing or buckling before punch bottoming. For the schematic geometry shown in Fig. 1-1, tearing occurs at the punch nose where radial tensile stresses are highest because of the reduced cross-sectional area. Buckling, or wrinkling, occurs in the unsupported area near the die radius, where compressive hoop stresses are highest because of the perimeter reduction. The magnitude of the radial and circumferential stresses at these points depends on the size of the constraining force on the material during the forming process. This constraining force can be influenced by a draw bead or, as in this work, by the binder force acting on the part flange. A lower binder force will reduce the radial stress but will also increase the hoop stress, through higher draw-in, and cause earlier buckling (Fig. 1-2(a)). Conversely, a higher binder force will increase the radial stress and cause earlier tearing (Fig. 1-2(b)).

Figure 1-3 shows the trends in failure height for a range of binder forces. Buckling failure occurs before tearing at low binder forces and

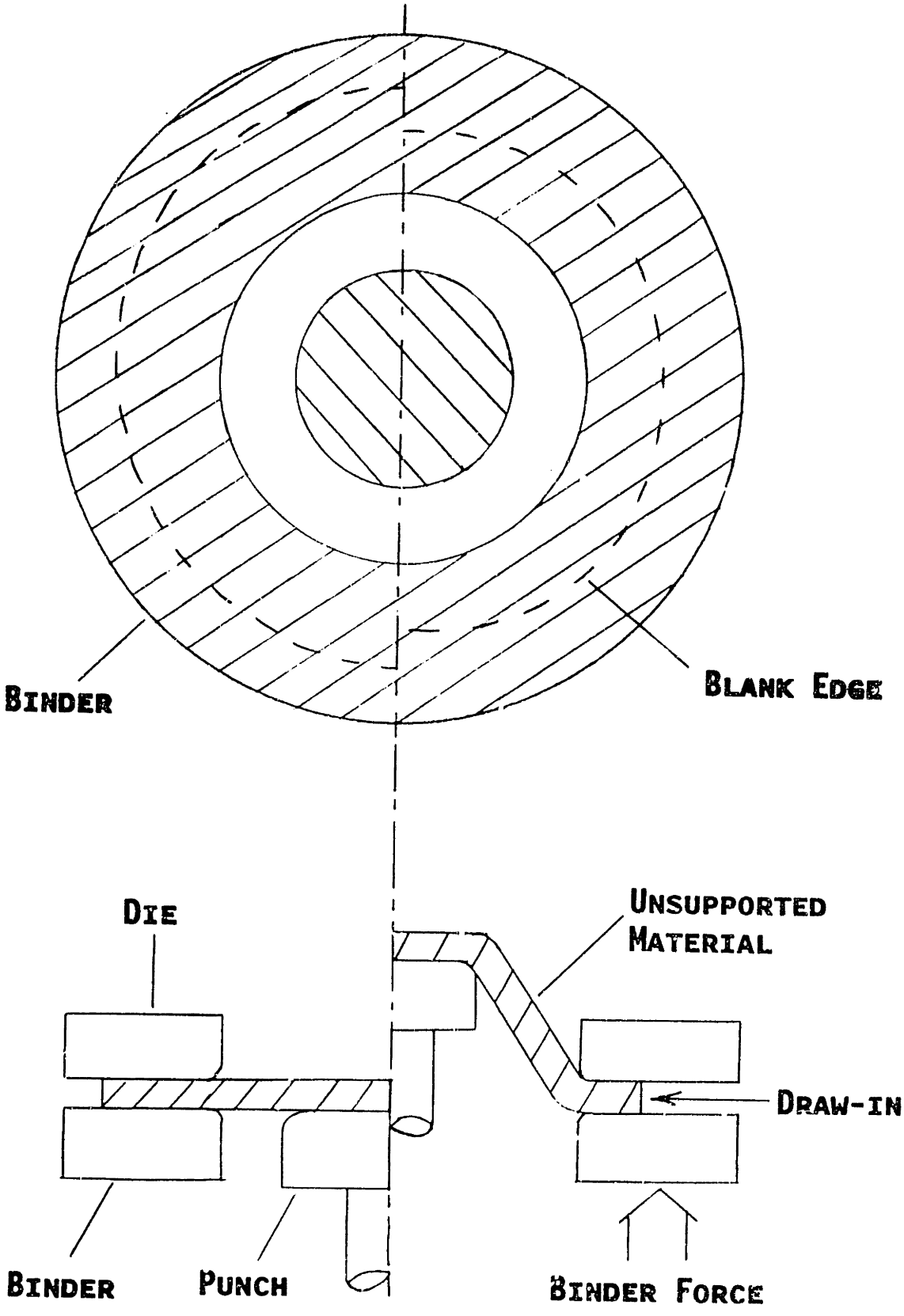

Fig. 1-1 Cylindrical Cup Forming Machine Geometry

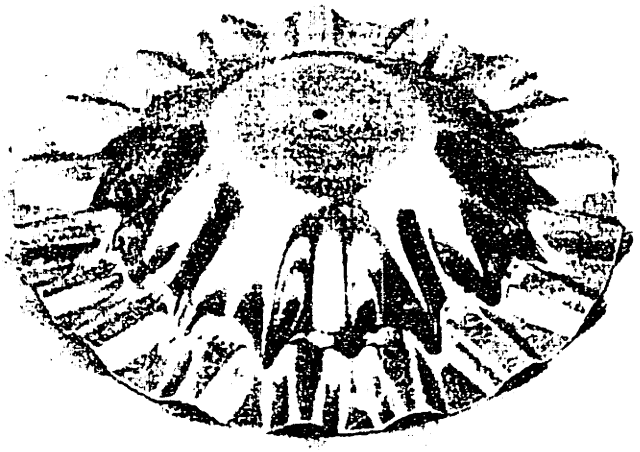

(A) SEVERE BUCKLING

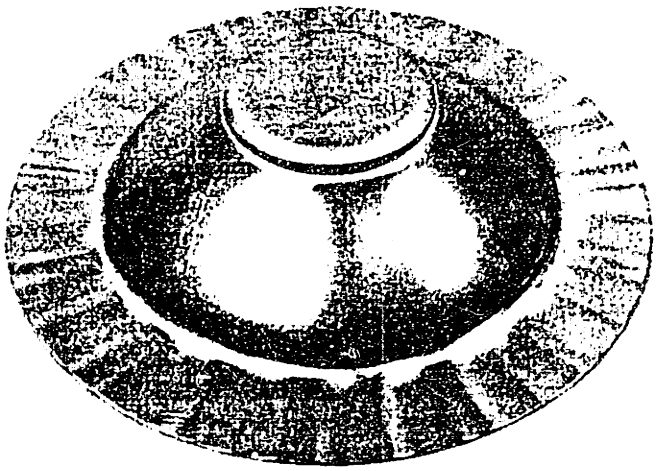

(B) SEVERE TEARING

Fig. 1-2 Examples of the Two Failure Modes

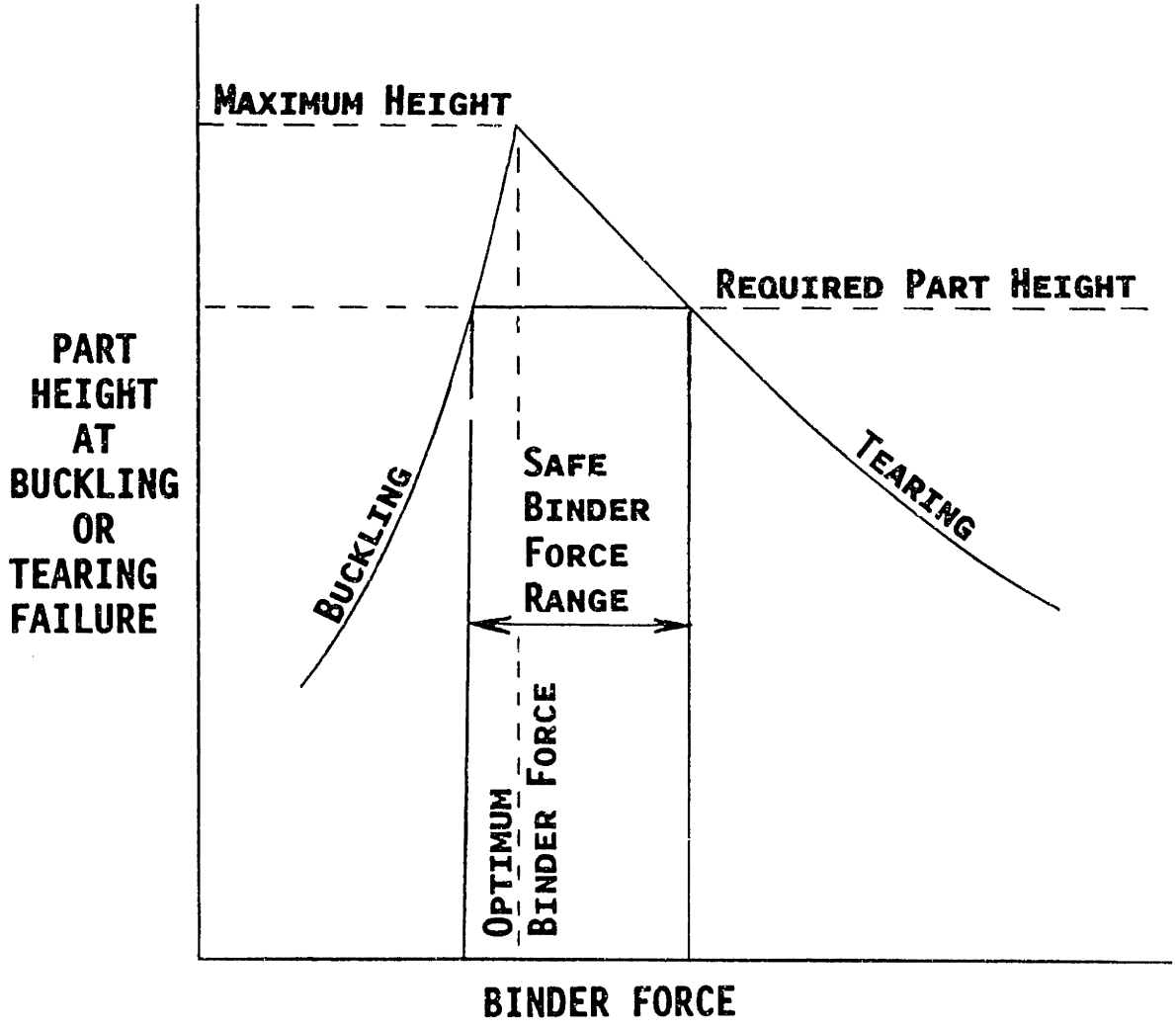

Fig. 1-3 Typical Failure Height Curve from Constant Binder Force Tests

tearing failure precedes buckling at high binder forces. An optimum failure height exists at an intermediate binder force. This binder force causes simultaneous tearing and buckling failure as represented by the intersection of the curves in Fig. 1-3. The optimum binder force is difficult to predict consistently because of variations in the forming conditions. Variations in the material properties, tooling condition, lubrication and blank dimensions all have significant effects on the process . These variations affect the position of the tearing and buckling limits and change the optimum binder force. The failure height curve of Fig. 1-3 is typical of production drawing operations as well as the drawing tests in this thesis. During production these variations are significant (Siekirk [1]) and the exact position of the maximum of the failure height curve is unknown. Forming failure often occurs because of inappropriate binder force.

For any given final part depth and forming condition, there is a range of "safe" binder forces which avoid part failure (Fig. 1-3). For deep and complex parts the buckling and tearing failure curves of Fig. 1-3 may be lower relative to the required part height. The safe binder force range for these parts may be too narrow to give consistent forming success. In this case, even small process variations may shift the optimum binder force sufficiently to cause failure before punch bottoming. The goal of this work is to construct a method that continuously determines the proper binder force required by the unknown conditions affecting each blank. It should predict the optimum binder force with sufficient accuracy to ensure that it lies within the safe range, although this may be narrow. The method should require only

limited knowledge about the process conditions to ensure simple implementation and wide applicability.

Control of the Process

This problem could be addressed by predicting the optimum binder force from the initial press and blank conditions. However, for general application this method requires techniques such as finite element method plastic analysis which cannot be used in real-time because of the computational load. Therefore this method cannot be used to respond to in-process uncertainty, which is a primary source of unexpected forming instability. To allow real-time binder force adjustment for individual blanks, the work here uses closed-loop control techniques. This approach uses in-process measurements to evaluate forming conditions and calculate the optimum binder force as forming progresses.

Ideally, the stresses and strains of the part would be monitored directly for closed-loop control. Direct measurement and control of the strains at the punch nose could eliminate premature tearing, and direct measurement and control of the stresses at the die radius could prevent premature buckling. However, direct measurement of stress and strain are impractical for every part because of the lack of adequate sensors. Fortunately, other process parameters can be more easily measured. Punch force and flange draw-in are more accessible than stress and strain and can be used to calculate useful approximations of stress and strain. These stress-strain estimates, can be used for real-time control of material condition. Optimum trajectories of these stress-strain correlates can be derived from a combination of standard tests

and analysis. The closed-loop control system manipulates the binder force to bring the estimates of stress and strain to the known optimum values. In this way the binder force is adjusted to the optimum value and premature failure is avoided.

Two closed-loop control techniques were developed here that use different methods of estimating material condition. The performance of these control algorithms was tested under simulated production conditions, which included variations in lubrication, blank diameter, blank thickness, blank location, and material properties. In addition, the control methods were tested on three die geometries (Fig. 1-4(a), 1-4(b), and 1-4(c)). The first configuration was a conical cup which was used for initial feasibility tests. Two subsequent square pan geometries tested the applicability of the closed-loop control technique to more asymmetrical, production-like parts. The results showed a large reduction in the effect of forming disturbances on the maximum formed height. In production this reduction of forming variability would increase the range of operating conditions giving successful stampings, thereby minimizing the number of scrap panels produced.

Thesis Overview

This thesis first examines the current understanding of the sheet metal drawing process. Studies of the effect of binder force manipulation on buckling and tearing failure are central to the application of closed-loop binder force control. In Chapter 3, two main methods of material condition estimation are defined. One technique estimates stress at the punch nose and another method estimates the

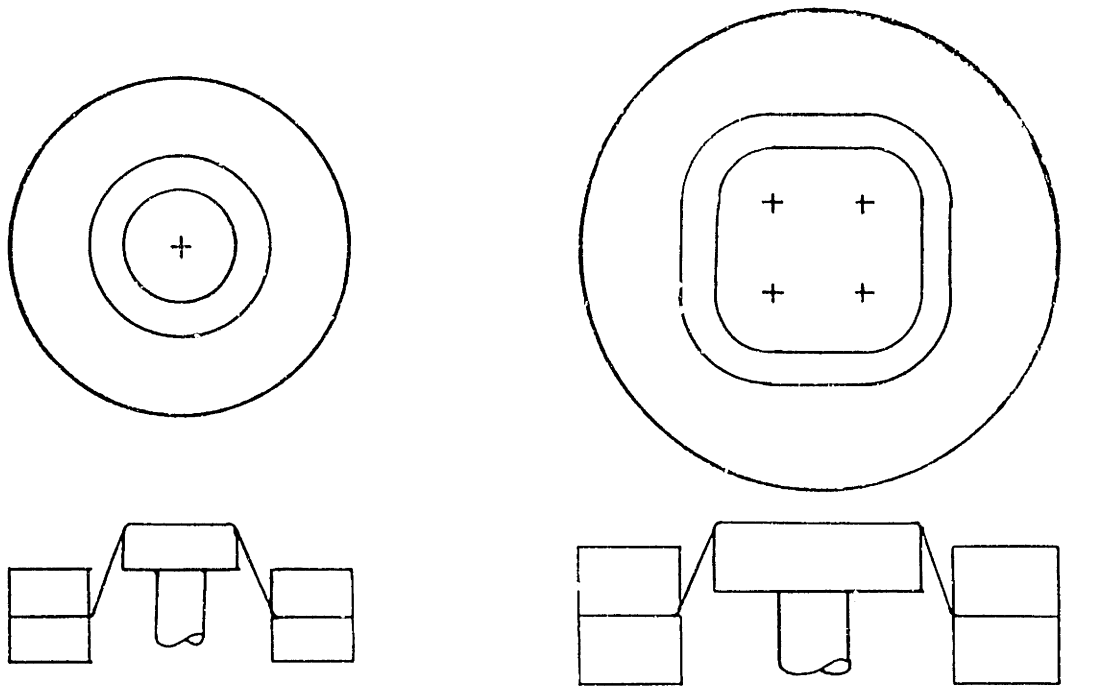

(A) CONICAL CUP

(B) EQUAL CORNER RADII PAN

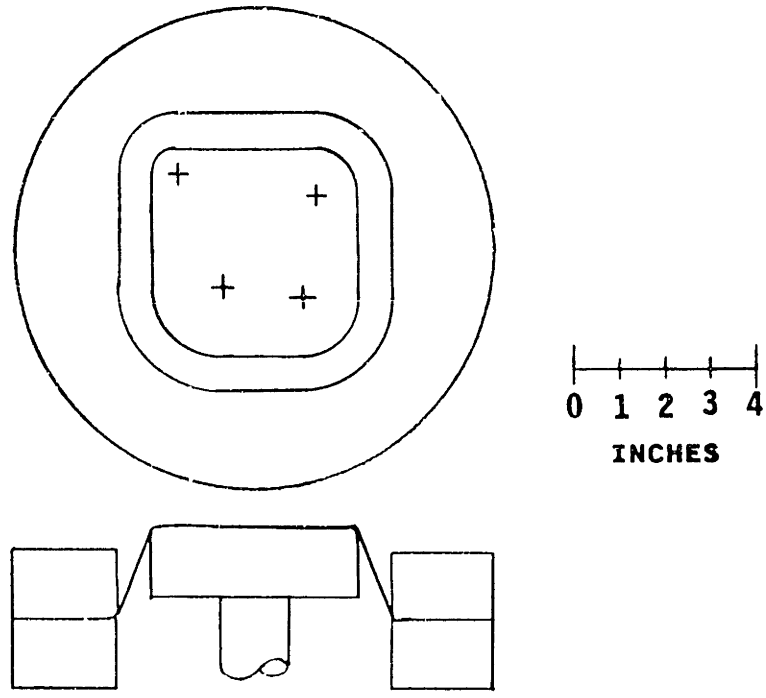

(C) UNEQUAL CORNER RADII PAN

Fig. 1-4 Drawings of the Three Die Set Geometries: a) Conical Cup Geometry, b) Equal Corner Radii Square Geometry, c) Unequal Corner Radii Square Geometry

average strain across the entire unsupported area in the die cavity. The advantages and disadvantages of each method are discussed including instrumentation issues. Chapter 4 describes the critical process of control target selection and presents the results of a complete set of closed-loop tests of the control methods. Control system performance for three die geometries and typical production process variations is documented. Chapter 5 summarizes the control strategy formulations and test results.

Chapter 2 BACKGROUND

Research into the stability of sheet metal forming has concentrated on topics such as material properties, circular grid strain analysis, forming limit diagrams, and finite element analysis. Below is a brief review of studies involving tearing, buckling, and forming limits.

The frequently used forming limit diagram, developed by Keeler [2] and Goodwin [3], is a good indicator of the tearing strains. For a given material, these diagrams are developed by using a hemispherical punch stretch test and plotting the circumferential and radial strains (Keeler[4]). Once the diagram is developed it can be applied, along with circle grid strain analysis of the formed sheet metal part, to help analyze specific tearing problems in the press shop. Fig. 2-1 shows a typical forming limit diagram.

There is a large body of research into flange buckling by Senior [5], Yu and Johnson [6], and Yossifon and Tirosh [7]. Although their work analyzes buckling, they do not focus on the buckling in the unsupported region which is critical in this thesis. Also, this work can not be used for closed-loop control because it does not predict binder force changes required during unknown process variations.

Havranek [8] did perform experiments on buckling in the unsupported region of conical cups. By measuring the circumferential and radial strains on the unsupported region, he discovered a wrinkling curve on the forming limit diagram, as shown in Fig. 2-1. Because the original

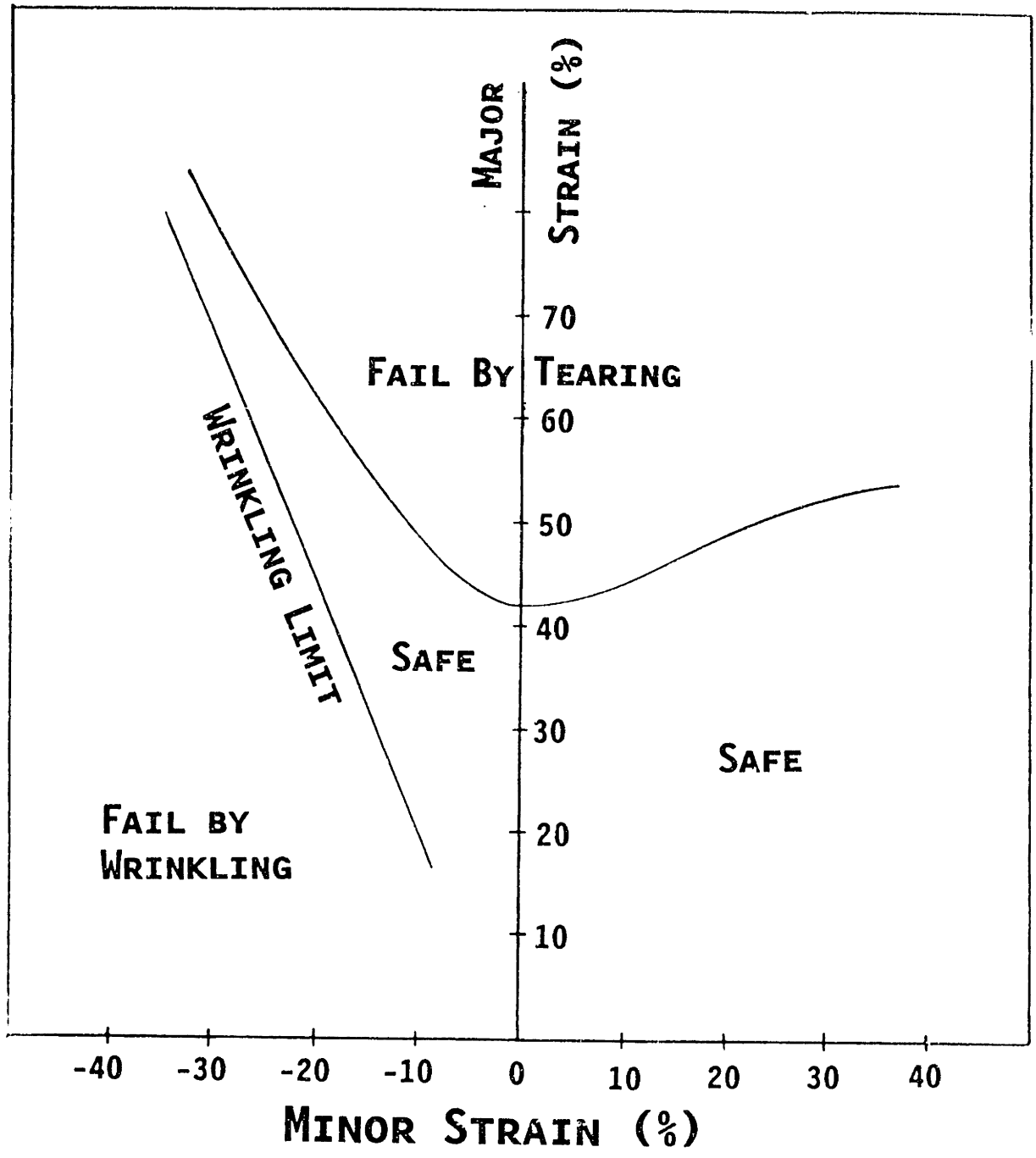

Fig. 2-1 Typical Forming Limit Diagram with Wrinkling Limit

location of wrinkling is not always obvious, its practical use is not as straightforward as using the forming limit diagram to analyze tearing. Another limitation of the wrinkling limit criterion is that it can not be used when there is considerable bulging. As a follow-up to Havranek's research, Hobbs [9] analyzed the stability of production sheet metal parts. By including the wrinkling curve in the forming limit diagram and using circle grid strain analysis, Hobbs reported alleviating both buckling and tearing failures of sheet metal parts.

The maximum height to which a conical cup can be successfully formed under constant blank holder force conditions is well established (Yoshida and Hayashi [10], Havranek [11]). Yoshida and Hayashi [10] stated that restraint conditions on the flange have little influence on the maximum formed depth of a conical cup if the corresponding optimal binder force is used. Others have investigated the effects of variable binder force on punch force, limiting draw ratio, and maximum cup height. Swiatkowski and Muzykiewicz [12] reported that the maximum formed height is increased by continuously decreasing binder force during forming. Romer, Fischer, and Breun [13] used mechanically produced binder force trajectories peaking near 50% punch displacement. These binder force trajectories were theoretically scaled to produce terminal compressive stresses at the buckling limit, resulting in significant increases in limiting draw ratio. The optimum binder force for non-axisymmetric parts was derived by Doege and Sommer[14] using buckling theory and experimental results. Manabe, Nishimura, and Hamano [15] derived the optimum binder force trajectory based on maintenance of the expected maximum punch load just below the fracture limit. This

resulted in a variable binder force, which is a minimum near mid-stroke, and a 2% increase in maximum formed cup height.

Much of the work discussed above used empirical methods to optimize formed height and minimize forming failures. Circle grid analysis is a classic example of this approach. Other investigations relied on simplified models of the forming process to make the calculations of parameters, such as binder force, more tractable. The recent advances in computers allow the use of a new approach using the finite element method (FEM). Solution of more complex models that more accurately represent the drawing process is possible using finite element formulations. Recent work by Logan [16] used the FEM to investigate the effect of material properties on forming stability. Sim and Boyce [17] developed a technique, using the FEM, to analyze forming stability for the geometries and conditions used in this thesis. This off-line code helps to understand the material states causing forming instability. The goal of this parallel FEM work is to suggest improvements to the closed-loop control strategies developed below.

None of the approaches described above can address the needs of real-time control during rapid process variations. The FEM is the most accurate but is computationally intensive and slow, which prevents its use on-line, and all of the methods require detailed knowledge of forming parameters, such as friction conditions, which is not often available.

A new method of adjusting binder force to prevent failure during rapid process changes was proposed by Lee and Hardt [18]. They used closed-loop control to adjust binder force to compensate for changes in process conditions. The sensitivity of cup failure height to binder force was reduced by controlling either flange wrinkling amplitude or average sheet thickness in the unsupported frustum to predetermined levels using binder force. This thesis pursues this concept of closed-loop control using in-process measurements that was developed in Lee and Hardt [18].

Chapter 3 CONTROL METHODS, APPARATUS, AND EXPERIMENTS

The objective of this work is to eliminate part failure during the forming cycle due to sheet instability. Premature failure occurs because poor strain distribution leads to excessive local stress and strain values. Binder force modulation can be used to control part strain by affecting the flange restraining force and draw-in of the part edge during forming. The draw-in in turn affects the stress and strain throughout the unsupported sheet area including the two potential failure zones at the punch nose and die radius. The ideal control system would measure and control the stress and strain at both critical areas. However, it is impractical to measure either stress or strain directly (e.g. with strain gauges) for each part which is formed. Also, it is not possible to vary the strain near the punch nose independently from die radius strain by manipulating binder force. Therefore the selection of binder force must be based on a stress or strain estimate which is related to the material condition in both critical areas of the part.

Two global calculations of material condition are described below. The first estimates the stress at the punch nose and the second estimates the average strain in the entire unsupported region of the forming part. A third estimate of part condition, which is based on measurement of flange buckling, is described last. Once methods of strain estimation are found, closed-loop control techniques can be used to regulate the strains to desired values.

Tangential Force

Tearing failure is closely related to the tensile stress within the part. For the conical cup geometry (Fig. 1-4(a)) and constant material thickness, the radial engineering stress will be directly proportional to the force in the direction of the material in the frustum (Fig. 3-1):

$$F_t = \frac{F_p}{\sin(\theta)} \qquad (3\text{-}1)$$

where

F_p = Punch Force
θ = Angle of the Frustum to the Horizontal

This tangential force (F_t) is a measure of material loading and it can be a basis for binder force changes because of its close relationship to stress at the punch nose. The circumferential stress as well as radial stress contributes to tearing failure as described by the forming limit diagram. However, in this forming geometry, the circumferential stress is small and relatively constant because of early "lock-up" where the material stops sliding over the punch. The effective result is straining at the punch nose which produces results similar to standard stress strain curves when F_t is plotted against unsupported meridian length (Fig 3-2). In Fig. 3-2 the rapid onset of plastic deformation is shown by the near vertical F_t slope at small strains.

The relationship between F_t and material engineering stress depends on the initial material thickness and die geometry. Changes of material

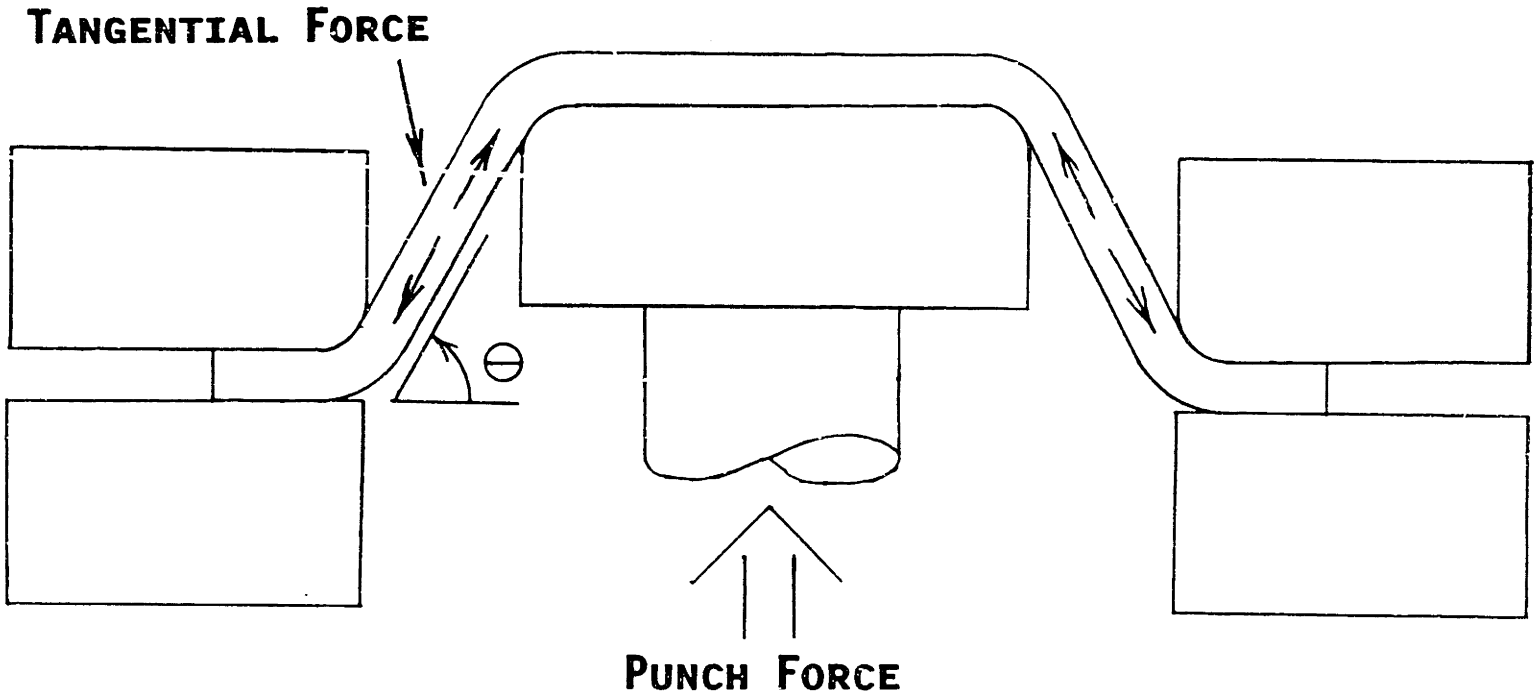

$$\text{TANGENTIAL FORCE} = \frac{\text{PUNCH FORCE}}{\sin \theta}$$

$$\theta = \theta\,(\text{PUNCH HEIGHT, DIE DIA., PUNCH DIA.})$$

Fig. 3-1 Definition of Tangential Force (F_t)

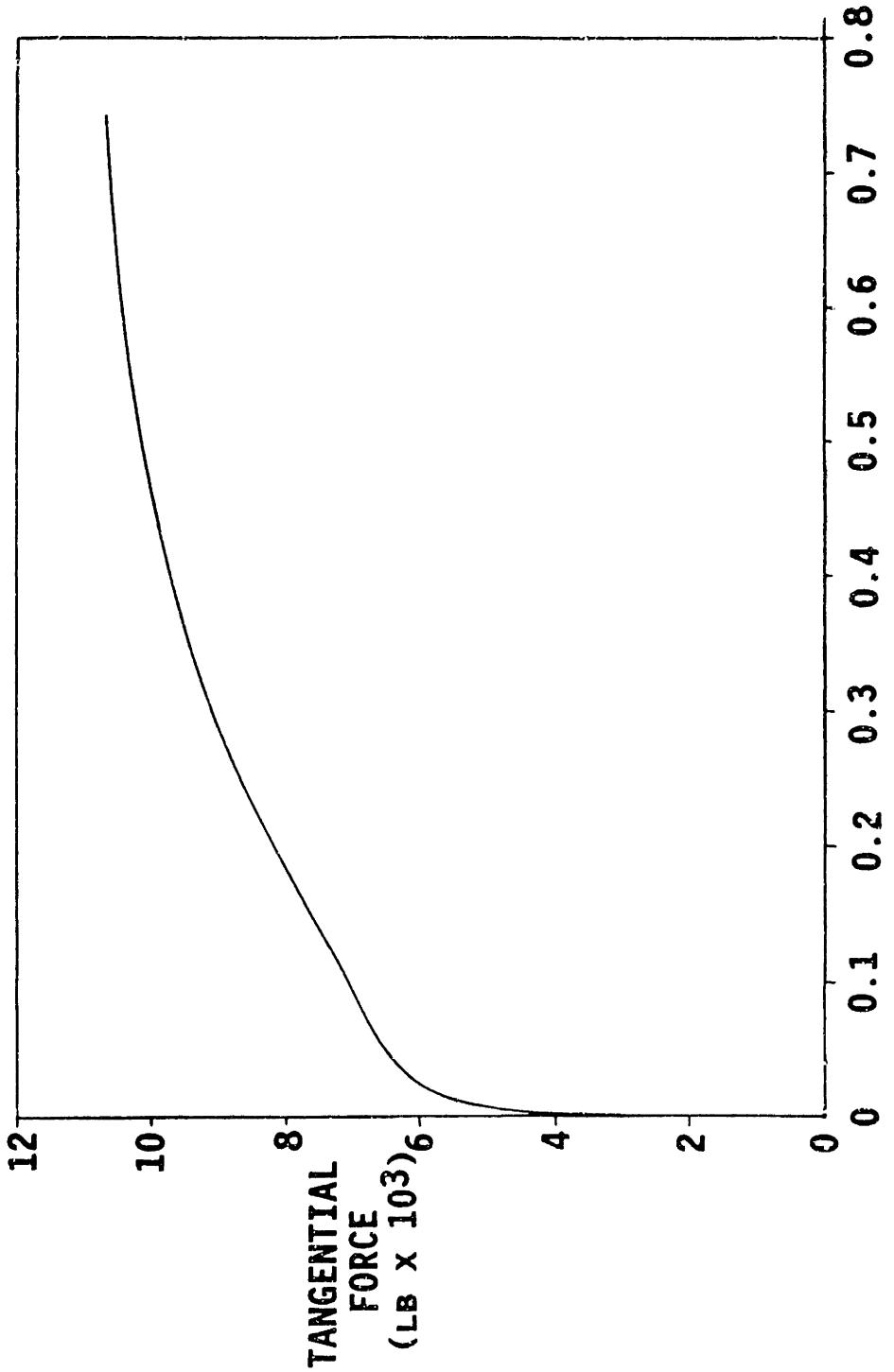

Fig. 3-2 Typical Tangential Force Trajectory: Similarity to the Stress-Strain Curve

thickness during forming do not affect the proportionality of F_t to engineering stress. Because of radial symmetry, the punch load is equally distributed around the punch perimeter. Localized straining will occur at the punch nose immediately before tearing failure. However, engineering stress around the punch perimeter will still be quite uniform over most of the punch stroke owing to symmetry.

During the forming cycle, the geometry changes because the effective punch nose diameter increases with punch height. As a result, the area of the material supporting the punch load changes, which affects the ratio of F_t to stress. However, the resulting error is minimal because the nose radius is small relative to the punch diameter. The typical punch diameter at failure height is used here for F_t calculations. Use of a constant punch diameter results in only a 1% stress error for punch height deviations of 0.18 in. at failure. Thus, the absolute error is small, but, more significantly, the effect is very repeatable, which allows automatic compensation of this systemic error during the control target selection process described later.

An important advantage of F_t for control purposes is the simplicity of required instrumentation. Only punch force measurement is required to supplement the punch displacement and binder force control loops. Force measurement implementation is straightforward and inexpensive, and the signal produced has low noise levels. A disadvantage is the global nature of F_t resulting from the single punch force value. The calculation of average stress, rather than the stress at particular failure points, requires special interpretation of F_t for non-

axisymmetric parts.

Normalized Average Thickness

The in-plane strains that determine the height at failure are closely related to the thickness strain of the material. For plastic deformation, the sum of the principle strains is zero, i.e. the sum of the in-plane strains is equal to the opposite of thickness strain. If in-plane strains have a particular ratio, then the thickness strain determines the in-plane strains. In this way thickness strain and thickness itself are related to the strains causing part failure.

The thickness of the unsupported area between the punch and the die can be estimated from the flow into the region and the area of the region at each instant in the forming cycle (Fig. 3-3). A "normalized average thickness" (t_{avg}) in the unsupported area is estimated from:

$$t_{avg} = \frac{V_f}{A_f * t_i} \qquad (3\text{-}2)$$

where

V_f = volume of the frustum formed by the part
A_f = surface area of the frustum
t_i = initial material thickness

As forming progresses, the area will increase as a function of punch displacement, while the volume can increase only if new material flows in from the binder. This flow can be measured by sensing the change in radius or circumference of the outer edge of the blank as it is drawn into the forming region. The expressions used to calculate t_{avg} are

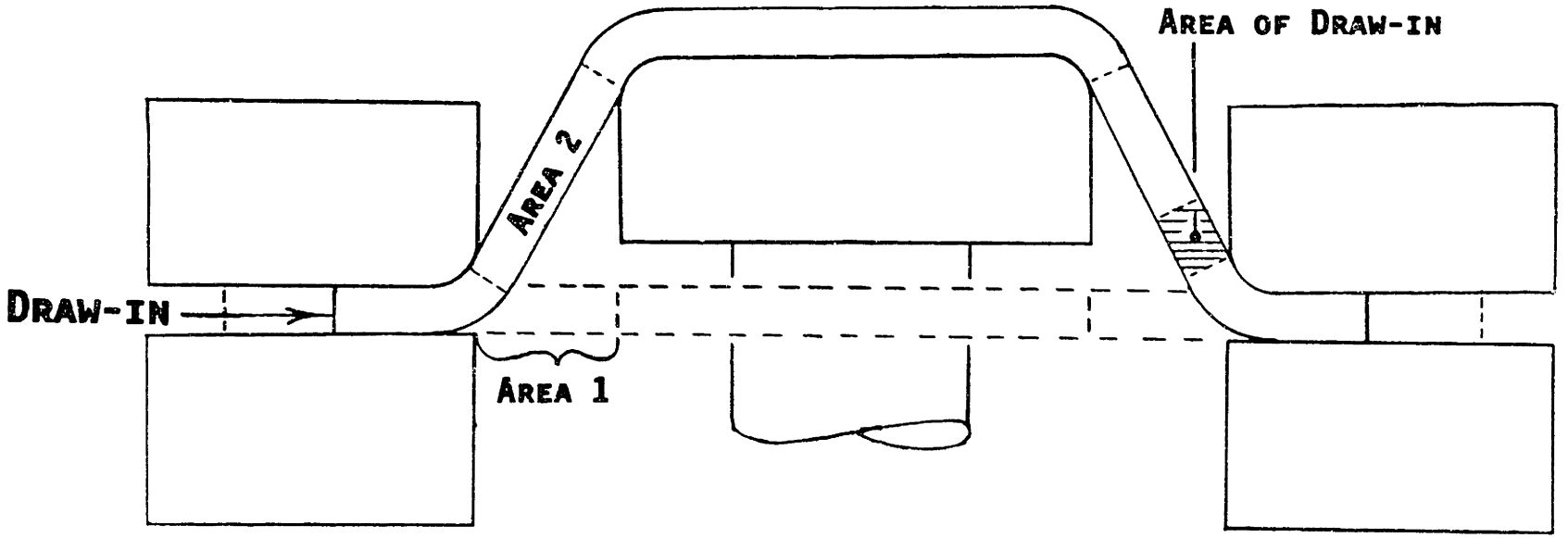

$$\text{NORM. AVERAGE THICK.} = \frac{\text{VOLUME OF FRUSTUM}}{\text{AREA OF FRUSTUM}}$$

$$= \frac{[\text{AREA 1} + \text{AREA OF DRAW-IN}] * T}{\text{AREA 2}}$$

Fig. 3-3 Definition of Normalized Average Thickness (t_{avg})

listed in Appendix A.

The conditions at the two potential failure points on the frustum, (the punch nose and die radius) are closely related to the average thickness of the entire frustum. The changes in the state at the two critical areas parallel the change in the average material state which is estimated by the thickness calculation described above.

An advantage of t_{avg} is its dimensionless formulation. The requirement for blank thickness measurement is eliminated and the sensitivity of the target selection to material strength is weaker than in the case of force based methods such as F_t control. Another advantage of t_{avg} is the possibility of making measurements at local areas of the part. By measuring draw-in at a particular point on the flange of an asymmetrical part, the t_{avg} value that is more representative of the conditions at the failure location might be found. Control of the localized thickness might allow attenuation of process disturbances which affect various areas of the part unevenly.

The calculation of t_{avg} does not include the material flow into the frustum from the top of the punch. However, this material flow is small because "lock-up" over the punch occurs early in the forming process. Measurements of this over-punch flow were done for parts formed using "standard" cup forming conditions and moderate (6,000 lb.) binder force. The "standard" conditions for cup forming are STP lubrication, type "C" material, 0.020 in. thickness, and 6.25 in. diameter blanks (see Standard conditions section of Chapter 4). These conditions produced

over-punch material flow of 0.045 in. A small, 2.4% t_{avg} error is caused in this case by incorrectly assuming over-punch flow to be zero. The repeatability of this effect allows automatic compensation during closed-loop control as described below.

During drawing, the flange typically thickens as forming progresses. Flange thickening affects the volume drawn into the die cavity and the average frustum thickness, however the calculation of t_{avg} here uses a constant flange thickness. This is acceptable because the flange thickness change is small and the corresponding effect on t_{avg} is minimal. By the end of the forming stroke, the conical flange edge gains less than 0.0005 in. of thickness for a 5,000 lb. binder force. The time averaged thickness change over the forming process is approximately 50% of this (i.e. 0.0003 in.). The error due to a zero thickness change assumption is less than 0.3% in this case. This error is small and predominately systematic which is corrected during control implementation.

The usefulness of t_{avg} depends on accurate calculation of material flow from the flange into the die cavity. An edge draw-in measurement can be made to estimate this flow. Often this draw-in reading is noisy because material anisotropy causes erratic "earing" of the flange. The low precision of the draw-in can cause large errors in the flange material flow calculation. For example, a 0.01 inch draw-in error causes a 0.009 t_{avg} error at 1.3 in. punch height for the conical geometry. Since the range of t_{avg} over the forming cycle is only about 0.1, this small draw-in error gives a significant error of 9% of t_{avg}

range. To reduce the sensitivity of t_{avg} values to unequal draw-in, a method using circumference measurement was developed which finds the average draw-in around the entire perimeter of the flange (see Measurement Techniques below).

The accuracy of the calculated t_{avg} value of a 1.3 in. deep cup (Fig. 1-4(a)) was checked by measuring the various thicknesses along a meridian and weighting by surface area. The part average thickness was 0.0190 inch which gives t_{avg} = 0.956 for 0.020 inch blank material. The calculated t_{avg} value was 0.900. The difference of 0.056 between the measured and calculated values of t_{avg} is caused by two primary effects. The discrepancy is the sum of 0.022 due to 0.045 inch over punch flow, and 0.020 due to 0.02 inch part height springback. This calibration test shows that t_{avg} values are based on physical part features, but small measurement inaccuracies cause significant t_{avg} inaccuracies. However, most of the error is due to systematic influences which do not compromise the control results when control targets are experimentally derived.

Binder Displacement

Because the compressive circumferential strains are largest in the flange area, wrinkling may start in the flange before occurring in the frustum under certain conditions. This flange buckling can be detected by measuring changes in the parallel gap between the die and binder. If buckling always occurred first in the unimportant flange area it would be a good predictor of imminent buckling in the frustum and would be a useful basis for control. In Lee and Hardt [18], experiments were

performed where the binder displacement was under computer control. Low initial binder forces caused small flange wrinkles to develop. When flange wrinkling increased the binder-die gap to a preset limit, computer control of binder force prevented the binder gap from exceeding the limit. Significant increases in failure height during process variations were produced for 0.032 in. thick cups.

However, flange buckling does not usually precede unsupported region buckling in the current work with thinner, 0.020 in., 0.025 in., and 0.030 in. material. For a wide range of binder forces, frustum buckling begins before flange buckling. In this case, control of flange buckling can not prevent development of buckling instability in the frustum. Because binder displacement is not always a good indicator of the condition of the material in the frustum of thin parts, it is not used here for control purposes.

Closed-Loop Control of F_t and t_{avg}

The concepts of F_t and t_{avg} are useful because they allow approximation of the critical stresses or strains during the forming process. Using these measurements, control systems can be developed to continuously regulate F_t or t_{avg} to target values, which will in turn regulate the stress and strain states. Such systems are illustrated in Fig. 3-4. In both cases, the manipulated variable is the binder force, but it now is dynamic and will assume whatever value is required to bring F_t or t_{avg} to the target. The key to exploitation of these regulators is, therefore, proper choice of the target trajectories, which in this work were defined by a series of experiments.

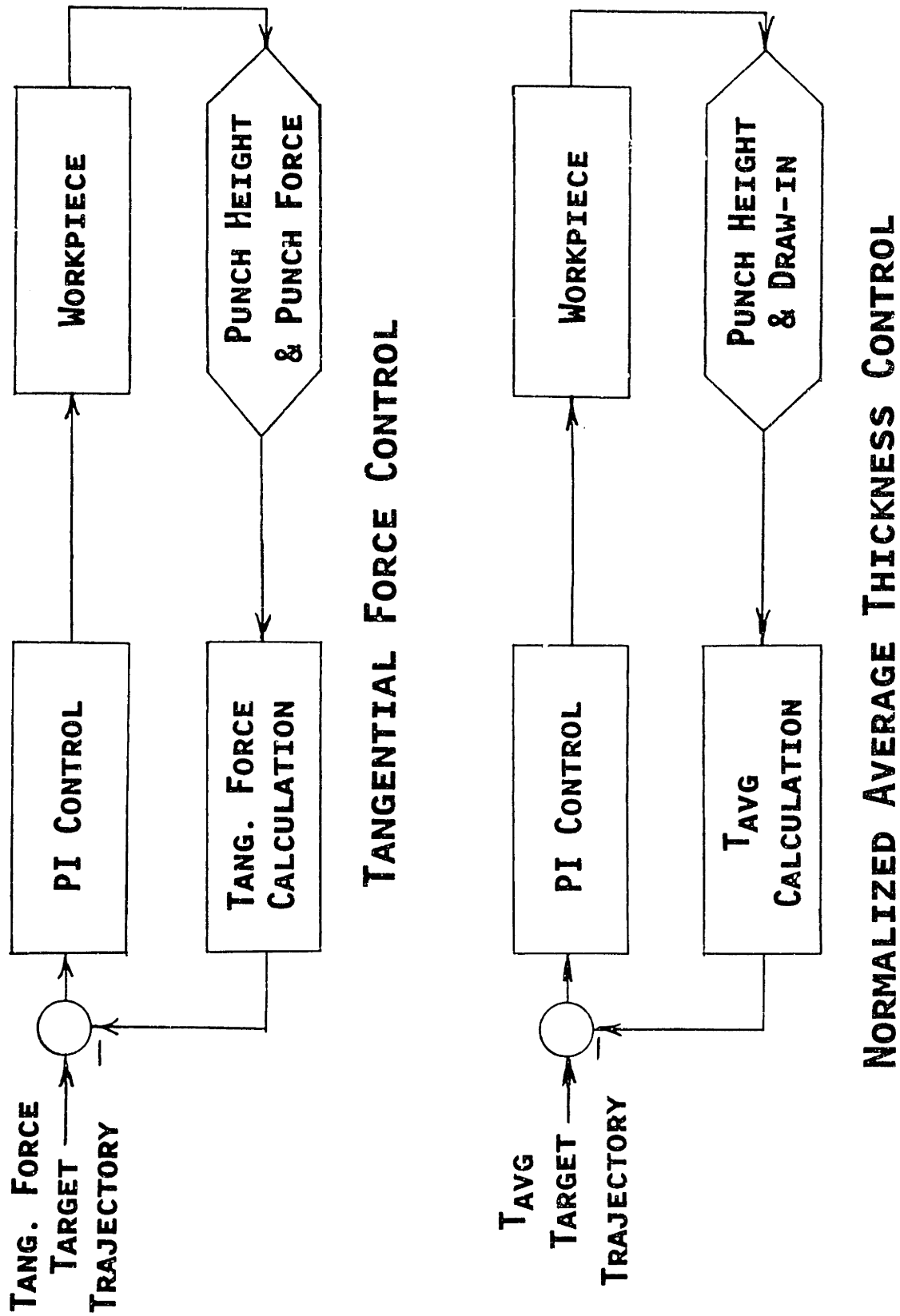

Fig. 3-4 Closed-loop Forming Stability Controllers

For each of the three die geometries (Fig. 1-4(a), 1-4(b), and 1-4(c)) a set of tests was performed under standard conditions but with various constant binder forces. The binder force of each test was selected iteratively while searching for the optimum binder force giving the maximum height at failure. Once this optimum test has been completed, the recorded "signature" trajectories of F_t and t_{avg} are modified to give target trajectories for closed-loop control. After the F_t and t_{avg} target trajectories are found experimentally for each geometry under standard conditions, scaled target versions can be created analytically for non-standard conditions. This method uses simple experimental and analytical techniques to satisfy the goal of ease of application.

Apparatus Design

The experimental stampings were formed on a double action hydraulic press specially built for this work (Fig. 3-5). The punch moves upward during forming and the press structure is designed to give access to the convex surface of the parts above the punch. The die and top plate are annular to allow instrument placement on the part surface for in-process punch height and buckling measurement (See Measurement Techniques section below and Lee [19] for details.) The punch capacity is 34,000 pounds and the binder capacity is 64,000 pounds. The flatness of the die, binder and supporting structure is critical to consistent experimental results. Small deviations from flatness result in large local changes in draw-in which severely compromise t_{avg} precision. Flatness of the press restraining surfaces must be better than thickness

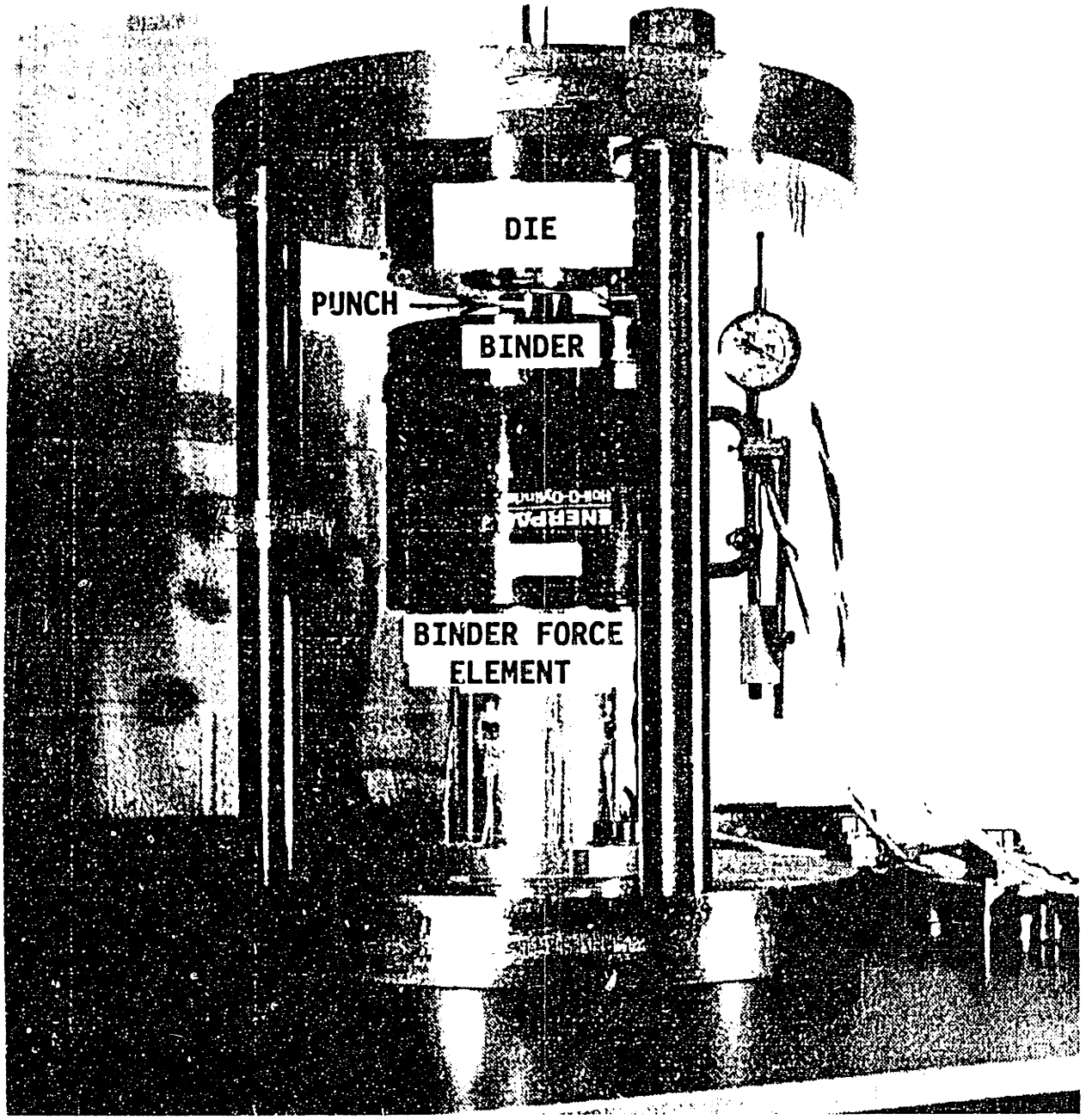

Fig. 3-5 Hydraulic Press Apparatus

deviations within each blank. Restraining surfaces should be very hard to limit scratching.

Procedures

Circular blanks are used here for both the cup and square geometries. The standard circular shape for cup forming was also used for the square pans because it approximates the ideal shape giving equal flange width. High side wall draw-in and low corner draw-in tends to equalize the flange width as pan forming progresses. The blanks used here were made in lots of approximately 60 by turning on a lathe. Oversize squares were tightly "sandwiched" between two thick plates which were compressed between the lathe chuck and tailstock. A 1/8 in. rod through the stack prevented sheets from flying out if clamping pressure were lost. An initial trepaning cut, then final turning gives accurate diameter blanks with no burr which could cause inconsistent friction force.

Four lubrication conditions are used in the tests: STP mixture, silicone oil, teflon particulate spray, and no lubrication (dry). The first two lubricants are liquids and can be metered by counting drops. One drop of these liquid lubricants is applied to each side of the 6.25 in. degreased cup blanks, and 2 drops are applied to each side of the 9.078 in. pan blanks. A saturated pad is used to spread the lubricant evenly across the blank surface. The teflon spray was used over a STP film and the uniformity of teflon application is visible because of its white color. Dry conditions required complete removal of mill oil using an organic solvent (hexane). The punch, die and binder were wiped after

each test to guarantee even lubrication. Conventional water soluble drawing lubricant was tested but was discontinued due to uneven wetting of the surface and varying degrees of evaporation before stamping. Pure 20W oil was also discontinued because it produced stiction at the punch nose and noise in the punch force signal. This stiction problem also occurs under dry conditions.

Orientation of the material rolling direction with the square die sets has a significant effect on failure height and is standardized. The rolling direction is perpendicular to a side of the equal corner radii pans. The rolling direction is perpendicular to the side between the 0.5 in. and 1.5 in. radii of the unequal corner radii square pans.

Measurement Techniques

Blank edge or 'draw-in' displacement can be a local value measured by a single LVDT or an average value for the entire circumference. One local draw-in measurement may not be representative of the average draw-in because of local process variations or material anisotropy. The variations in final draw-in around a cup perimeter can be estimated from measurements of the diameter of the cup flange. Fig. 3-6 shows ranges in flange diameters around a typical cup formed using "standard" conditions (STP lubrication, 0.020 in. thickness, and 6.25 in. diameter blanks) and 6,000 lb. binder force. The maximum flange diameter variation is 0.09 in. different from the average. The unequal draw-in of this example is caused by blank anisotropy and non-uniformity of friction conditions. If this diameter variation were caused by a draw-in variation on one side, the t_{avg} error could be as large as 0.08,

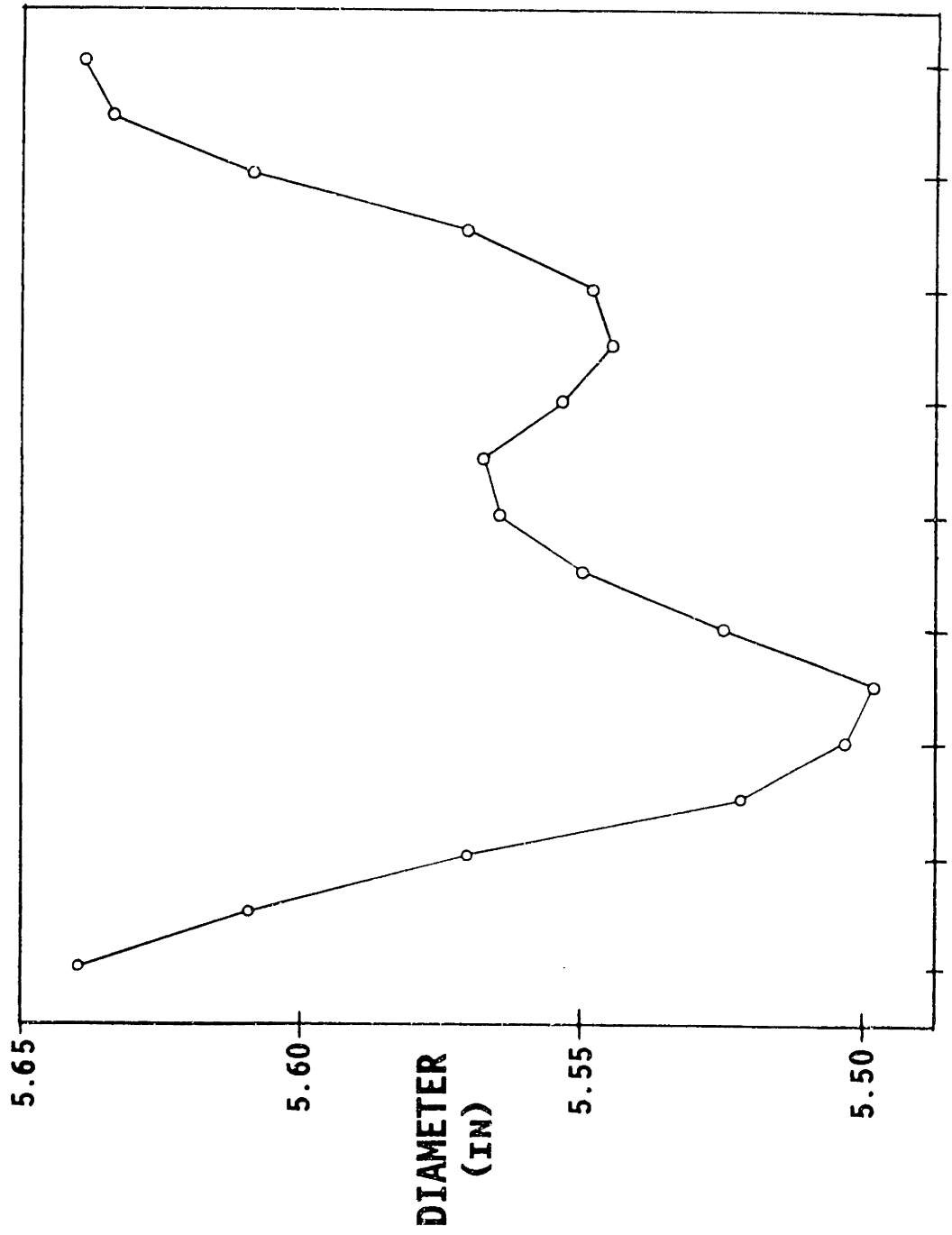

Fig. 3-6 Typical Cup Flange Diameter Showing Variability

which is more than 50% of normal t_{avg} range. The particular error would depend on the position of the LVDT edge measurement.

To reduce the effects of random local draw-in variations, a measure of average draw-in was derived from measurements of the part edge circumference during forming. The circumference changes were measured using a 0.008 in. lubricated and tensioned nylon line wrapped around the part edge (Fig. 3-7). During the forming cycle, the perimeter reduction caused the movement of the free end of the line, which was measured using an LVDT. This estimated average draw-in is found by dividing the circumference change by 2 . The flange in Fig. 3-7 has four "ears", which are typically produced by anisotropic material. The effect on t_{avg} accuracy of the new "average" draw-in as well as the local draw-in can be calculated using the idealized geometry of Fig. 3-7. High draw-in accuracy is required for accuracy of the frustum area that is used in the t_{avg} calculation. Use of the local draw-in produces an area error of 4.6% while the circumferential method gives only 0.8% error. This special method of measuring average draw-in can reduce t_{avg} error by more than 80% if the part edge deviates significantly from circularity as in Fig. 3-7.

Real-time buckling measurement is important to these experiments because it allows accurate determination of failure height. Without real-time measurement, an unreasonable number of tests would be required to find failure height to sufficient accuracy. The instrument used to measure buckling of the conical parts as cup forming progresses is shown in Fig. 3-8. The lower edge of the 0.007 in. spring steel cylinder

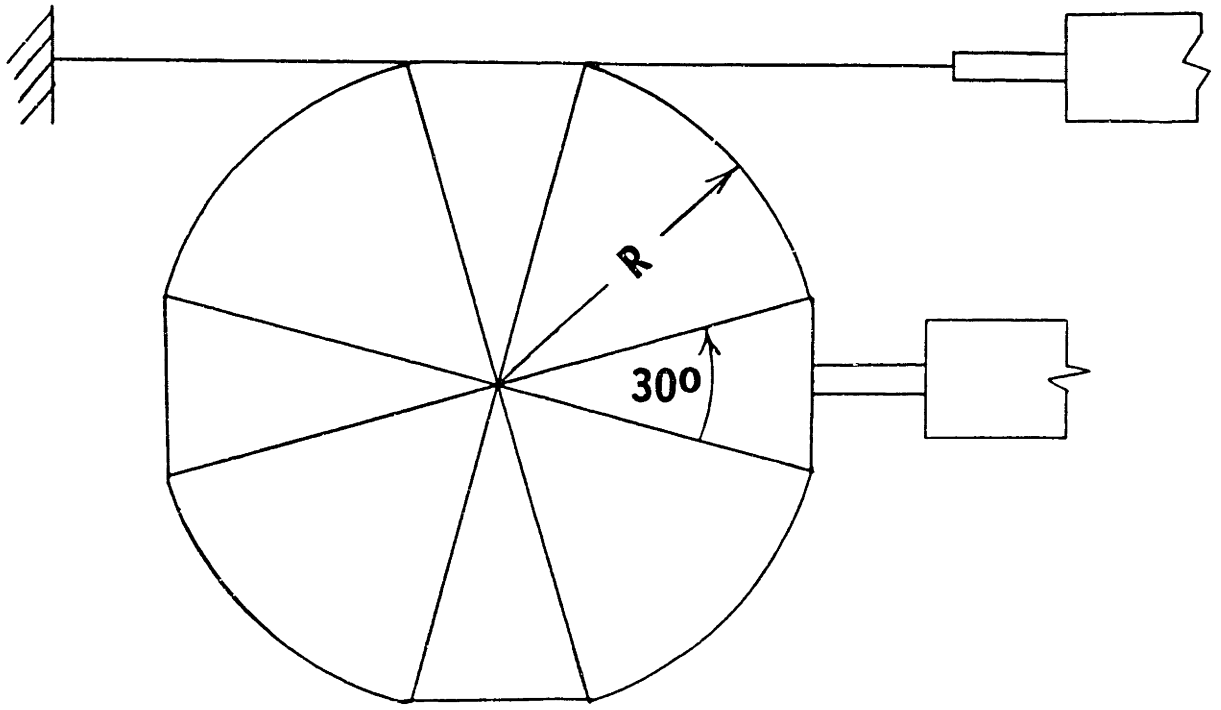

ACTUAL AREA	3.10 R^2	
AREA FROM LOCAL DRAW-IN	2.93 R^2	(ERROR=4.6%)
AREA FROM CIRCUMFERENCE	3.12 R^2	(ERROR=0.8%)

Fig. 3-7 Geometry of Circumferential Measurement Technique

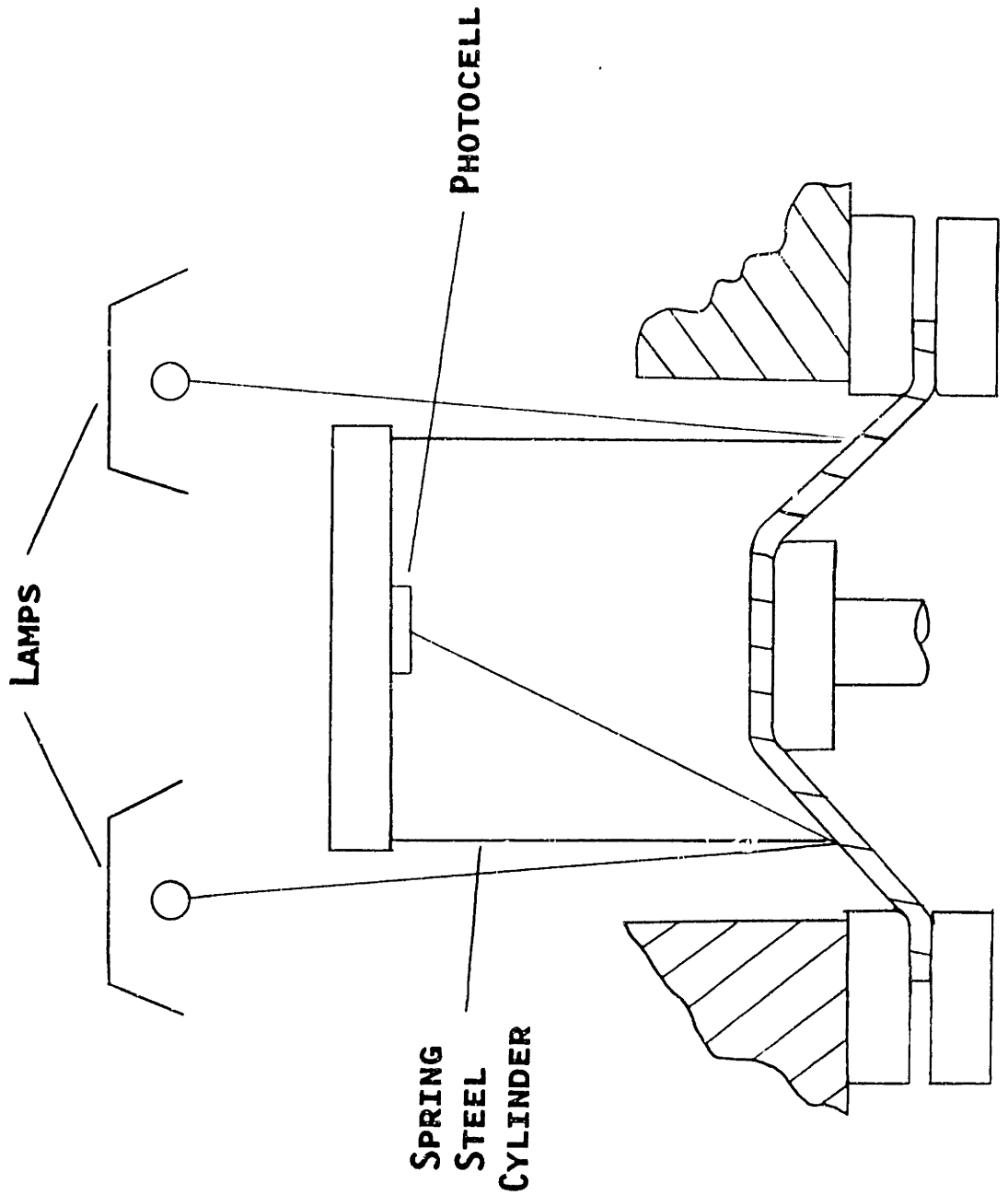

Fig. 3-8 Sensor for Measurement of Buckling Amplitude

rests on the nominally circular cross-section of the unsupported sheet near the die. As the material flows past the die and cylinder edge, the cylinder is dithered about its axis to ensure a good light seal. When large amplitude, short wavelength buckling occurs, the edge of the cylinder no longer conforms to the part along its entire length. Gaps between the cylinder and the part allow light from the outer annular space to enter inside the cylinder. Two 500W quartz lamps and foil lined cylinder and die surfaces assure high intensity light at the gaps. A sensitive cadmium sulfide photocell inside quantifies the light leak which is proportional to the area of the gaps around the cylinder. The high impedance photocell circuit is buffered from the analog to digital converter by an operational amplifier.

Buckling of parts produced by the two square die sets can not be measured by the sensor described above. Buckling of the square pans first occurs in the side, where the wall buckles inward along its entire length. The asymmetrical pans shown in Fig. 1-4(c) usually buckled first at the wall between the smallest and largest corner radii. The buckle shape allows simple, manual buckle detection when a straight edge made of spring steel is held against the side wall during forming. Early in the forming cycle the straight edge contacts in the center of the side wall. When buckling occurs the straight edge contacts at the corners of the side wall. This change in side wall curvature can be detected by noting the change in straight edge contact points while sliding the edge perpendicularly to the meridian. The square pans are considered buckled if the side wall is bowed inward by more than 0.002 in.

The degree of buckling is not a single displacement but rather is a measure of the curvature, or second derivative of displacement, of wrinkles on the frustum. The curvature of the wrinkles determines the visibility of this type of part defect when painted. The measure of buckle curvature used by Logan [16] is the value of buckle height divided by buckle wavelength. When this ratio is greater than 0.002 a part is considered failed by buckling.

The ability of the buckling sensor to distinguish between ovalness, (due to anisotropy or die shape) and actual buckling is very important. The response of the buckling sensor to cups with ovalness and wrinkles was tested. One full height cup without wrinkling, as determined manually, and another cup with wrinkling of ten times sensor sensitivity were examined. Each cup was centered on a lathe chuck and spun slowly by hand while measuring the buckle amplitude at each meridian with a stationary dial gauge. Figure 3-9(a) shows the high frequency waves of a cup identified by the sensor as buckled. Figure 3-9(b) shows the radii of an unbuckled cup, which has predominately smooth, low frequency variations. This test shows that the sensor described above is effectively a spatial frequency filter which is sensitive predominately to high frequency, short wavelength buckling.

The frequency "cutoff" of this filter is adjusted by varying the weight forcing the cylinder onto the forming cup. A one kilogram weight provided the optimum signal difference between characteristic 1/2 in. wavelength buckles and 3 in. wavelength anisotropy effects. Sensitivity

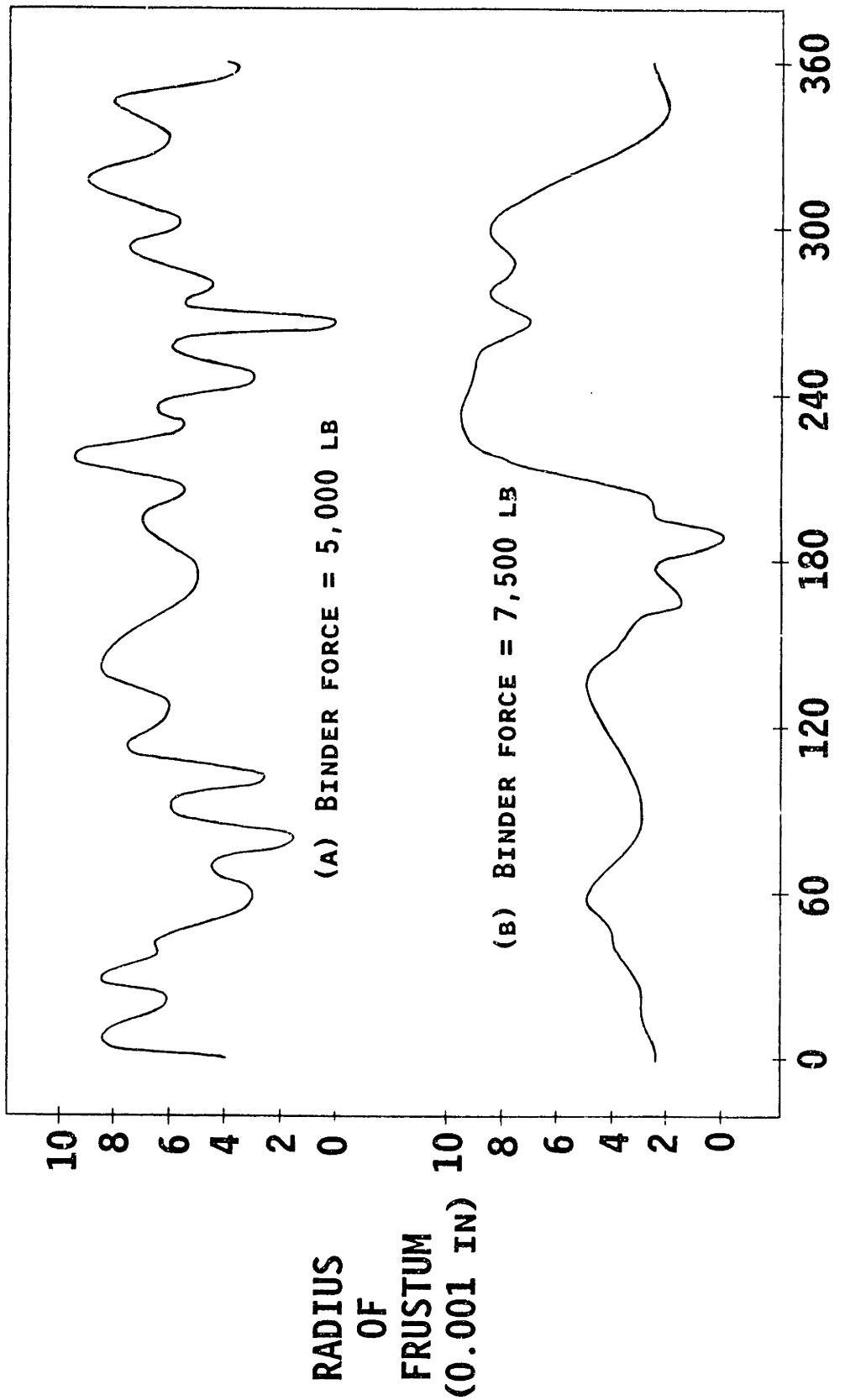

Fig. 3-9 Buckling Amplitude Plots: a) Buckling at 10 Times Sensor Threshold, b) No Buckling Detected by Sensor

of the sensor is better than the 0.002 amplitude/wavelength criteria suggested by Logan. For the initial conical die geometry used here, the buckling wavelength is approximately 0.5 in. and the sensor sensitivity is better than 0.001 in. buckling amplitude. The sensor reacts slowly at these low light levels because of the two second time constant of the photocell but the slow punch speed eliminates the need for a rapid response.

Instrumentation and Control Implementation

The experimental apparatus is instrumented for various force and displacement measurements. The forces measured are punch force, which is used to calculate F_t, and binder force which is controlled by a hardwired closed-loop servo. Strain gauges attached to the press structure allow measurement of these forces. The measurements of displacement are punch, blank edge, binder-die displacement and frustum buckling amplitude. All displacements except buckling are measured with LVDTs. The punch displacement is the independent variable in the tests and the punch velocity is approximately 0.75 in./minute.

An IBM PC with an Intel 8088 CPU and Intel 8087 math coprocessor controls the press. An interactive menu allows changing and recording important experimental parameters for each test. This computer initiates data acquisition, calculates F_t and t_{avg}, and determines appropriate changes to the binder force based on the target trajectories for F_t and t_{avg}. Voltages from the process transducers are converted to digital format and used to calculate F_t and t_{avg}. A proportional plus integral (PI) control algorithm compares the actual values of either F_t

or t_{avg} to the target values and calculates the desired binder force. The commanded binder force from the two control schemes is converted to a voltage by a digital to analog converter, and this voltage becomes the force target for an electro-hydraulic servo-valve controlled force loop. A detailed discussion of the control algorithm formulation is presented in Appendix B.

Tests were done to characterize the response of F_t and t_{avg} to binder force changes so that the controller gains could be determined from control theory. Step changes to binder force were done at various starting binder forces and heights within the forming cycle. These responses are the deviations of F_t or t_{avg} from their trajectories without a binder force step. Because the process is highly non-linear and can not be described by a simple model, conservative control gains were calculated to give F_t and t_{avg} responses with little overshoot (Appendix B). These theoretical proportional and integral control gains were reduced by an average of 68% because binder force was often driven to zero or saturation by control action. However, detuning to prevent saturation did not effect failure height during tests because rapid convergence of F_t and t_{avg} to the target was still achieved. The resulting values of the gains were constant for all tests of each control type. In an effort to simplify the use of the control methods, no adjustment of the gains was done for varying conditions.

The speed of the punch movement is limited by the computer processing time of one control cycle. The computer operations of data acquisition, updating of six real-time plots, F_t and t_{avg} calculations,

control algorithm calculations, and binder force output altogether require 0.3 seconds. The resulting total elapsed time for a test is typically 100 seconds for 340 control cycles. The speed of the hardware force servo loop is much higher than the 3Hz PC output and does not limit control speed. The speed of the control system could be drastically increased by eliminating real-time plotting and only making the necessary control calculations.

Chapter 4 RESULTS AND DISCUSSION

In the introduction, a typical plot of cup failure height versus constant binder force was presented that shows how failure height is reduced drastically by small deviations of the binder forces from the optimum (Fig. 1-3). Similarly, if random process variations mandate binder force changes to maintain optimum cup height but actual binder force is left unchanged, the formed height at failure is reduced. One such variation in formed height is caused by unpredicted changes in friction coefficient lubricant which affect flange restraint. This could result from: changes in lubricant composition and application, mill dependent changes in the blank surface, changes in the die condition due to wear, etc. A test series using three lubrication conditions was done using "standard" cup forming blanks (Fig. 4-1). Test results cited in the following sections are all performed using the cup geometry (Fig. 4-1*(a)) and "standard" conditions (Table 4-1) unless otherwise noted. Standard conditions for cup forming are 0.020 in. thick material "C", 6.25 in. blank diameter, and STP mixture lubrication. The steep shoulders of the curves in Fig. 4-1 mirror the sensitivity to binder force selection of Fig. 1-3. For example, if the binder force was correctly chosen as 6000 pounds while using STP lubricant, a change to teflon lubricant would cause a 21% reduction in failure height, since the part would now fail prematurely by buckling. Similarly, if no lubricant were present, early failure by tearing would result. Changes in part flange width also require adjustment to binder forces during forming. Flange width affects flange restraint through variations in hoop stress, which is particularly important at lower

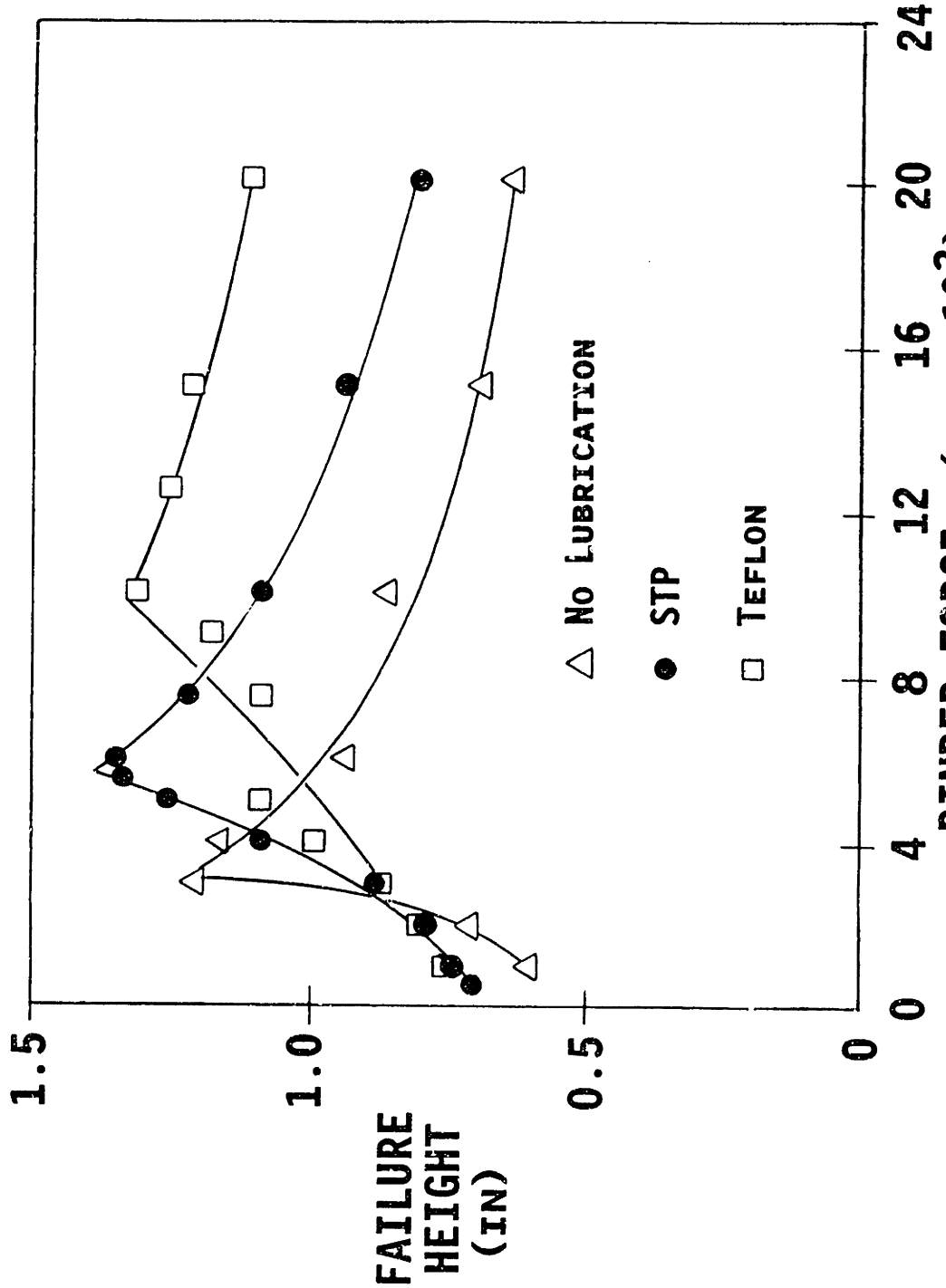

Fig. 4-1 Constant Binder Force (Open-Loop) Tests: Effect of Lubrication on Failure Height (cup geometry, 0.020 in. material "C", 6.25 in. diameter)

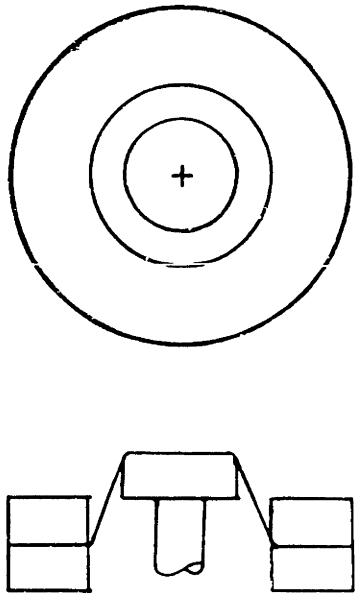

(A) CONICAL CUP

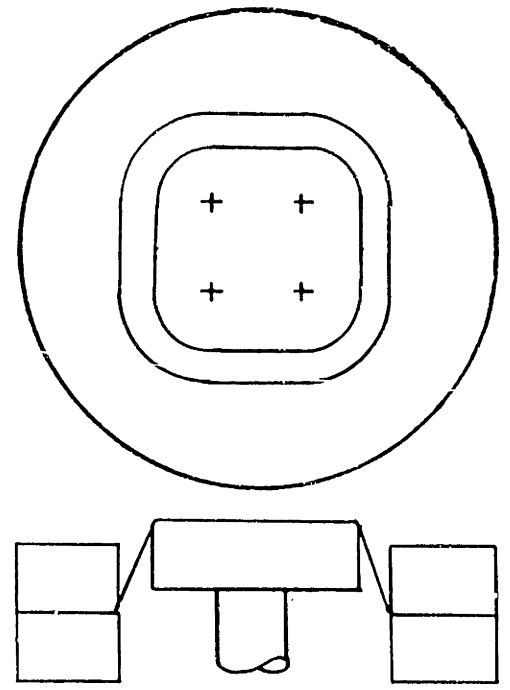

(B) EQUAL CORNER RADII PAN

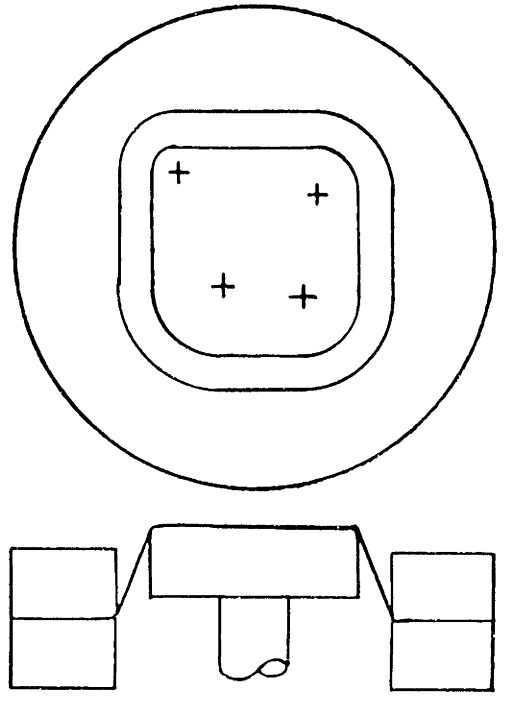

(C) UNEQUAL CORNER RADII PAN

Fig. 4-1* Drawings of the Three Die Set Geometries (repeat of Fig. 1-4): a) Conical Cup Geometry, b) Equal Corner Radii Square Geometry, c) Unequal Corner Radii Square Geometry

binder forces. Tests were done to determine the effect of flange width variations on failure height. Figure 4-2 shows the variation in failure height curves for flange width variations caused by blank diameter changes and eccentric blank positioning.

The control systems implemented in this study automatically adjust the binder force toward the optimum value, which maximizes failure height for the particular conditions. A typical binder force trajectory during closed-loop control is shown in Fig. 4-3. After an initial period of constant binder force, the controller turns on and controls the binder force on a safe trajectory to the optimum force level. The sections below describe the implementation of the F_t and t_{avg} control algorithms.

Scope of Experiments

A comprehensive experimental program was completed to test the F_t and t_{avg} control methods. Initial tests for each die geometry were done under a set of standard conditions. Subsequent tests used process perturbations for each die geometry to test the robustness of the two control strategies. The die geometries, standard conditions and process perturbations are described in the section below.

Die Geometries:

Tests of the control techniques were completed on three die set geometries. Early tests used a standard conical cup configuration (Fig. 4-1*(a)) that was chosen for the following reasons:

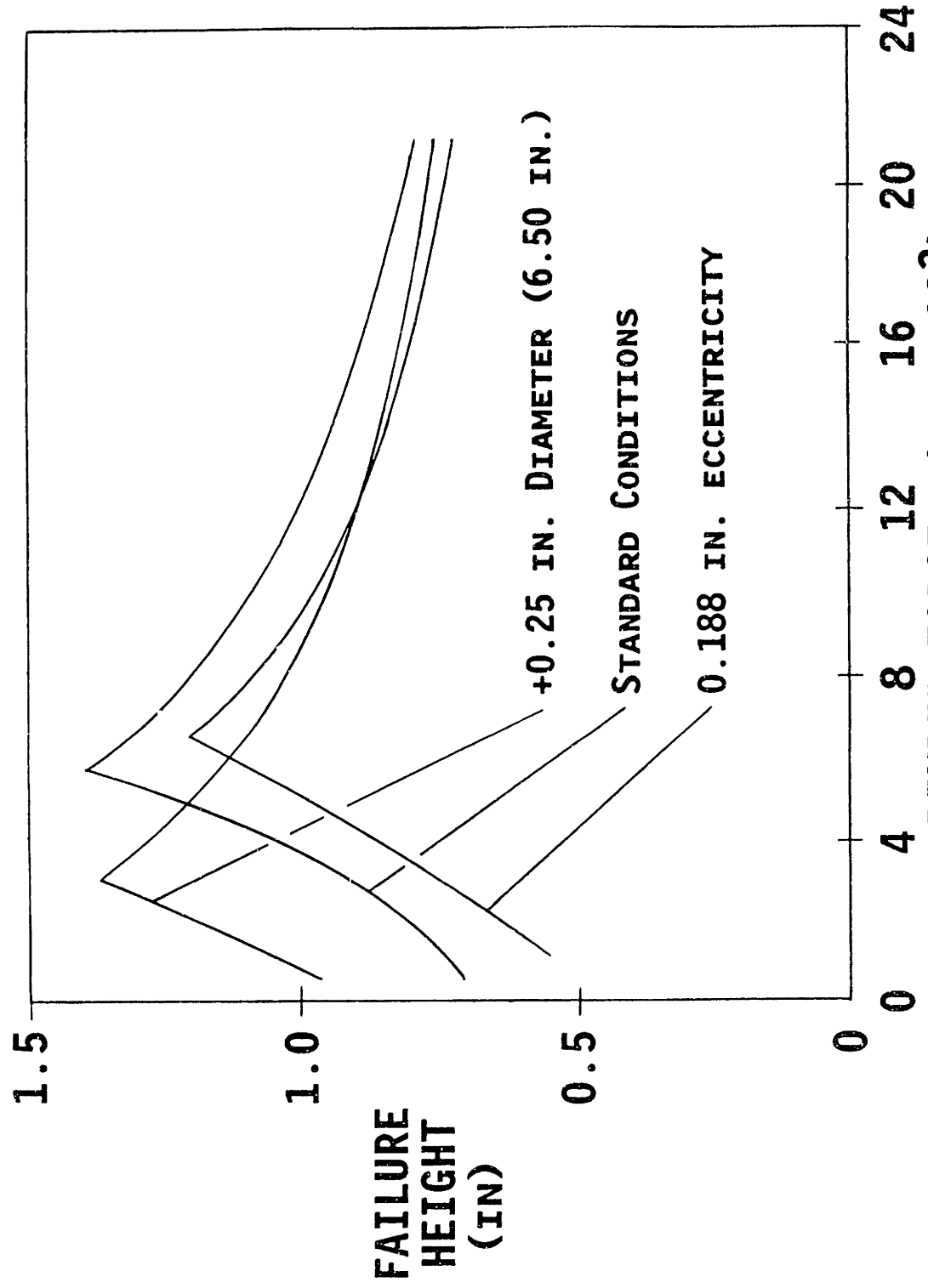

Fig. 4-2 Constant Binder Force Tests: Effect of Flange Width on Failure Height (cup geometry, 0.020 in. material "C", STP)

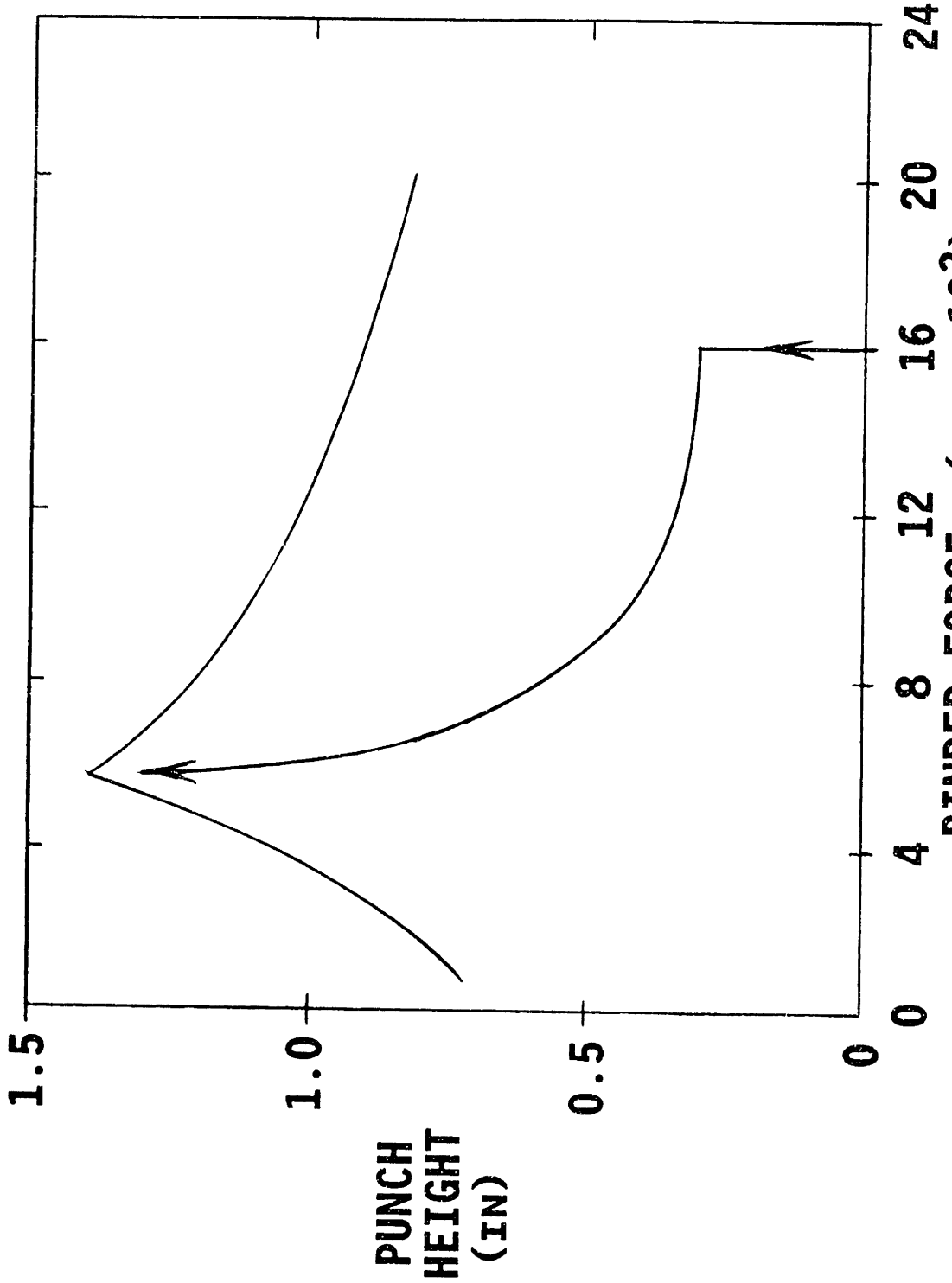

Fig. 4-3 Controller 'Finds' Optimum Binder Force

1. The basic geometry, with a peripheral blank holder, unsupported region, and "dead" metal region on the punch, allows study of the critical phase of die-stamping prior to bottoming of the die set.
2. The flat topped circular punch gives a well defined area at the punch nose where tensile stresses are maximum and failure occurs. This allows tearing failures to be easily analyzed.
3. The geometry permits easy evaluation of forming performance by comparison of the maximum cup height achieved before failure.

This cup die set has punch and die diameters of 2.5 in. and 4 in. respectively, and profile radii of 0.25 in.

The second and third die sets both produce square pans but have different corner radii (Fig. 4-1*(b), 4-1*(c)). Both punches are 4.5 in. across and both dies are 6.0 in. across. All profile radii remain 0.25 in. as in the conical configuration. The gap between the punch and die is 0.75 in. as for the cup geometry. The first square geometry has four equal punch corner radii of 1.25 in. which is equal to the cup punch radius. The four die radii are 2.00 in. as for the circular die. The second square die set has the least symmetry because of unequal corner radii. The four punch radii are 0.5, 1.0, 1.25, and 1.50 in. and the corresponding die radii are 1.25, 1.75, 2.00, and 2.25 in. This die set was chosen to be more representative of typical asymmetric production parts while retaining common elements with the earlier configurations. The original punch-die gap, profile radii, and certain corner radii were preserved in the square configurations. This square geometry facilitates study of the effect of punch asymmetry on punch nose stresses and F_t values. The effect of die asymmetry on draw-in and

t_{avg} values was also studied.

Standard Conditions:

Initial tests on each of the three geometries were done under three sets of standard conditions. Perturbations from the standard were then done to check the robustness and general applicability of the control algorithms. The standard conditions for the three geometries are given in Table 4-1.

	Conical	Square with Equal radii	Square with Unequal Radii
1. Material	"C"	"A"	"A"
2. Lubrication	STP Mix	Dry	Silicone
3. Blank Diameter	6.25 in.	9.078	9.078
4. Thickness	0.020 in.	0.025	0.025
5. Eccentricity	0 in.	0	0

Note: Details of forming conditions are described in the perturbation section below.

Table 4-1 Standard Test Conditions

A thin 0.020 in. material was chosen to promote buckling failure of the original cup geometry which allowed thorough testing of the controller algorithms. The 6.25 in. blank diameter for the conical tests was the minimum size that prevented draw of the cup into the die cavity before failure. The 9.078 in. diameter of the pan blanks was chosen to make the initial flange width at the equal radii die corners equal to the initial cup flange.

Perturbations:

Tests of the control methods were done using a variety of perturbations from the standard conditions listed above. The scope of the variations in the process conditions is described below.

1. Material

The material type used throughout is drawing quality cold-rolled steel sheet. The six materials used are listed in order of ascending tensile strength in Table 4-2.

Code	Thick	Yield	UTS	Elong	R_b	r	r	%C
A	0.025	29ksi	47ksi	39%	46	1.63	0.66	0.04
B	0.025	33	49	28				
C	0.020	36	51	35				
D	0.020	47	58	31	63	0.96	0.25	0.12
E	0.025	44	64	27	69	1.63	0.44	0.11
F	0.030	42	65	32	66	1.46	0.67	0.09

Table 4-2 Properties of Materials Used in Tests

2. Lubrication

The lubricants used in the tests are listed from lowest to highest friction coefficient:

- o Teflon particle aerosol spray
- o STP Mix - 3 parts 20W motor oil and 1 part STP
- o No lubricant with die cleaning between tests
- o DC 200 - 100 centistoke viscosity silicone oil

3. Blank diameter

Tests using blanks 0.25 in. larger than the standard were done (i.e. 5.50 in. and 9.078 in.).

4. Blank Thickness

The thicknesses used in tests were 0.020, 0.025, and 0.030 in.

5. Misalignment of Blank with Press Centerline

The effect of 3/16 (0.188) in. eccentricity of the blank centerline with respect to the die was tested.

Table 4-3 summarizes all tests of the two main control methods under various conditions.

Perturbation	Conical	Square with Equal radii	Square with Unequal Radii
"A" 0.025	F_t, t_{avg}	F^*	F_t^*, t_{avg}^*
"B" 0.025	F_t, t_{avg}		
"C" 0.020	F_t^*, t_{avg}^*		
"D" 0.020	F_t		
"E" 0.025	F_t	F_t	
"F" 0.030			F_t
Teflon	F_t, t_{avg}		
STP Mix	F_t^*, t_{avg}^*	F_t	F_t,(note 1)
Dry	F_t, t_{avg}	F_t^*	
Silicone Oil			F_t^*, t_{avg}^*
6.25 in. blank	F_t^*, t_{avg}^*		
9.078 in. blank		F_t^*	F_t^*, t_{avg}^*
+0.25 in. blank	F_t, t_{avg}		F_t
0 eccentricity	F_t^*, t_{avg}^*	F_t^*	F_t^*, t_{avg}^*
0.188 in. eccen.	F_t		F_t,(note 1)

"*" - Standard Conditions

F_t - Tangential Force Control

t_{avg} - Normalized Average Thickness Control

Note 1: All perturbations are done singly except one test of eccentricity with a lubrication change.

Table 4-3 Summary of Process Perturbations

Two control algorithms were tested with the various geometries and process conditions described above. The implementation and performance of the tangential force and normalized average thickness control strategies are discussed in the sections below.

Tangential Force Target Selection For Cups

The calculated value of tangential force (F_t) is an estimate of the average stress around the punch nose, as described in Chapter 3. Trajectories of F_t for five tests using different constant binder forces and conical geometry are shown in Fig. 4-4. The failure height for each condition is indicated by the position of the end of each curve. The 30,000 lb. binder force causes high F_t and premature tearing. The 500 lb. binder force results in low F_t and premature buckling due to the large draw-in. An intermediate binder force of 6,000 lb. gives the optimum height at failure because of near simultaneous tearing and buckling. This optimum F_t trajectory was found during iterative tests using various constant binder forces. If the stress of the material were controlled to this "signature" trajectory that was produced by optimum conditions, consistently high formed height would be expected. A linear target trajectory for F_t was chosen which approximates this optimum trajectory.

It is most important that the target is a good approximation of optimum F_t level at the end of the forming stroke. The chosen target value is 5% higher than the optimum F_t at failure and usually causes failure by tearing rather than buckling. This small shift from the optimum will give a higher <u>average</u> failure height. By favoring tearing

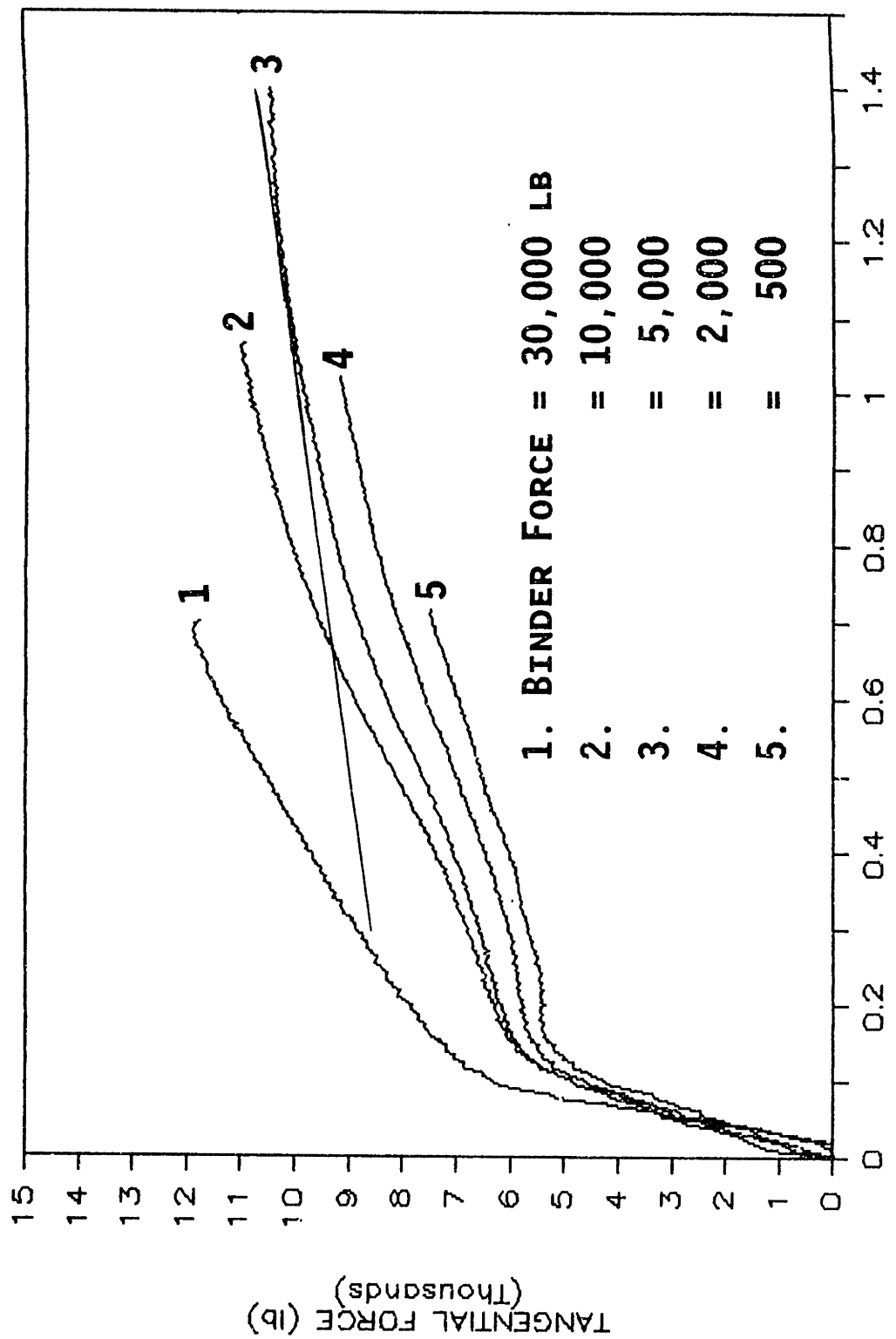

Fig. 4-4 Optimum F_t Trajectory and Target Selection for the Cup Geometry (cup geometry, 0.020 in. material "C", STP, 6.25 in. diameter).

rather than buckling, the shifted target will usually avoid a large reduction in formed height caused by failure on the steeper, buckling curve (Fig. 4-1). This target shift increases the robustness of the control system by reducing the sensitivity of the failure height to binder force errors. No specific rule is required for placement of the early F_t target values.

Values of the F_t target at the beginning must be within the safe envelope defined by the trajectories of Fig. 4-4. Typically these early target values will be significantly above the optimum so that the end of the target line is parallel to the optimum near the failure height. High initial F_t target values also ensure that low initial binder forces are not driven to zero by the controller if the early F_t trajectory is atypical. In general, early target position is not as important as final position because early binder force has much less impact on failure height.

Successful control during a variety of process disturbances requires that the optimum F_t trajectory does not change as conditions change. Any changes in the optimum F_t path would require corresponding changes to the F_t target line which would be difficult to predict. Significant variations in F_t trajectory occur during lubrication changes while binder force is constant (Fig. 4-5(a)), and for each lubrication condition, there is a different optimum binder force. However, the F_t trajectory variation is much smaller if the binder force is changed to the optimum constant value (Fig. 4-5(b)). The similarity of the curves indicates that the best target line does not change significantly as

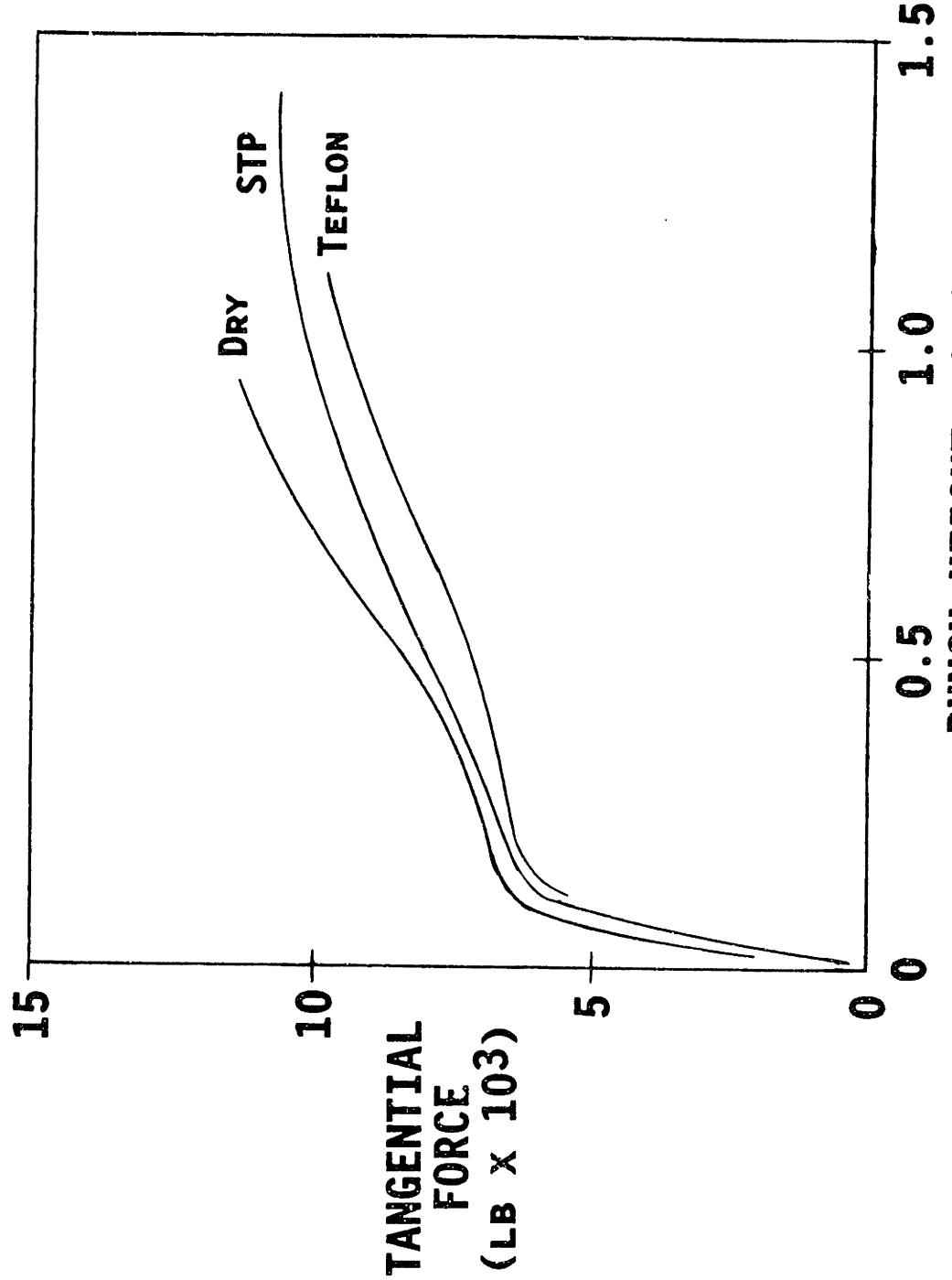

Fig. 4-5(a) Effect of Lubrication on the Tangential Force Trajectory: One Binder Force (binder force = 6,000 lb, cup geometry, 0.020 in. material "C", 6.25 in. diameter)

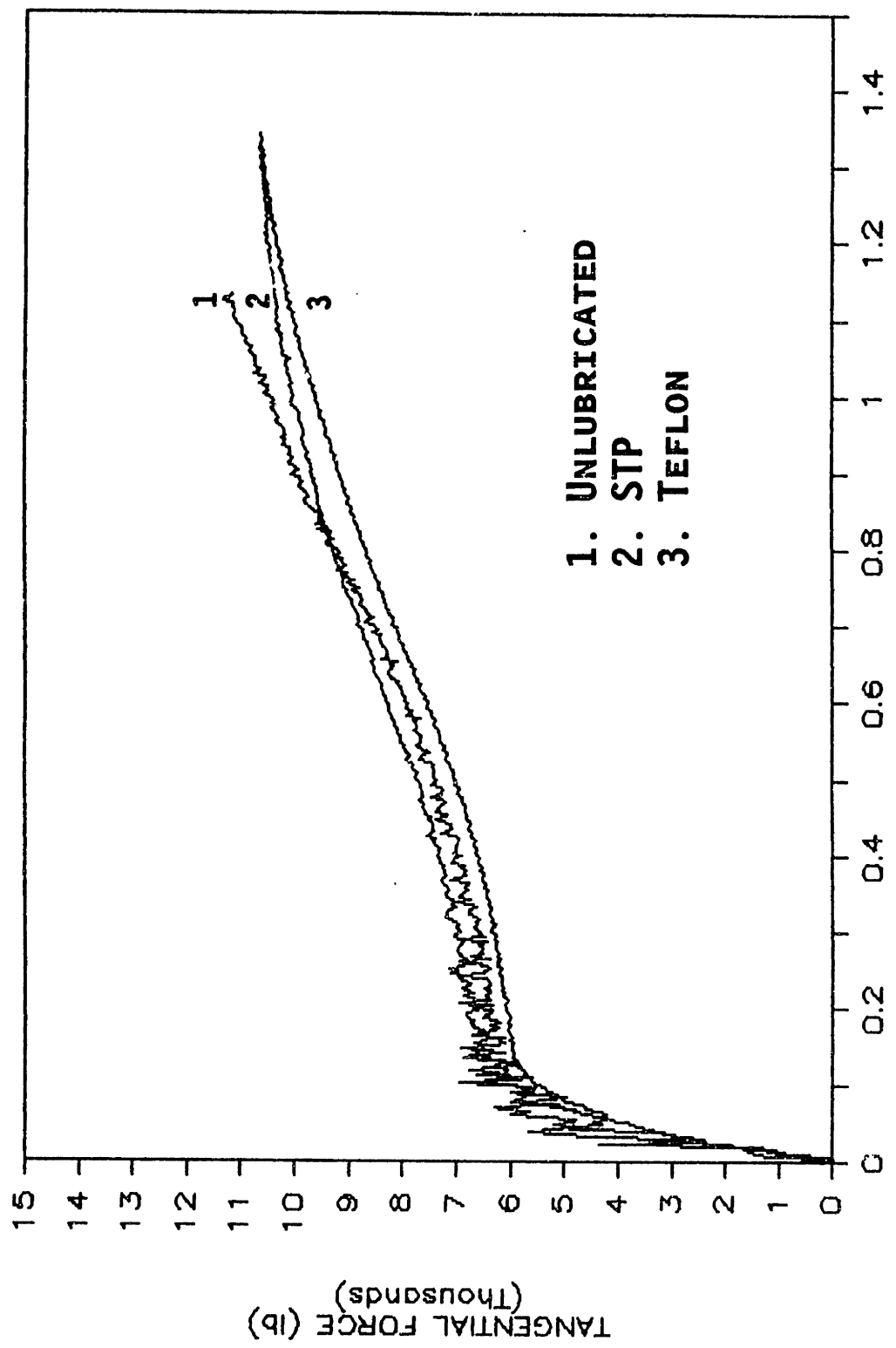

Fig. 4-5(b) Effect of Lubrication on the Tangential Force Trajectory: Respective Optimum Binder Forces (dry:2k lb, STP:5k, Teflon:10k, cup geometry, 0.020 in. material "C", 6.25 in.)

lubrication varies. One constant target line should give similar levels of control performance for any lubrication condition. The same argument for the use of constant target lines also applies to other types of disturbances. Figure 4-6(a) shows how F_t varies with blank diameter. However, the F_t trajectories are almost congruent when the binder forces are adjusted to their respective optimums (Fig. 4-6(b)).

Closed-Loop Tangential Force Control Of Cups

The development of the required F_t target line from cup experiments is discussed above. Once the target has been determined, the F_t control loop (Fig. 3-4) can be used to manipulate the binder force so that real-time F_t values follow the target trajectory. Regulation of F_t in this way minimizes the effect of process disturbances on failure height and is expected to minimize forming failure during production. Test results under standard conditions as well as during variations of lubrication, blank diameter, and eccentricity are discussed in the section below. No target trajectory alteration was required for these conditions that alter flange restraint conditions through frictional or hoop forces. The optimal targets are relatively constant because the maximum allowed tearing and buckling forces in the frustum are independent of the particular restraint conditions at the flange. However, target scaling for thickness and material property variations is necessary as described in a section below. These variations affect the load carrying capacity of the material and the resistance to buckling, which change the optimal control targets.

A comparison of the open and closed-loop failure heights for cup

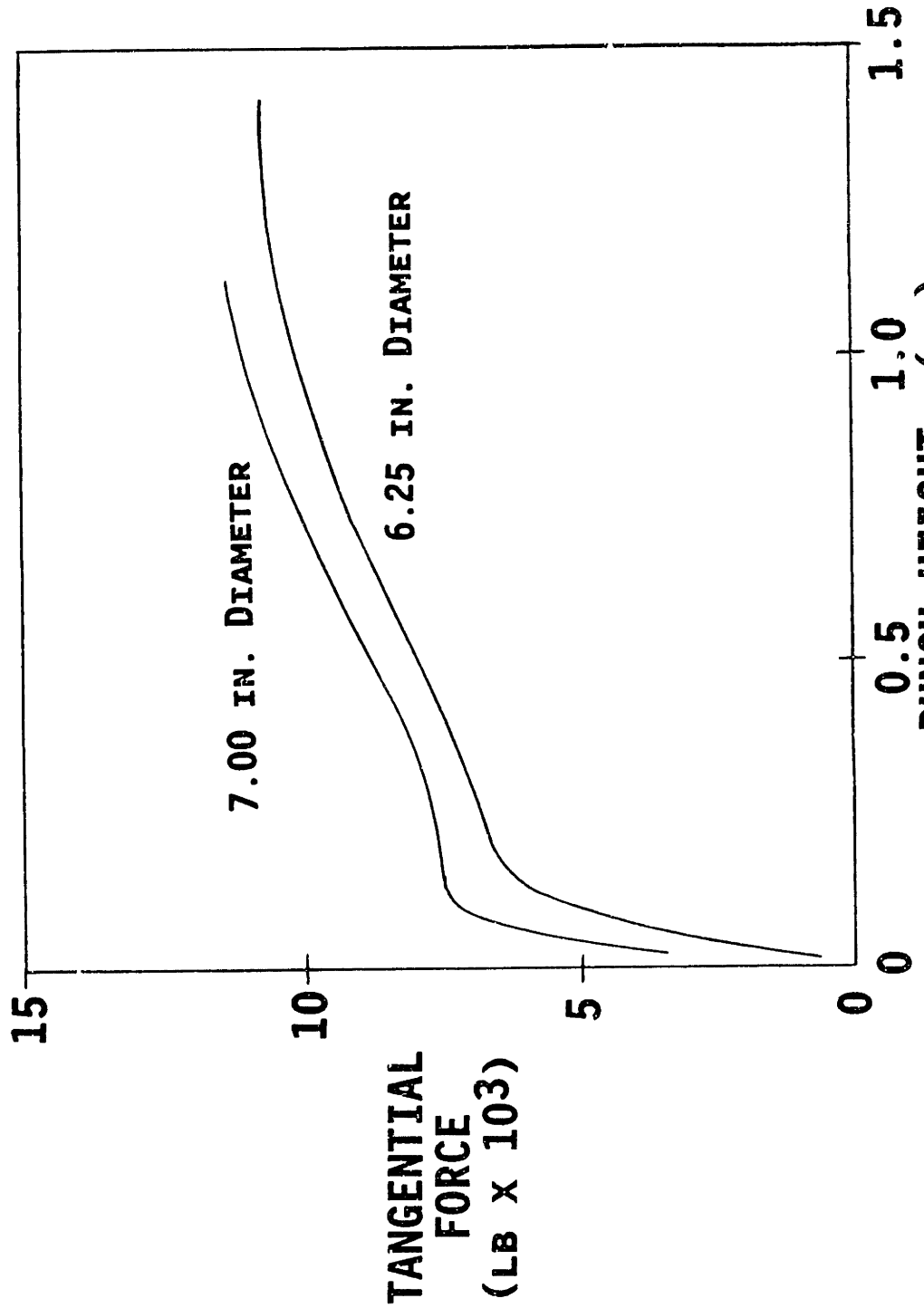

Fig. 4-6(a) Effect of Blank Diameter on Tangential Force Trajectory: One Binder Force (Binder force = 6,000 lb, cup geometry, 0.020 in. material "C", STP)

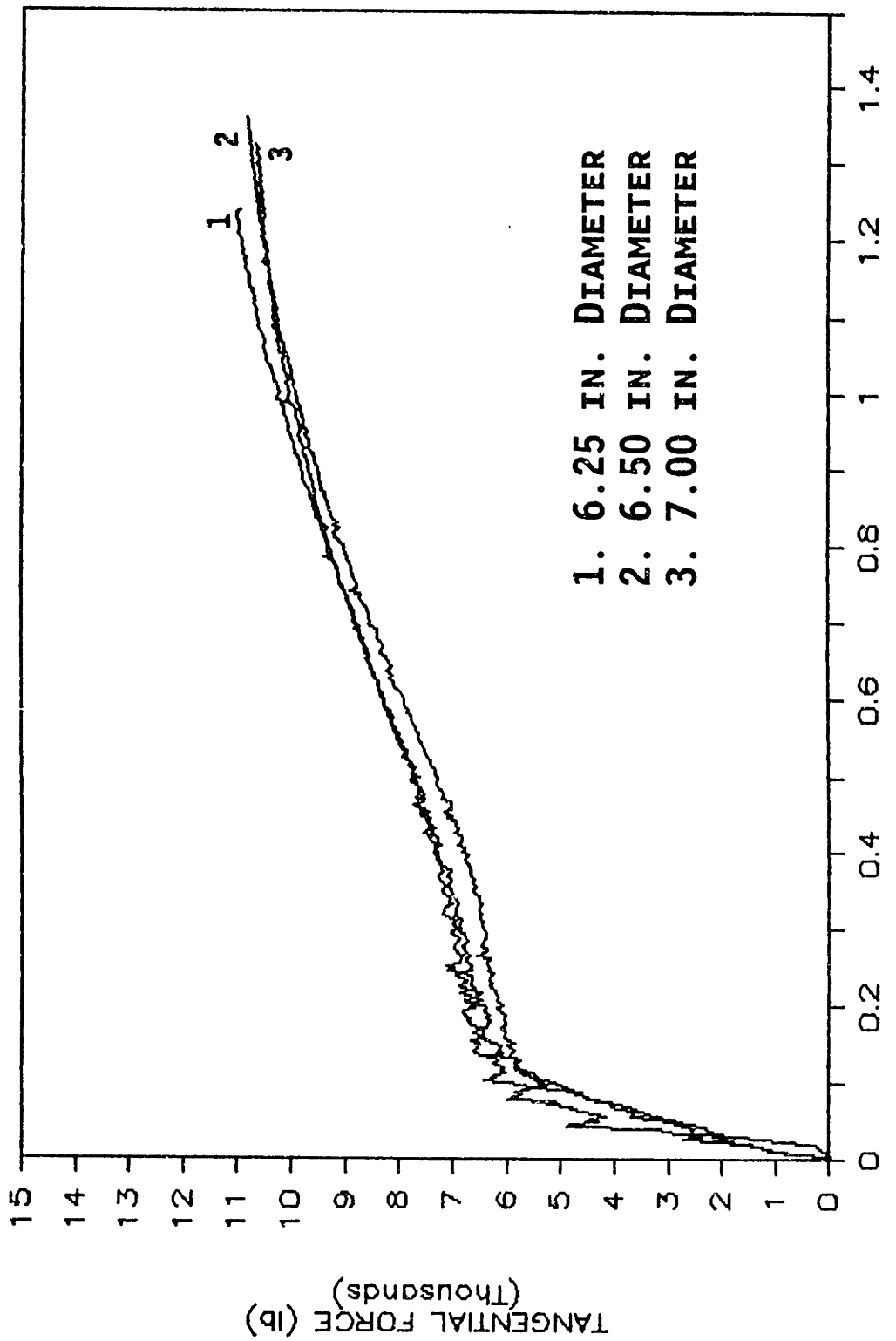

Fig. 4-6(b) Effect of Blank Diameter on Tangential Force Trajectory: Respective Optimum Binder Forces (6.25:5k lb, 6.50:3k, 7.00:1k, cup geometry, 0.020 in. material "C", STP)

forming under standard conditions is shown in Fig. 4-7. The open-loop plot shows the failure height for a range of binder forces which are constant throughout the forming process. In this case, accurate selection of the constant binder force value is required to maximize formed height. The closed-loop plot shows the failure height for a range of initial binder forces that are altered by the control system after 0.3 in. of punch height. The failure height is almost constant for the closed-loop case and is near the highest failure height produced by the optimum binder force. F_t control significantly reduces or eliminates the need for previous knowledge of the binder force giving the greatest formed height. The bars marked on Fig. 4-7 correspond to +/- one standard deviation. The results of the other tests shown below had levels of variability similar to Fig. 4-7. These "standard" tests used STP-oil mixture lubrication and 6.25 in. diameter blanks made of 0.020 in. thick "C" material.

The characteristic shape of the F_t versus punch height plots is similar to a typical uniaxial stress-strain plot (Fig. 4-6(b)). The slope up to 0.2 in. of punch height is largely due to elastic deformation occurring during the initial forming. As forming progresses, plastic deformation replaces elastic deformation over the frustum and the slope becomes smaller. Because of the radical difference between the elastic and plastic deformation processes, the closed-loop control system was designed only for the plastic deformation process. For this reason control system changes to binder force were allowed only after 0.3 in. of punch height. Conversely, it is important that the required binder force changes are not delayed too far into the

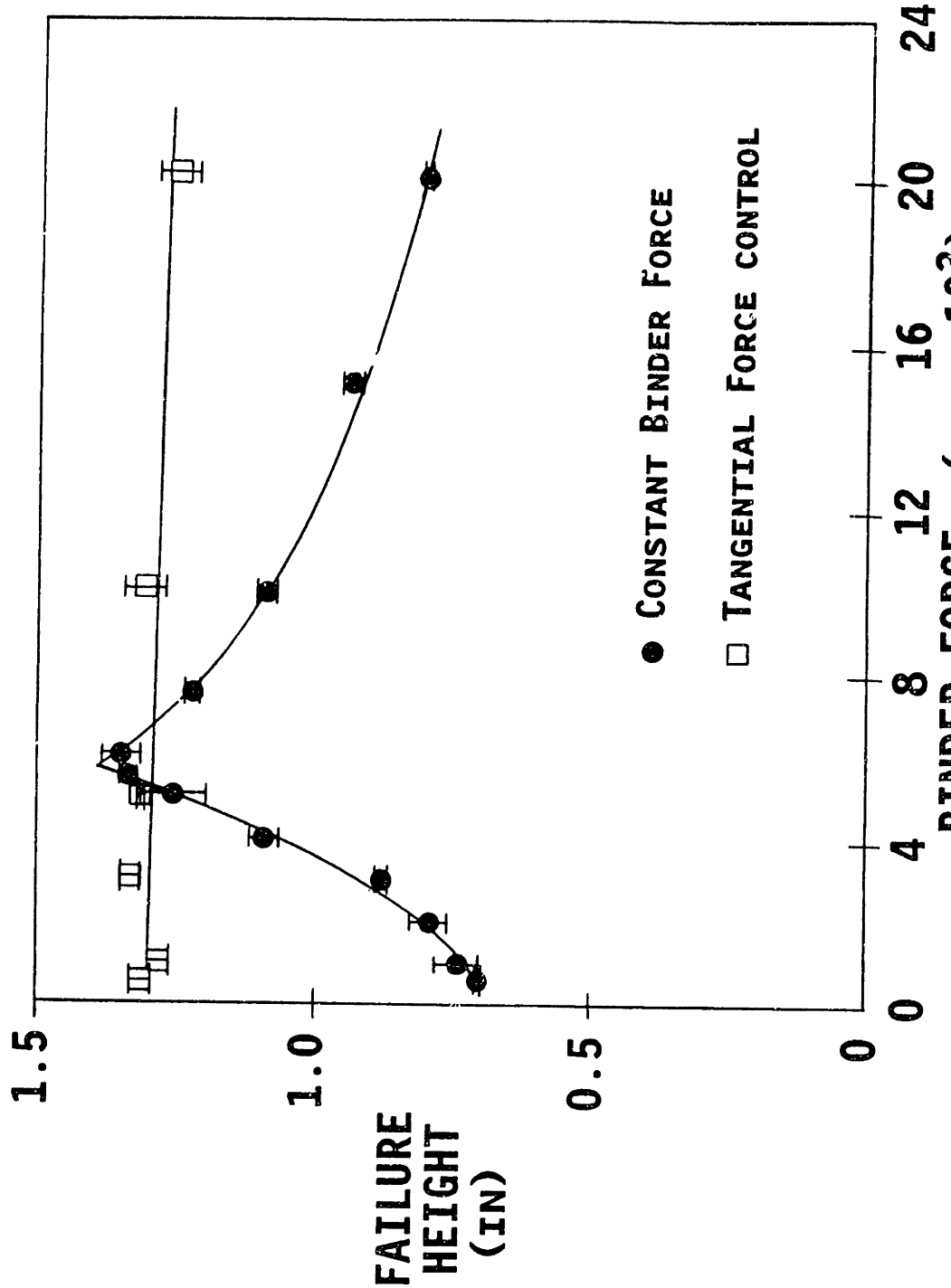

Fig. 4-7 Closed-Loop F_t Control: Cup Standard Test. The open-loop curve from Fig. 4-1 is included for comparison (cup geometry, 0.020 in. material "C", STP, 6.25 in. diameter).

forming cycle. If forming is allowed to progress too far while using an inappropriate binder force, failure height will be reduced. Figure 4-8 shows the loss in available part height when control action is postponed for varying punch heights.

The effect of closed-loop control on five F_t trajectories is shown in Fig. 4-9(a). The initial uncontrolled trajectories of the 500 lb. and 20,000 lb. binder force cases are quite different. However, the control system, after it is activated at 0.3 in., quickly brings the F_t values for both initial conditions to the target line. The result is similar material states for both over most of the forming cycle and near-optimum failure heights which are independent of initial binder force.

The binder force trajectories that produce the desired F_t trajectories can also be examined. Figure 4-9(b) shows two binder force trajectories which produce F_t trajectories like those in Fig. 4-9(a). To bring the F_t to the target line, the control system automatically adjusts the binder force toward the optimum value. If the forming conditions change, the control system "finds" the new optimum binder force regardless of starting binder force.

The closed-loop control system was tested using the same target line as above but with two other types of lubrication. Figures 4-10(a) and 4-10(b) show the constant binder force and closed-loop failure heights for the dry and teflon lubrication conditions. The optimum constant binder forces for the dry and teflon condition are shifted by -3,000 lb.

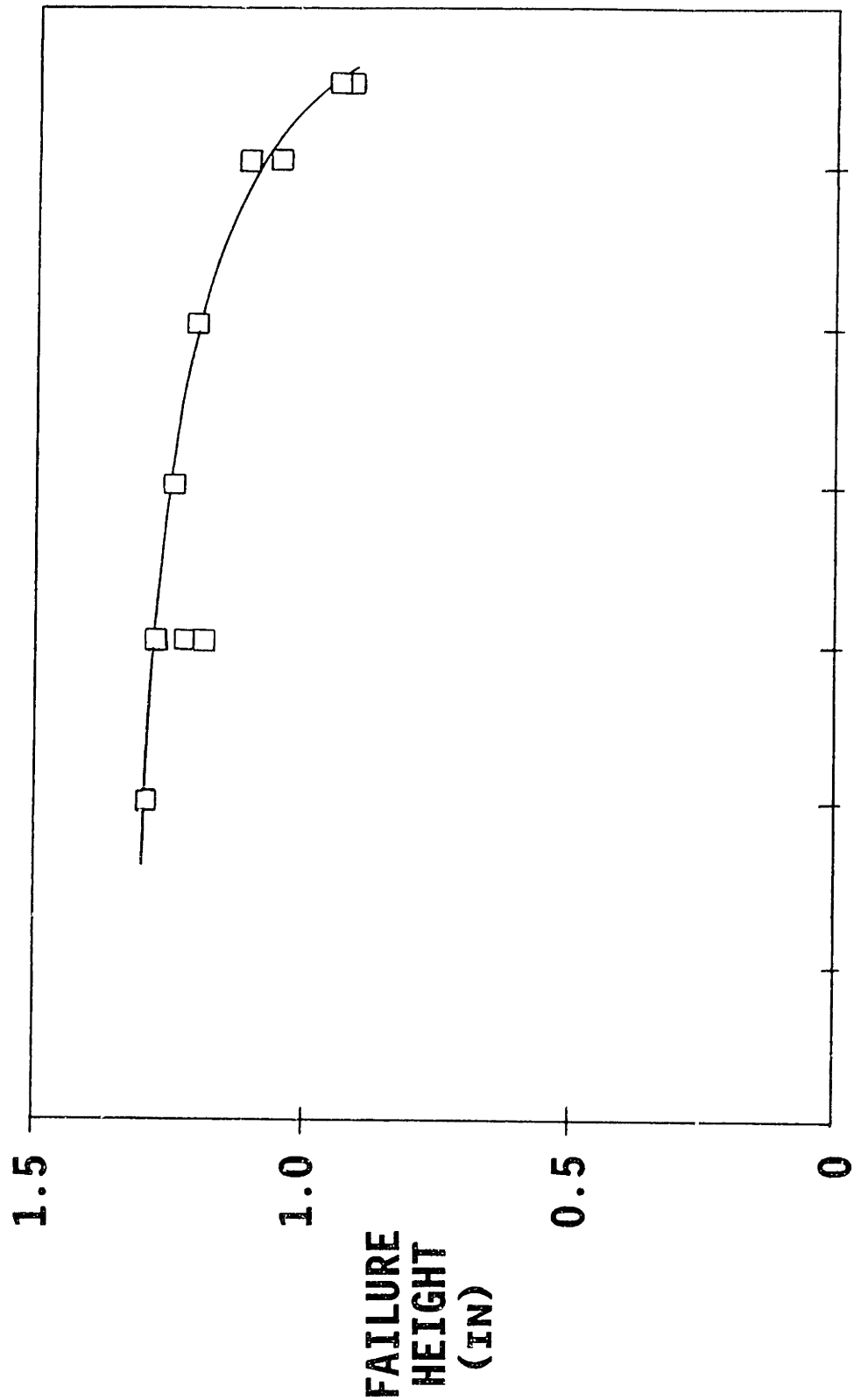

Fig. 4-8 Failure Height for Various Control Starting Heights (initial binder force = 20,000 lb, cup geometry, 0.020 in. material "C", STP, 6.25 in. diameter)

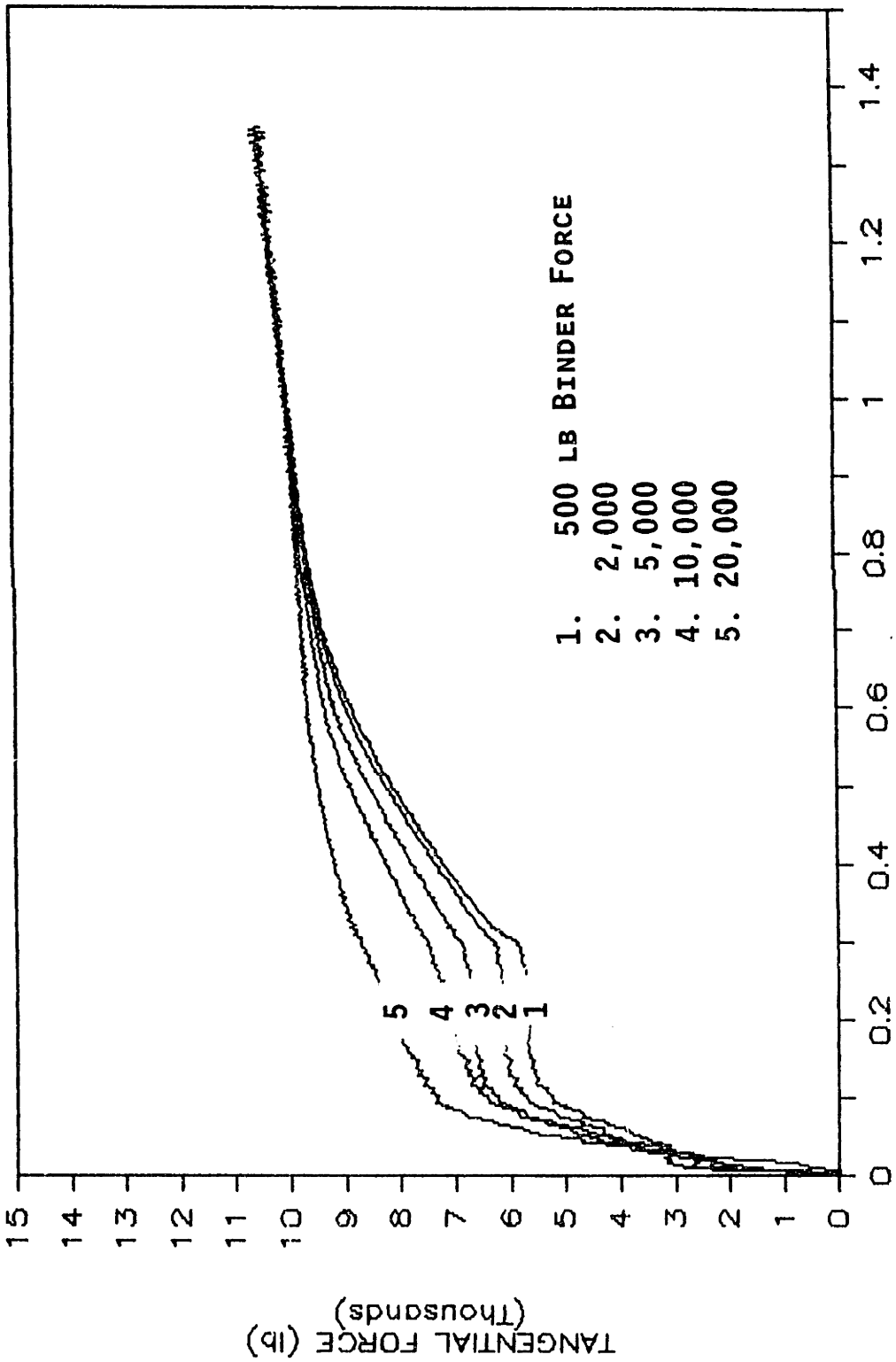

Fig. 4-9(a) Tangential Force Control Dynamics: Trajectories for different initial binder forces (cup geometry, 0.020 in. material "C", STP, 6.25 in. diameter)

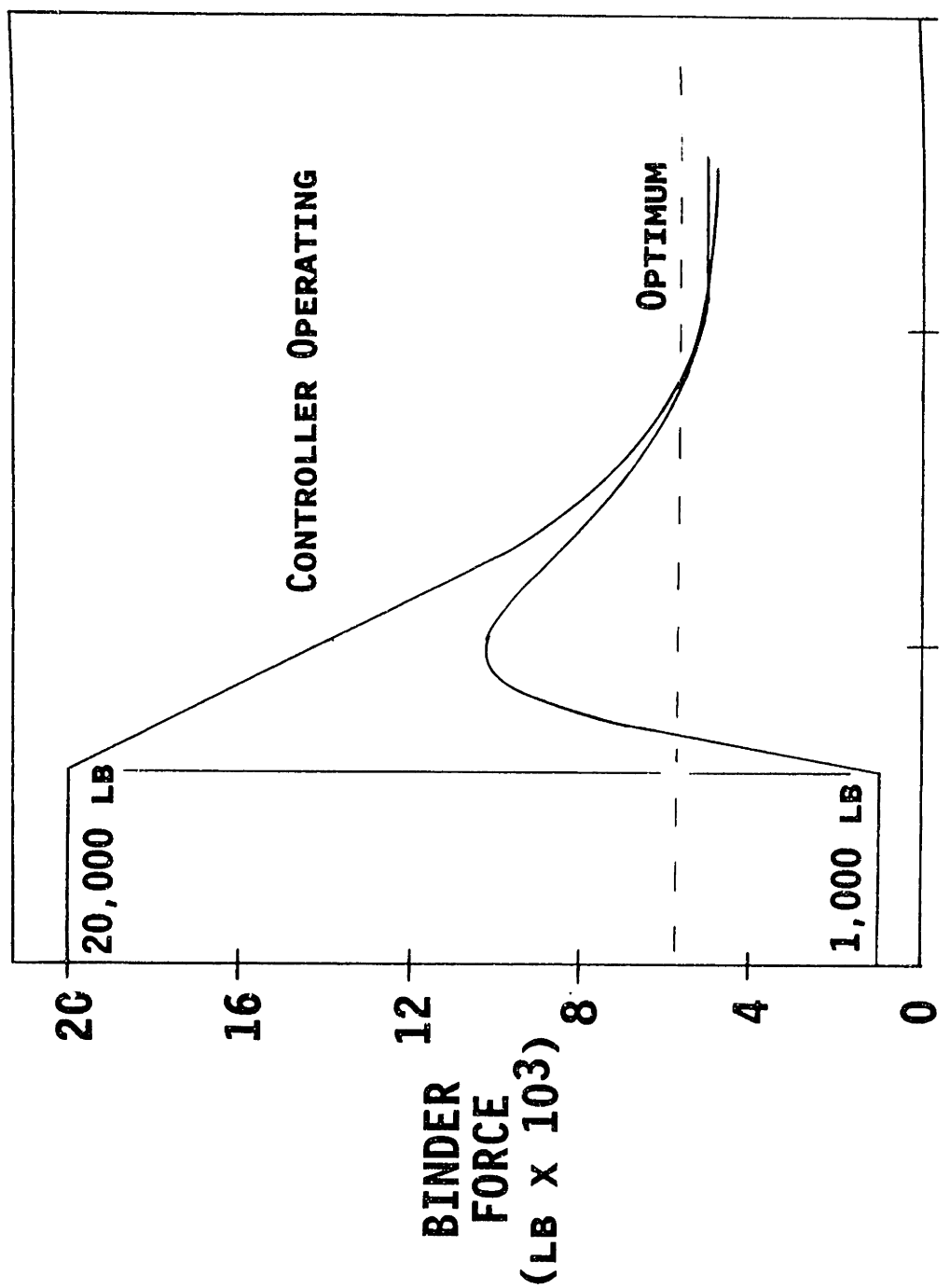

Fig. 4-9(b) Tangential Force Control Dynamics: Corresponding binder force responses (cup geometry, 0.020 in. material "C", STP, 6.25 in. diameter)

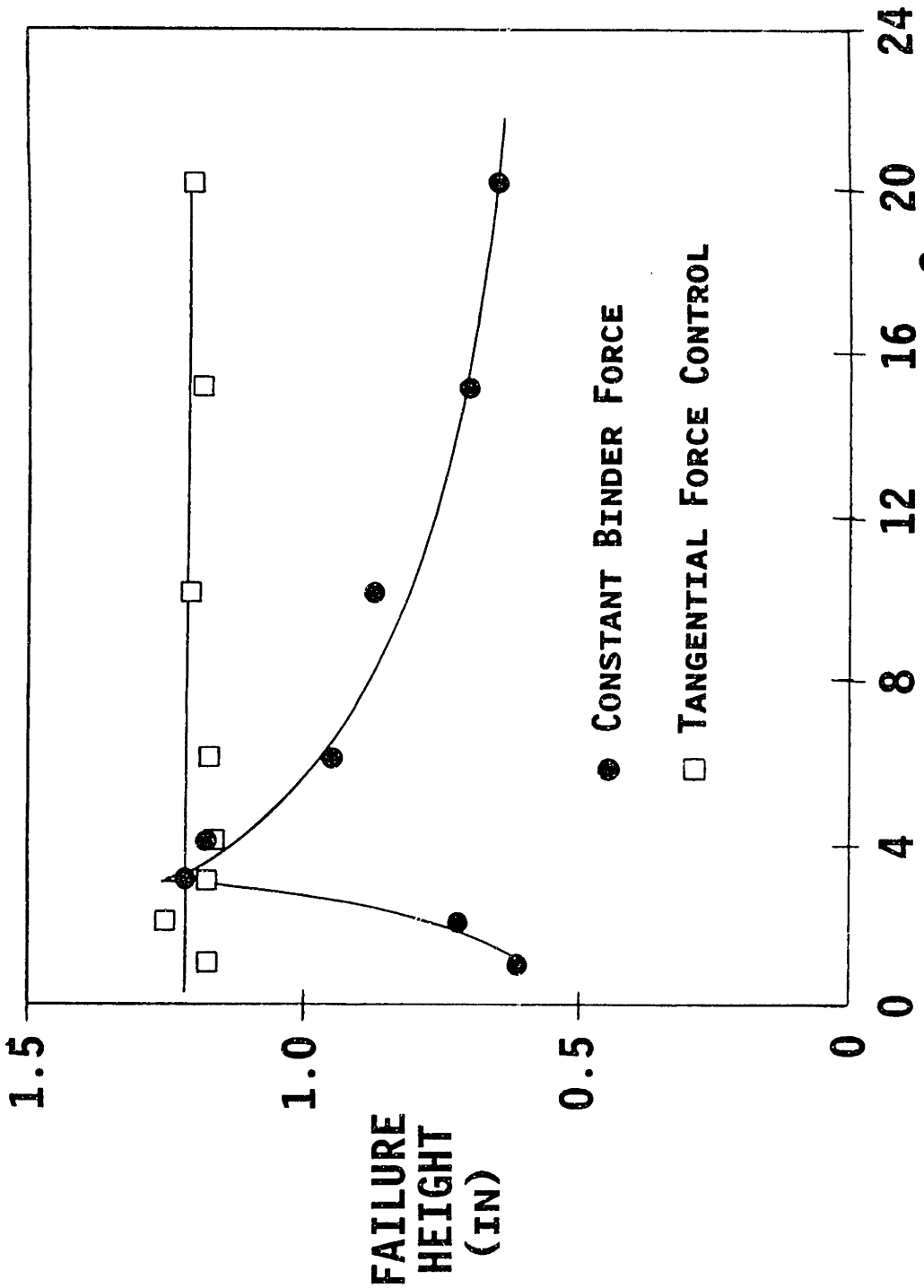

Fig. 4-10(a) Closed-Loop F_t Control: Change of Lubrication Conditions to Unlubricated (cup geometry, 0.020 in. material "C", 6.25 in. diameter)

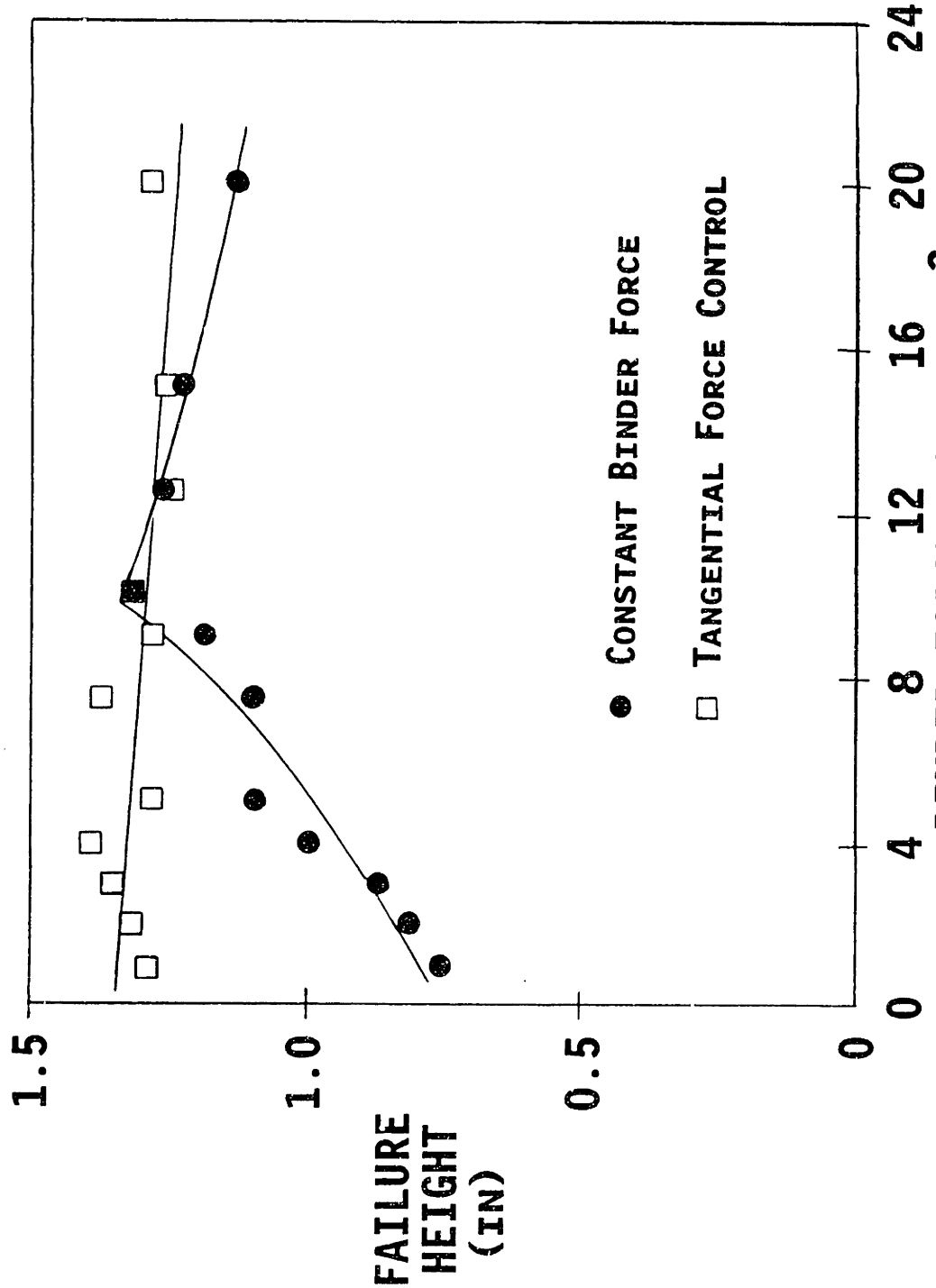

Fig. 4-10(b) Closed-Loop F_t Control: Change of Lubrication Conditions to Teflon Film (cup geometry, 0.020 in. material "C", 6.25 in. diameter)

and +4,000 lb. respectively from the value under standard conditions (Fig. 4-7). Under dry conditions the optimum binder force is low because the high friction coefficient acts to increase the restraining force in the flange. Conversely, the low friction conditions with teflon require a high binder force. In all three cases, closed-loop control almost eliminates the influence of initial binder force on failure height. Taken together, the tests indicate that the effect of lubrication changes is minimized by the control system.

There are process disturbances other than lubrication that affect flange friction forces. Changes in surface finish of the blanks, die or binder affect friction forces and change the optimum binder force. The effect of these variables is expected to be minimized by F_t control in the same way as lubrication variation.

The effect of larger blank diameter on failure height is shown in Fig. 4-11 for constant binder force and closed-loop control tests. Blanks of 6.50 in. diameter, which is 0.25 in. larger than the standard, were formed using the original controller target and gains. The controller again produces near optimum formed heights regardless of initial binder force estimate.

The effect of "off-center" placement of the blank within the die cavity was examined in the last test of F_t control without target scaling. Figure 4-12 shows that F_t control significantly reduces the effect of eccentric blank placement. Both blank size and eccentricity affect the distribution of hoop stresses in the flange. The effect of

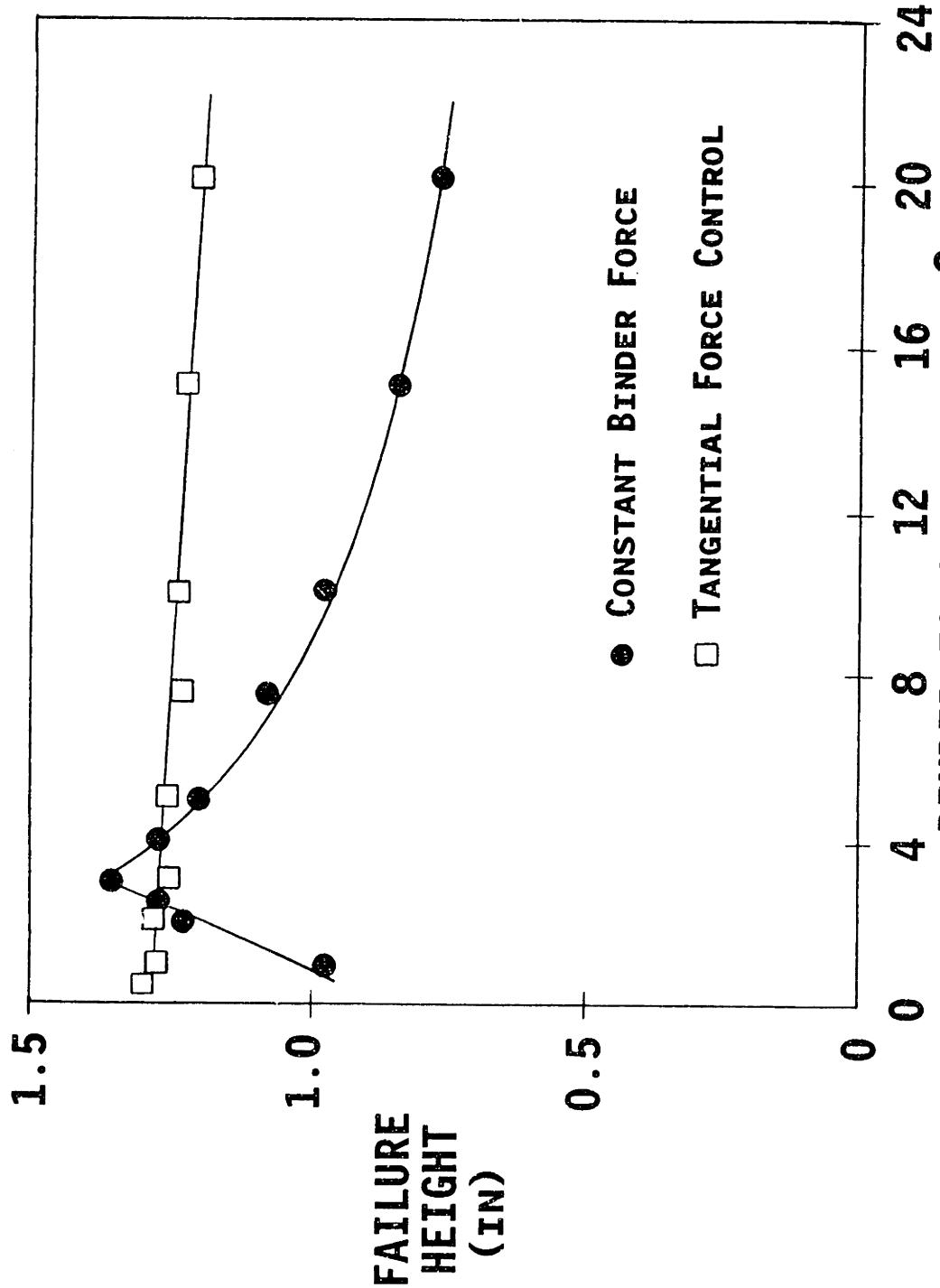

Fig. 4-11 Closed-Loop F_t Control: Change of Blank Diameter to 6.50 in. (cup geometry, 0.020 in. material "C", STP)

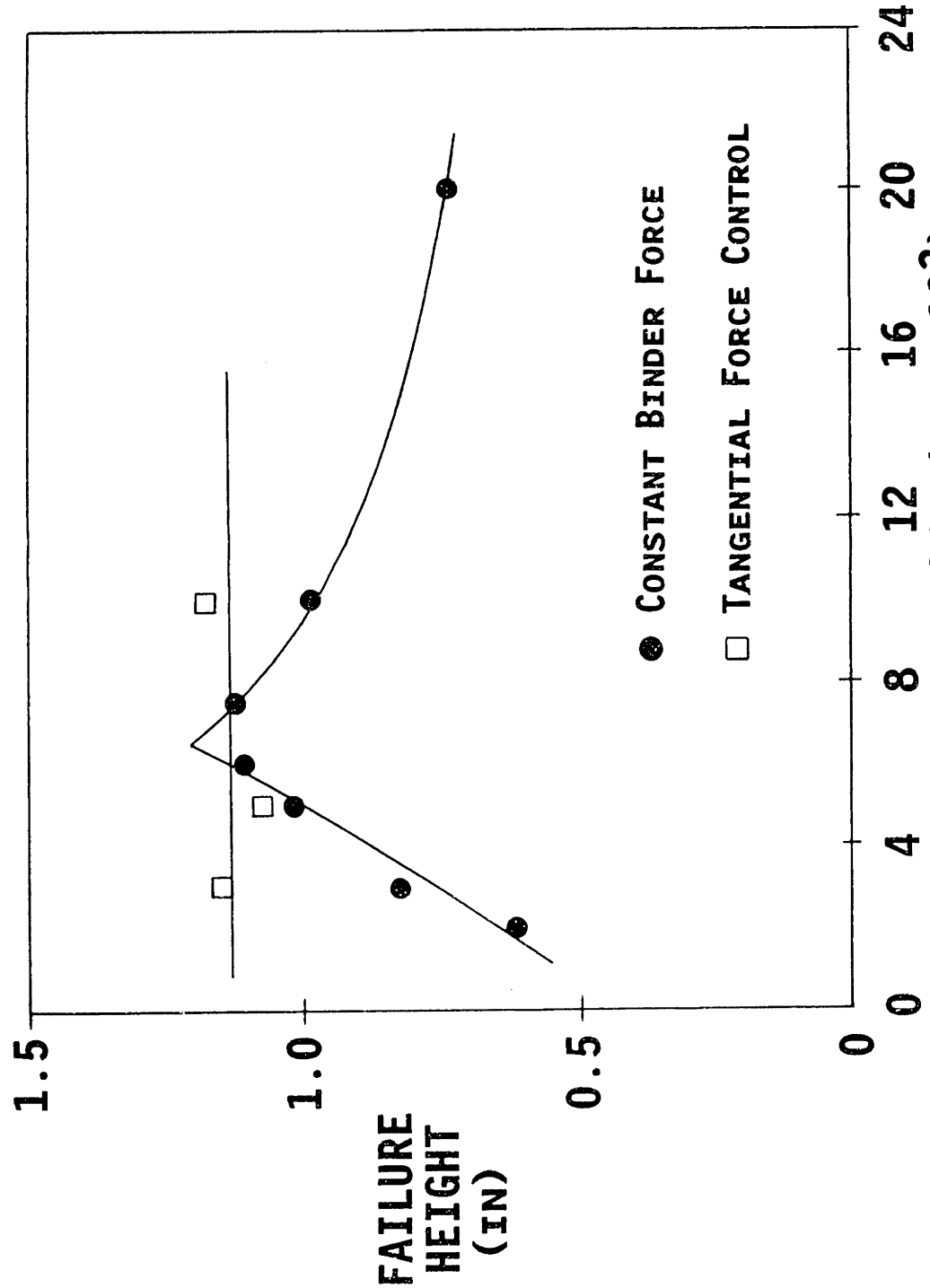

Fig. 4-12 Closed-Loop Control: 0.188 in. Eccentric Blank Position (cup geometry, 0.020 in. material "C", STP, 6.25 in. diameter)

these stresses in the flange is minimized by F_t control because F_t calculation is based on tearing forces at the punch nose.

The closed-loop failure heights for the eccentric and dry conditions are significantly below the closed-loop failure heights during standard conditions. This reduction in height is a reflection of the reduction in maximum possible height caused by non-standard conditions. In general, F_t control will only match the highest uncontrolled failure height under the same conditions.

Tangential Force Control Requiring Target Scaling

The process disturbances examined above did not require changes to the F_t target because they did not affect the permissible material forces. However the variations described in this section, thickness and material strength, affect both the maximum tearing and buckling forces. Other properties such as yield strength, maximum elongation, and r-value affect formability but exert only secondary effects relative to strength and thickness. Material strength (UTS) determines the maximum F_t that can be supported by the material. Thickness has the most important effect on buckling resistance. For these reasons target scaling factors are required for UTS and thickness changes.

Scaling for Thickness:

Because F_t is a measure of force in the material at the punch nose, the F_t target must be scaled for blank thickness changes. Equal stress at the punch nose would suggest F_t targets 25 percent higher for the 0.025 in. material. For this reason, the F_t target could be adjusted

upwards 25 percent to give the same stress levels as occurred in the thinner 0.020 in. material. Tests were done using a new 25% higher target line and, as expected, equal failure heights are achieved for the thicker material with the same properties because of control to equal stress levels (Fig. 4-13).

However, this 25% target adjustment does not give the greatest failure heights because it does not utilize the greater buckling resistance of the thicker material. The failure heights using the 125% target are well below the height for the optimum constant binder force (Fig. 4-14). Maximum failure height of the 0.025 in. material is 0.22 in. higher than for the 0.020 in. material (Fig. 4-15). The peak of the 0.025 in. curve is shifted upwards as the buckling and tearing curves move apart. Thicker material gives lower radial stress for a given binder force causing a shift of the tearing curve to the right. For a given binder force, the thicker material will draw in more and will have higher hoop stresses. However, the ability to withstand compressive stress is proportional to the thickness squared, as shown in Appendix C. Therefore, the buckling resistance effect predominates over the draw-in effect causing the buckling curve to shift to the left. The net result is a higher maximum failure height at approximately equal binder force.

The superior forming characteristics of the thicker material were realized using a F_t target scaled less than proportionately with thickness. A revised target was derived from the test data of Fig. 4-15 using the measured optimum binder force. This resulted in a F_t target for the 0.025 in. material which was 15% higher than that for the

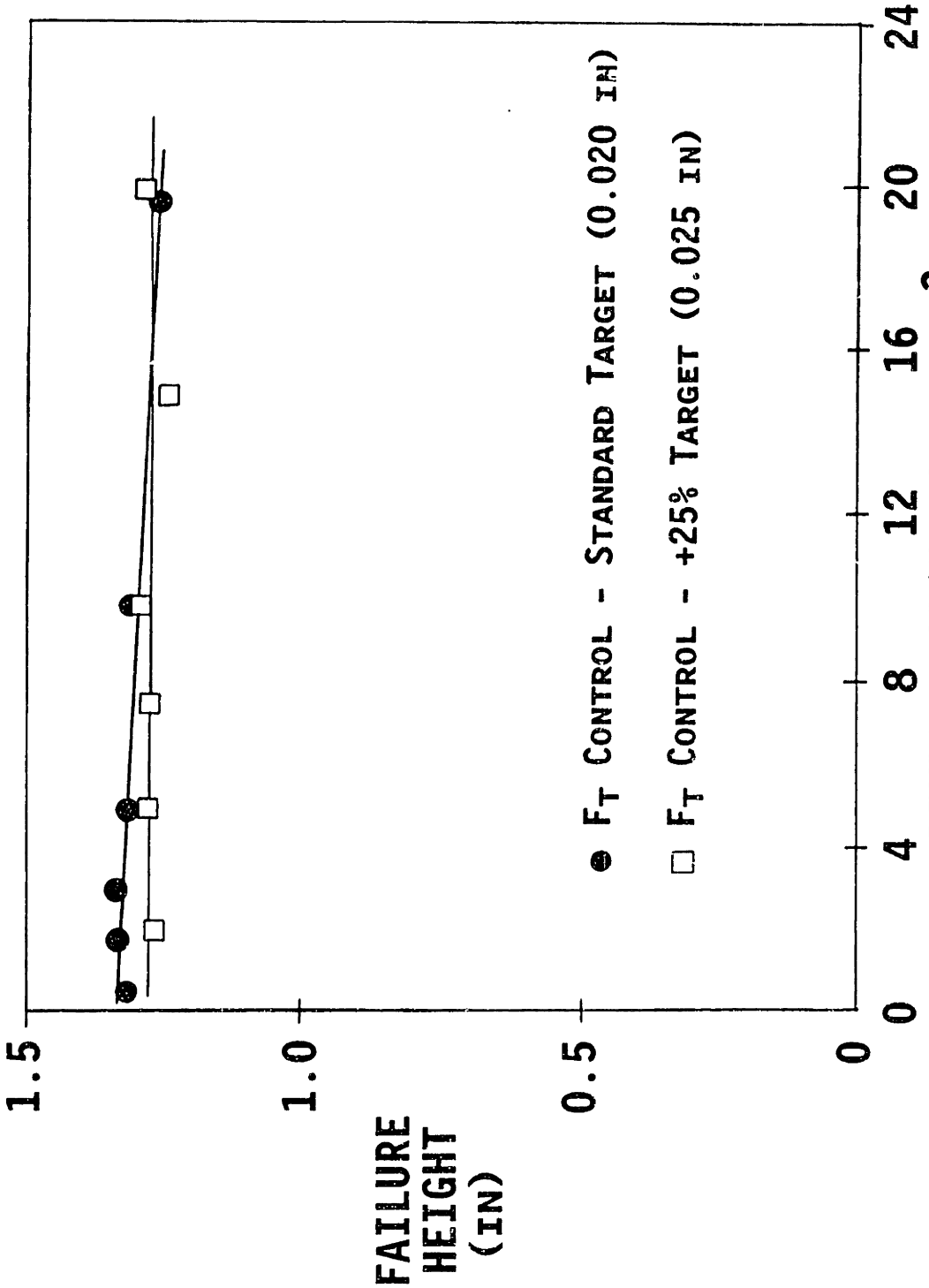

Fig. 4-13 Closed-Loop Control: Target Scaling Proportional to Thickness (cup geometry, 0.025 in. material "B" and 0.020 in. material "C", STP, 6.25 in. diameter).

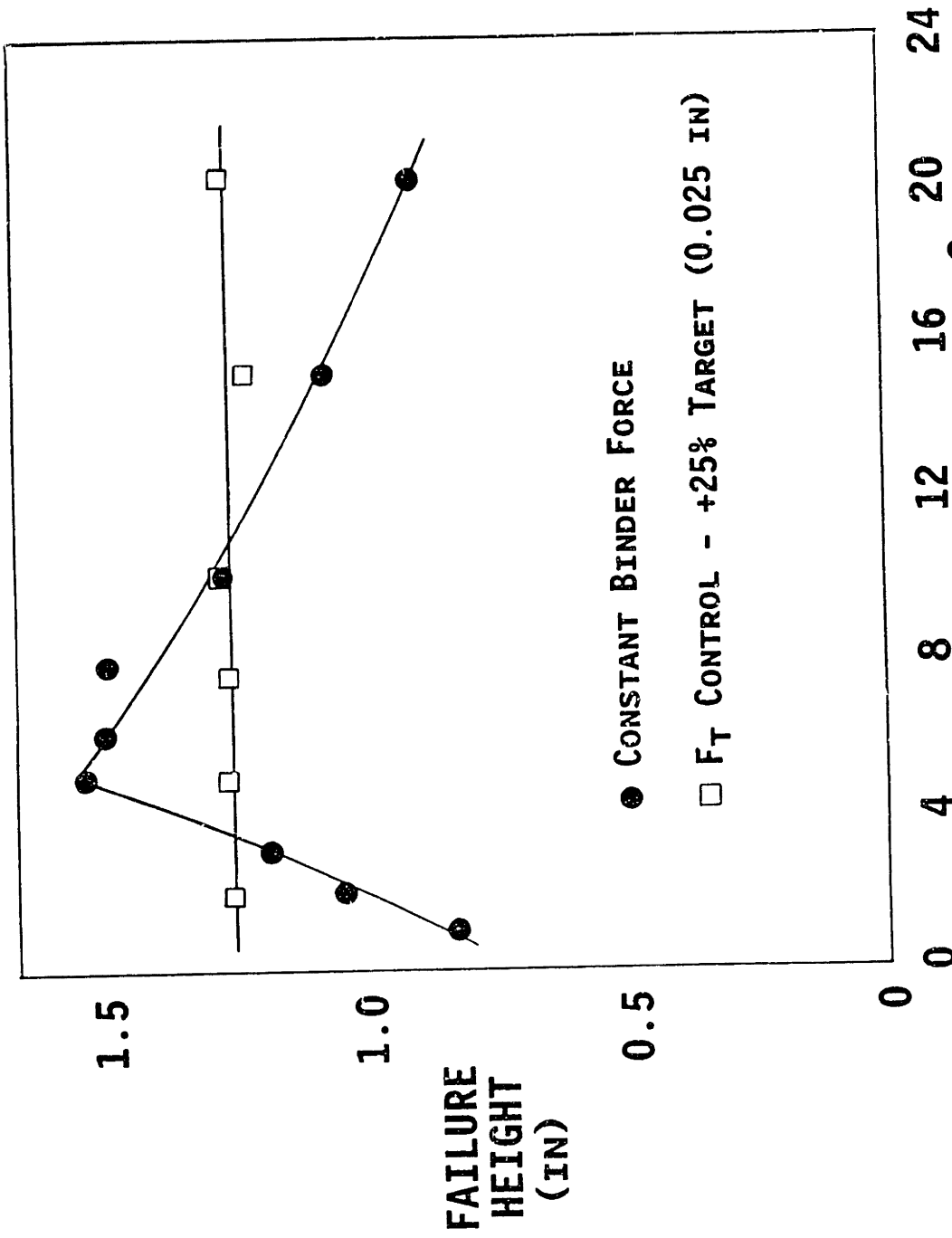

Fig. 4-14 Failure Height Using Proportional Target Scaling Compared to Maximum Height for Thicker Material (cup geometry, 0.025 in. material "B", STP, 6.25 in. diameter)

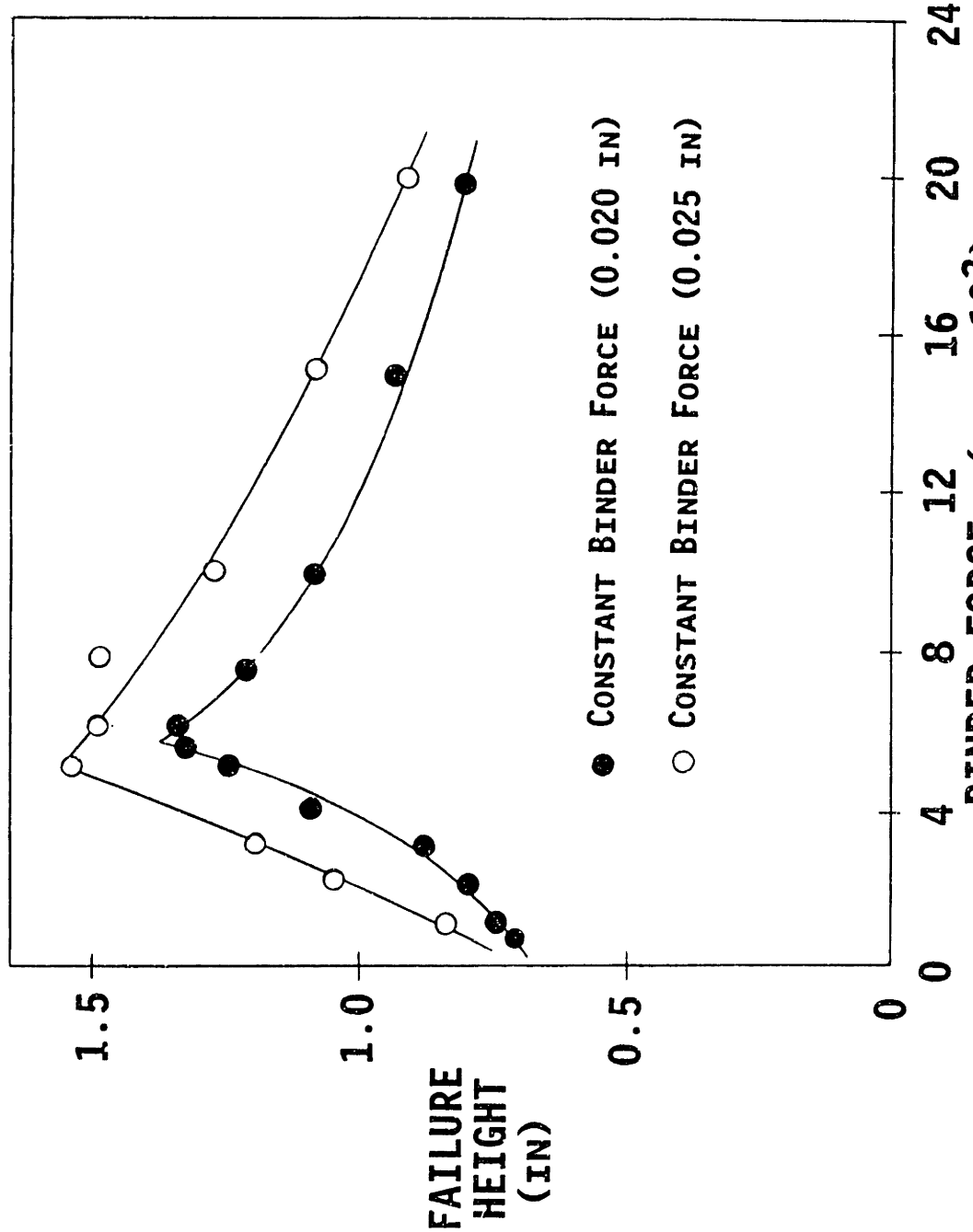

Fig. 4-15 Shift of Constant Binder Force Curve Caused by Thickness Differences (cup geometry, 0.025 in. material "B" and 0.020 in. material "C", STP, 6.25 in. diameter).

standard 0.020 in. material. This new target is shown in Fig. 4-16 with the original target and the 125% target. The improved performance while using this 115% F_t target is represented in Fig. 4-17.

In this work every effort was made to reduce the requirement for process knowledge and set-up tests. A technique was devised to avoid the need for additional tests to determine new F_t targets for blank thickness changes. This algorithm can be easily applied using thickness measurements available from simple press instrumentation.

Thickness scaling factors for the F_t and t_{avg} targets are derived in Appendix C. The degree of target precision required for practical use can be achieved by modifying experimentally determined standard targets rather than starting from first principles. For F_t target scaling there are two steps in the procedure. First, the target intercept and slope are both multiplied by the ratio of the new to standard thicknesses. This vertically scaled target would produce the same stresses as those of the standard test for the same material properties. The second step is scaling horizontally to compensate for the higher (lower) critical buckling strain of the thicker (thinner) material.

Appendix C shows that critical hoop stress and strain in a frustum shape are proportional to thickness squared. Plate buckling theory is applicable rather than shell theory because the wrinkles are aligned with the straight meridians of the frustum. The hoop strain is directly proportional to draw-in which is in turn directly proportional to frustum meridian length. The meridian length is related to punch height

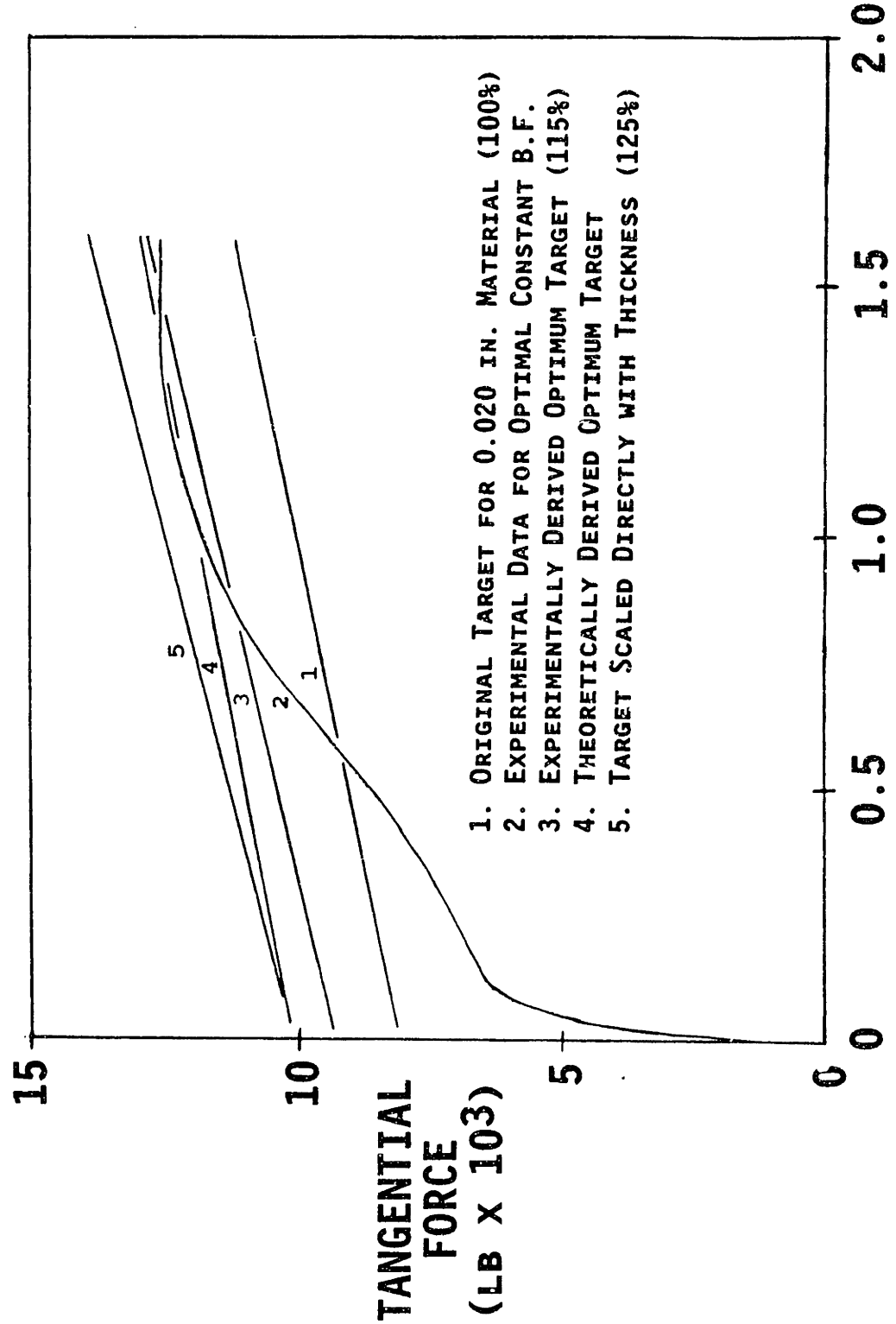

Fig. 4-16 Comparison of Theoretical Target to Experimentally Determined Optimum Target for Thicker Material (cup geometry, 0.020 in. "C", 0,025 "B", STP, 6.25 in.)

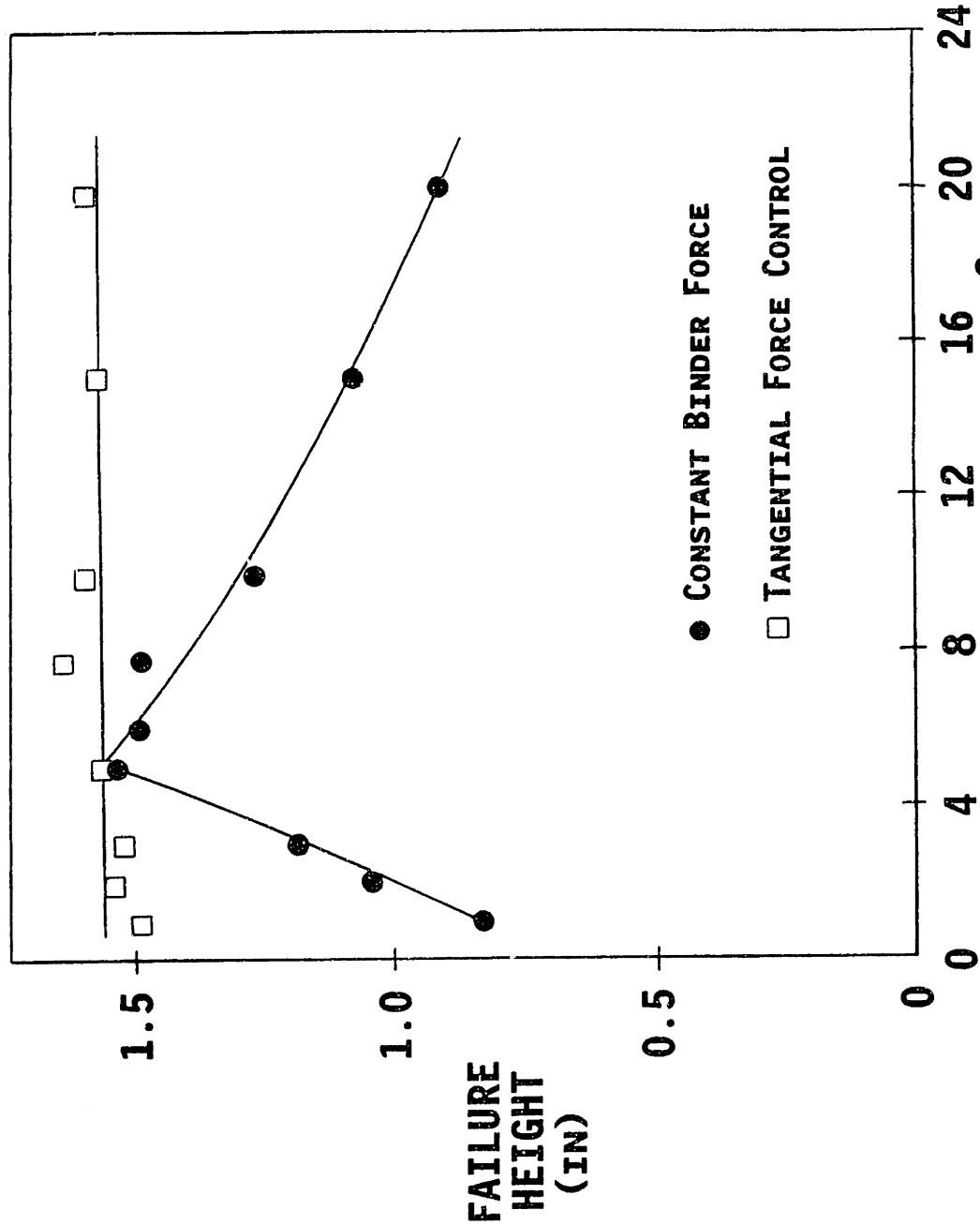

Fig. 4-17 Closed-Loop F_t Control: Optimum (115%) Target for Thicker Material (cup geometry, 0.025 in. material "B", STP, 6.25 in. diameter)

through the Pythagorean formula. These individual relationships can be combined to relate critical strain change to required punch height scaling. Appendix C shows that punch displacement change must be proportional to the 1.25 power of thickness change to give optimal failure heights.

In the case of 25% thicker material the F_t target line must be scaled horizontally by $1.25^{1.25} = 1.32$. Each value of F_t in the intermediate 125% target will be shifted to a punch height which is 32% higher. The resulting target line has a 125% intercept but a 95% slope, resulting in a 16.4% higher F_t value at failure compared to the standard F_t target line (Fig. 4-16). This scaling of punch displacement will produce critical meridional and hoop stresses simultaneously, resulting in maximum formed height.

The slope and intercept of the theoretically derived optimum target line are different from the optimum target found through experiments. However, near the failure height the two targets converge, giving only a 1.2% F_t difference at 1.570 in. (Fig. 4-16). The theoretical target produces 86% of required target correction for thickness change. Use of this theoretical target realizes 98% of the maximum possible height that is produced by the optimum constant binder force.

Scaling for Ultimate Tensile Strength:

Variations in material strength as well as thickness have a direct effect on the F_t at failure. The maximum F_t that the material at the punch nose can support is most closely related to the ultimate tensile strength (UTS). Failure to scale the target line for UTS changes will prevent the desirable simultaneous tearing and wrinkling failures which occur for the standard target under standard conditions. If the new material were stronger but otherwise equivalent in thickness and properties, use of the unchanged target would cause premature wrinkling. Figure 4-18 shows the less than optimal height produced by use of the original target with higher UTS (but identical thickness) material. All failures were by premature buckling as expected. A higher strength material will draw-in more for a given F_t target because of rapid F_t buildup, and control action reduces the binder force too much. If wrinkling occurs at a constant hoop strain and constant draw-in, F_t should be scaled vertically by the ratio of the UTSs to give critical meridional stress at the same height as critical hoop strain. For 0.020 "D" steel with UTS = 58ksi, the original target intercept and slope are multiplied by 58/51 = 1.14. Figure 4-19 shows how scaling by UTS ratio results in a target line tangential to the F_t trajectory at optimal constant binder force. This new target would give near-optimal failure height during F_t control. Tests presented below for the two square geometries show the effectiveness of scaling by UTS ratio.

The scaled target closely approximates the optimum trajectory even though property changes other than UTS were ignored. The 0.020 "D"

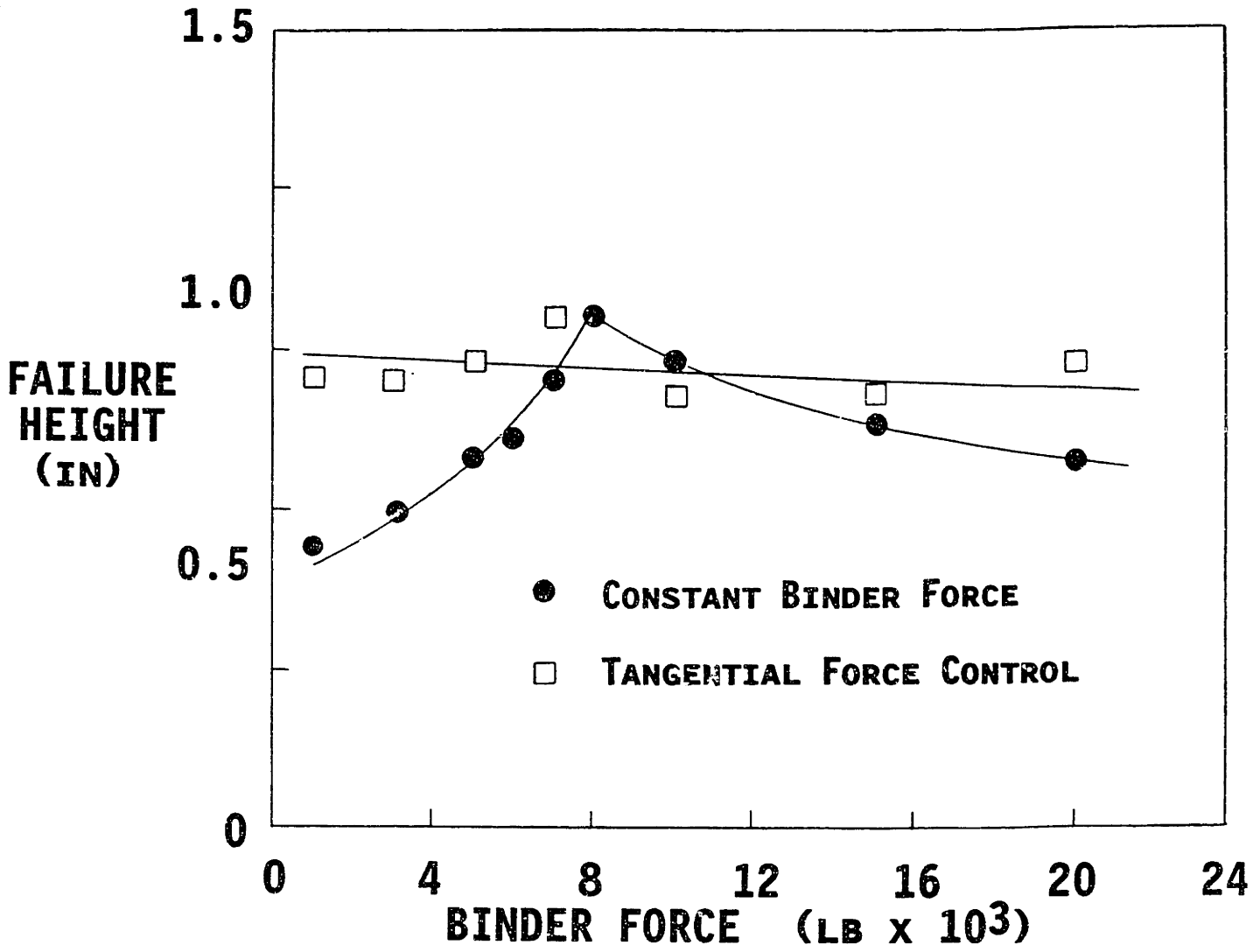

Fig. 4-18 Closed-Loop F_t Control: Use of Unaltered Target with New Ultimate Tensile Strength Material (UTS 58ksi, cup geometry, 0.020 in. material "D", STP, 6.25 in. dia.)

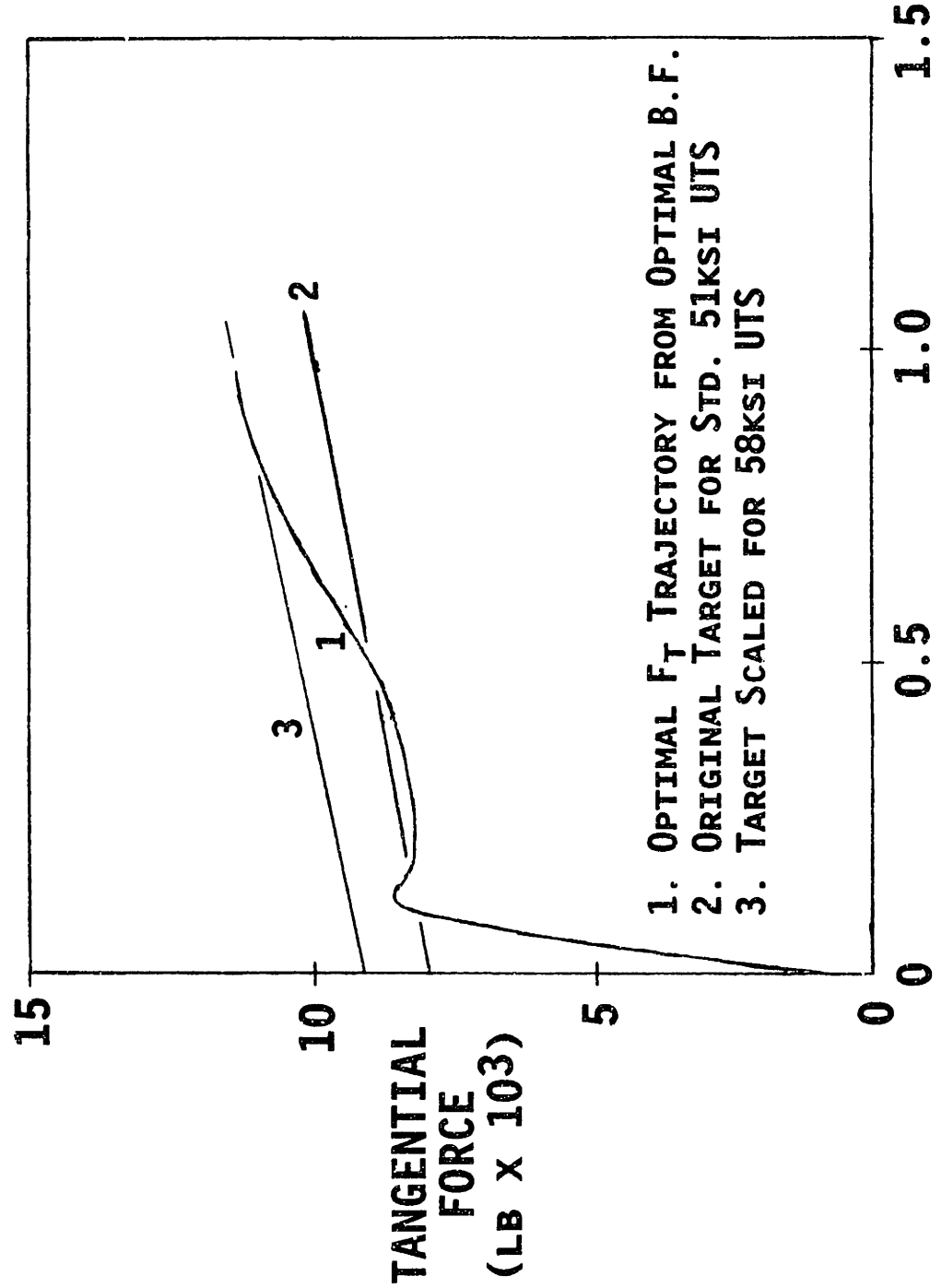

Fig. 4-19 Comparison of Theoretical Target to Experimentally Determined Optimum Target for New UTS (cup geometry, 0.020 in. material "D" (UTS 58ksi), STP, 6.25 in. dia.)

steel is not an aluminum killed steel and has a low r-value = 0.96. Yield point elongation in the form of "stretcher strains" was present during 0.020 "D" forming, unlike all other materials. Although many material properties such as yield strength, maximum elongation, and r-value affect drawing, UTS has the major influence on target scaling for F_t control. This is because of the strong correlation between maximum F_t and tensile strength. Control system compensation for very rapid UTS changes might be possible using on-line estimates of UTS. However, changes in UTS often vary more slowly than other forming parameters because of relatively uniform properties within particular coils and "heats". Off-line measurements can be used to adjust the F_t target if UTS changes occur slowly.

Tests were done on an "A" steel that had both thickness and property changes relative to the standard. A target was developed using vertical scaling by UTS ratio and thickness ratio. No horizontal scaling to utilize the increased buckling resistance was done. The new material had a UTS of 47ksi vs. 51ksi and a thickness of 0.025 in. vs. 0.020 in. The resulting target line has an intercept of 8,000 * (47/51) * (25/20) = 9,220 lb. and a slope of 2,000 * (47/51) * (25/20) = 2,300 lb./in. Figure 4-20 shows a controlled height which is approximately 0.3 in. below the optimum. This loss in potential formed height is the same as seen in tests without horizontal scaling on 0.025 in. "B" material in Fig. 4-14.

A horizontally scaled target can be calculated by dividing the slope by the factor $(25/20)^{1.25}=1.32$ as discussed above and in Appendix C.

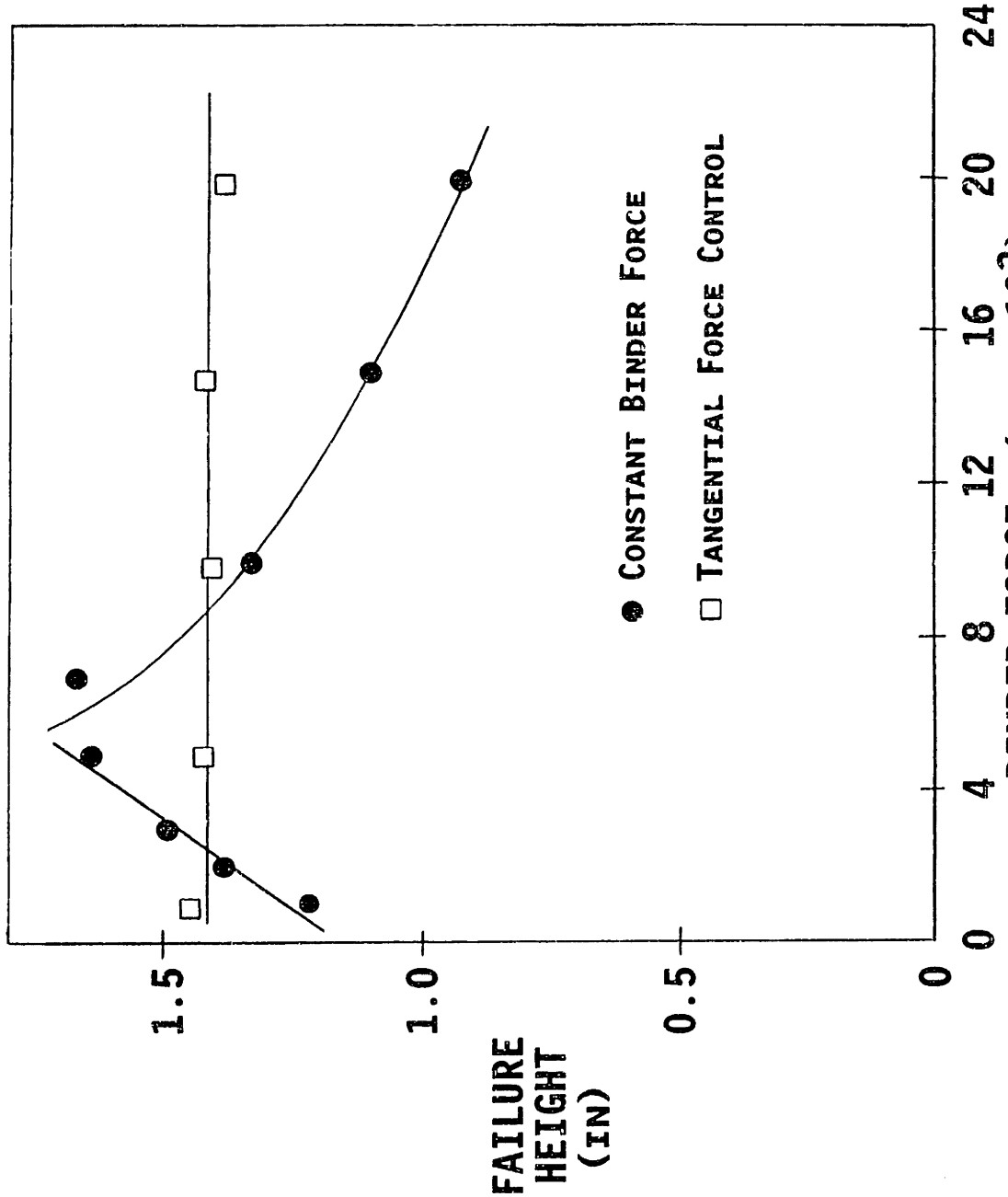

Fig. 4-20 Failure Height Using Proportional Target Scaling for UTS and Thickness Compared to Maximum Height (cup geometry, 0.025 in. material "A" (UTS 47ksi), STP, 6.25 in. dia.)

Figure 4-21 shows targets with and without horizontal scaling for this material. The target without horizontal scaling is higher than the optimum F_t trajectory. The horizontally scaled target which accounts for increased buckling resistance is nearly tangential at the critical area at the end of the forming stoke. This target should give significantly improved formed heights over the vertically scaled, equal meridional stress target. Tests described below using the unequal corner radii geometry and horizontal scaling show near-optimal failure heights.

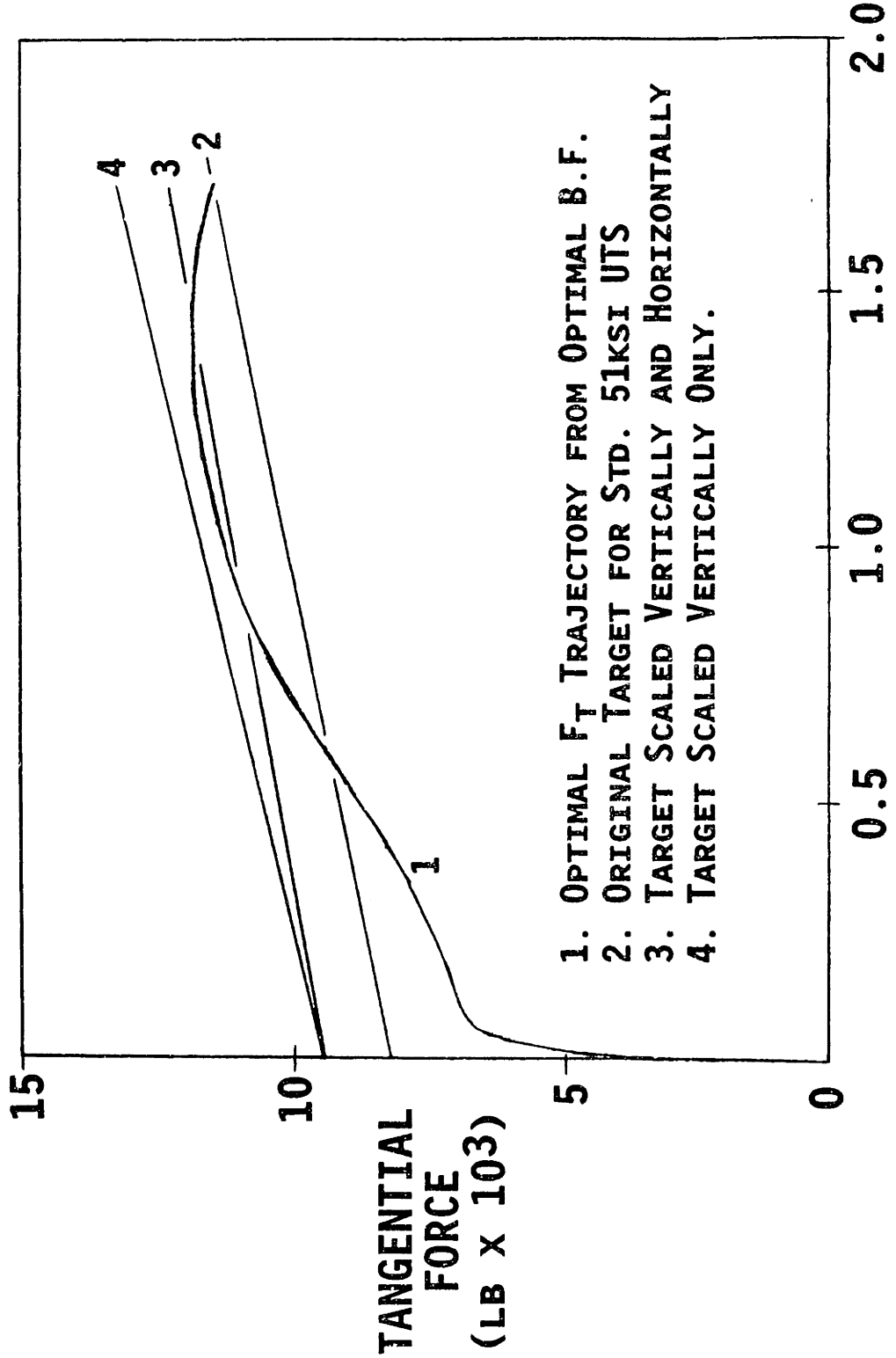

Fig. 4-21 Comparison of Theoretical Target to Experimentally Determined Optimum Target for New UTS and Thickness (cup geometry, 0.025 in. "A" (UTS 47ksi), STP, 6.25 in.)

Tangential Force Control for Square Geometry

In the section above, tangential force (F_t) control proved to be an effective method of reducing the effects of various process disturbances during cup forming. The radial symmetry of that geometry supported the assumption that F_t, an average tangential force value, was proportional to the tangential stress at each point on the punch nose. However, the applicability of this technique to non-axisymmetric geometries more typical of production can not be guaranteed by the cup results.

Tests of F_t control of two square parts were done to determine the efficacy of this control method. The first square geometry, with equal corner radii, is discussed below. The second square geometry, with unequal corner radii and thus less symmetry, is discussed in a following section.

The first square geometry shares many features of the original cup geometry. The square punch and die have corner radii equal to the cup punch and die. The square punch and die also share the same profile radii. The square geometry simply consists of quadrants of the punch and die separated by 2.0 in. wall segments.

As explained above, the theoretical derivation of all control targets is not attempted in this thesis. A new "standard" target is found experimentally for each different geometry and control method. A series of tests was done with this new geometry to determine the optimum constant binder force and the corresponding optimum F_t trajectory. This F_t "signature" trajectory that was produced by the optimum binder force

is then used as the standard F_t target. Type "A" 0.025 in. material was used for these new standard conditions rather than the previous 0.020 in. type "C" stock, which became unavailable. Dry conditions were used rather than the STP mixture lubrication used in the standard cup tests. Use of STP lubrication shifts the optimum binder force almost to the press capacity limit of binder force. Dry conditions were used because the benefits of F_t control for high initial binder forces could not be determined using STP lubrication.

The F_t trajectories for the optimum constant binder force and two other binder forces are shown in Fig. 4-22. The 16,000 lb. binder force caused premature buckling, and the 40,000 lb. binder force resulted in premature tearing. Buckling of this equal corner radii geometry, as well as the unequal radii geometry, always occurred in the side wall rather than the corner. Tearing occurred on the punch nose at one of the corners. A 28,000 lb. binder force resulted in the highest formed height. As above, a target line was fitted to the F_t trajectory produced by this optimum binder force. The target line with intercept = 15,000 lb. and slope = 6,000 lb./in. matches the optimum F_t trajectory. Determining the target was more difficult here because of noise in the F_t signal which is visible in Fig. 4-22. This signal noise and audible "popping" was caused by a stick-slip condition on the unlubricated punch nose.

Tests of F_t control were done for these standard conditions. The controller 'found' the optimum binder force and the full failure height was achieved for any initial binder force conditions (Fig. 4-23). The

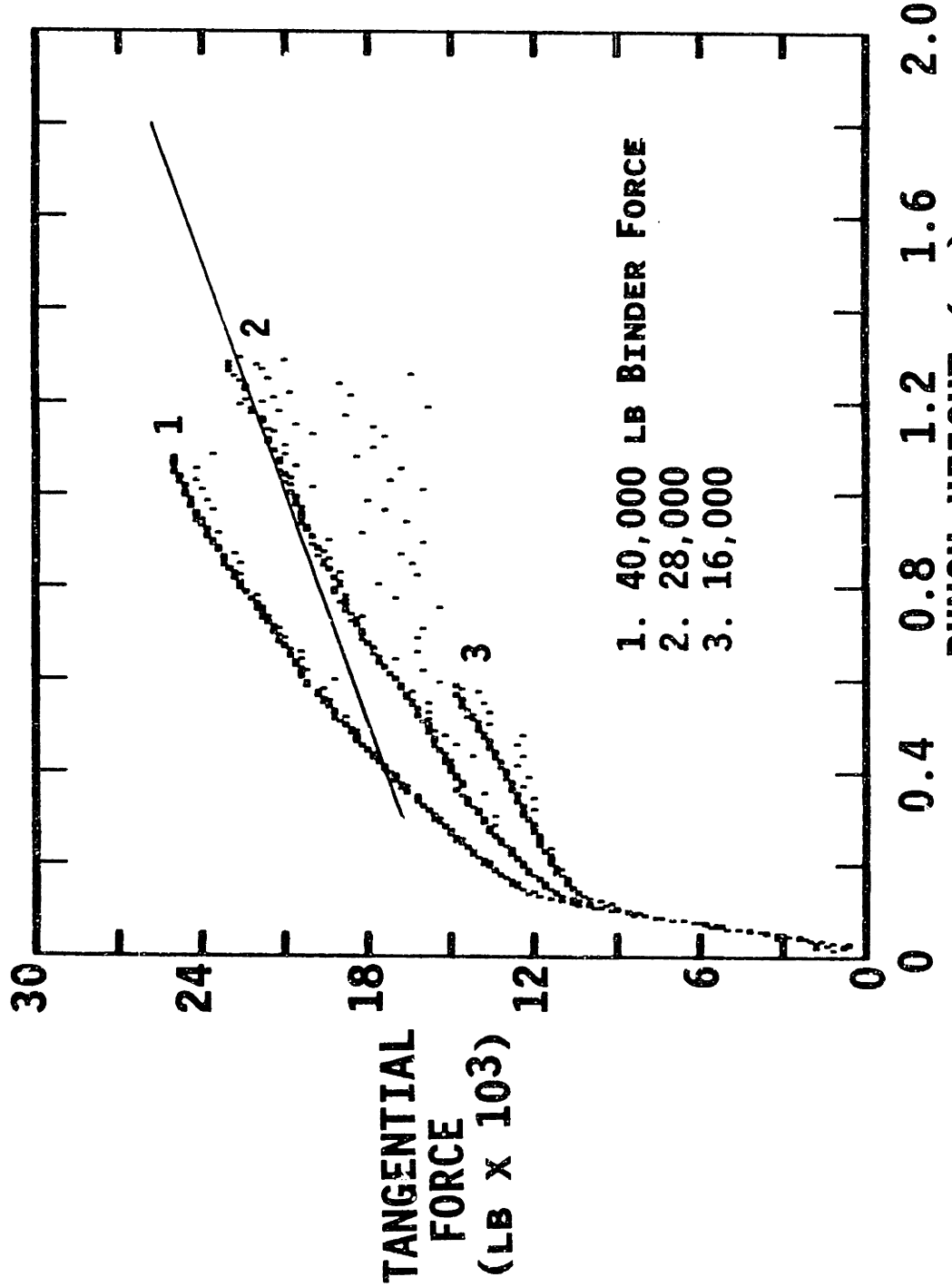

Fig. 4-22 Optimum F_t Trajectory and Target Selection for Equal Corner Radii Square Geometry (0.025 in. material "A", dry, 9.078 in. diameter)

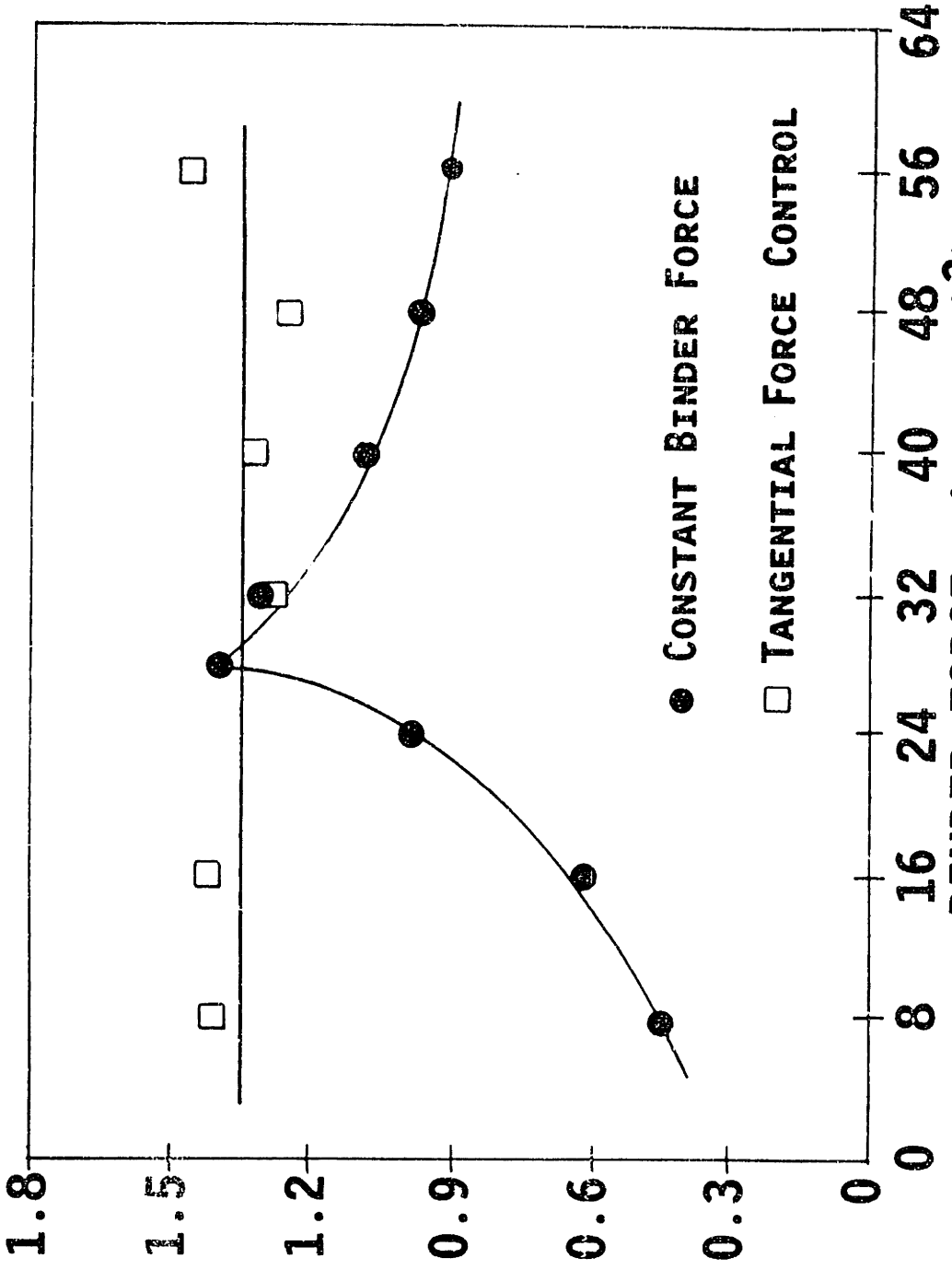

Fig. 4-23 Closed-Loop F_t Control: Equal Radii Square Geometry Using Standard Conditions (0.025 in. material "A", dry, 9.078 in. diameter).

control action amplified the noise of the F_t measurements as it controlled the average F_t value to the target (Fig. 4-24). Even though large oscillations in binder force and F_t were made during the forming cycle, the stick-slip conditions had little effect on the failure height. The robustness of the control algorithm is emphasized by the controller performance under these adverse conditions.

For effective F_t control under various conditions, the F_t target must not vary as process conditions change. Lubrication changes are an important source of flange restraint variations. The performance of F_t control can be predicted for new lubrication conditions by comparing the standard target developed above to the new optimum F_t trajectory. Tests using constant binder force were done, after changing to STP lubrication, and the F_t trajectory for the optimum binder force was found. The F_t values for both the standard dry conditions and the new STP lubrication were equal at the critical final values of the curves (Fig. 4-25). These results suggested that, as was the case for the conical cup, the F_t control target would not require changes to produce satisfactory performance. F_t control tests were done using the standard target for various initial binder forces. As predicted, the failure heights produced were equal to or better than the optimum constant binder force height (Fig. 4-26). The stability of the target line is an important feature of F_t control. Changes in lubrication or other variations affecting the friction coefficient can not often be predicted or measured. To be successful, a control algorithm must not require detailed information about friction conditions.

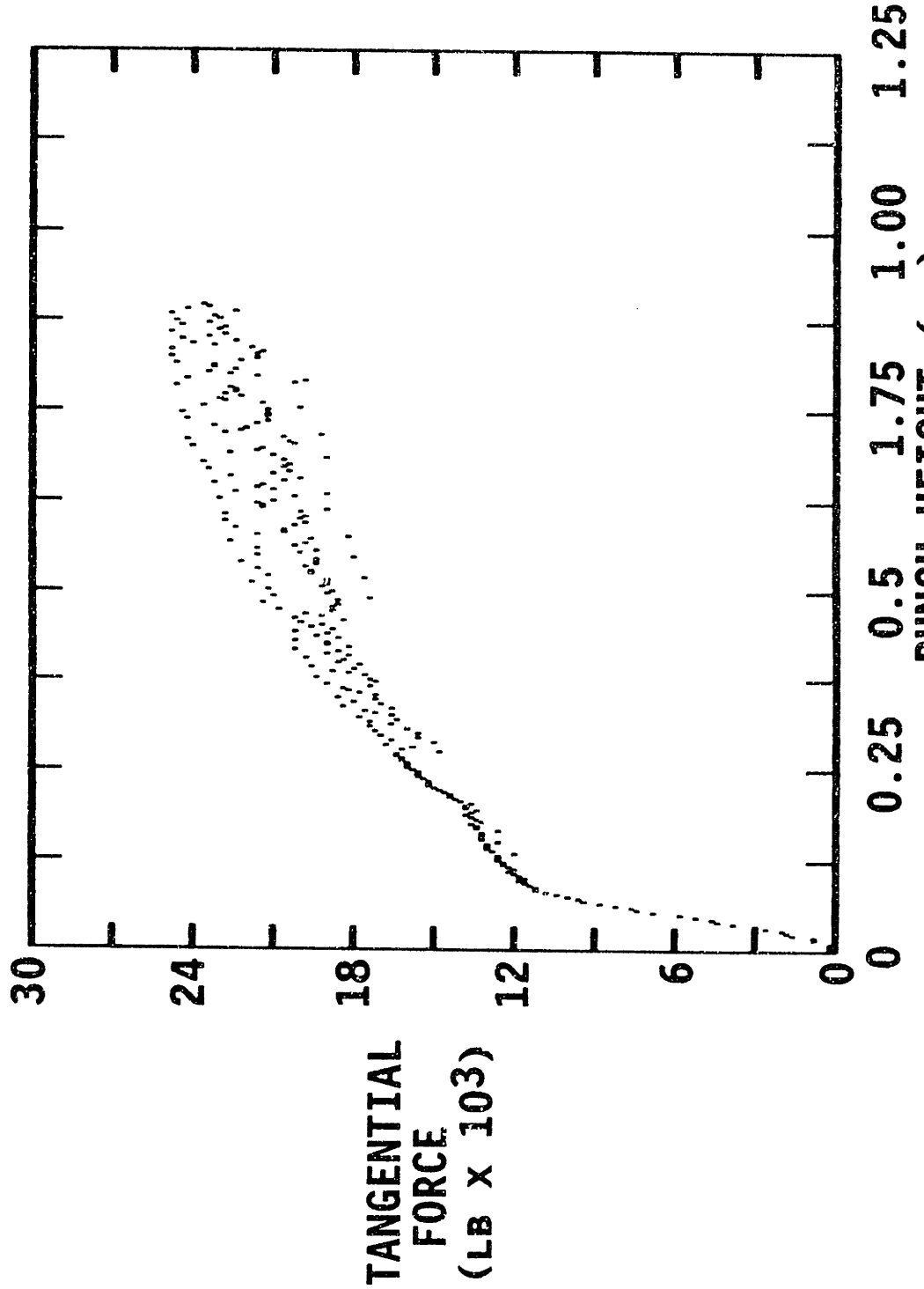

Fig. 4-24 Typical F_t Noise during Dry Forming (equal radii geometry, initial binder force = 24,000 lb, 0.025 in. material "A", 9.078 in. diameter).

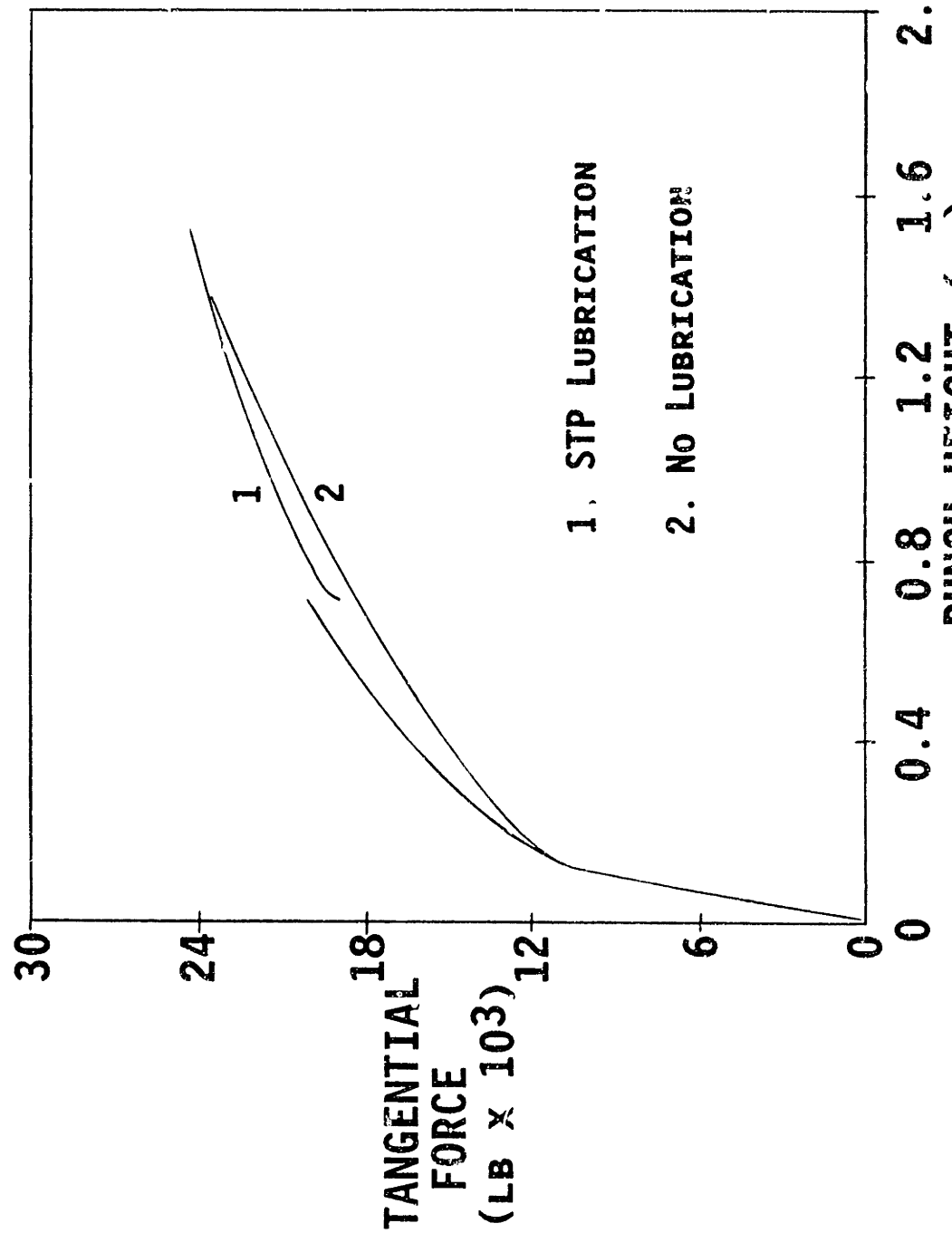

Fig. 4-25 Tangential Force Trajectories for Two Lubrication Conditions Using the Respective Optimum Binder Forces (ury:28k lb, STP:52k, equal, 0.025 in. "A", 9.078 in.)

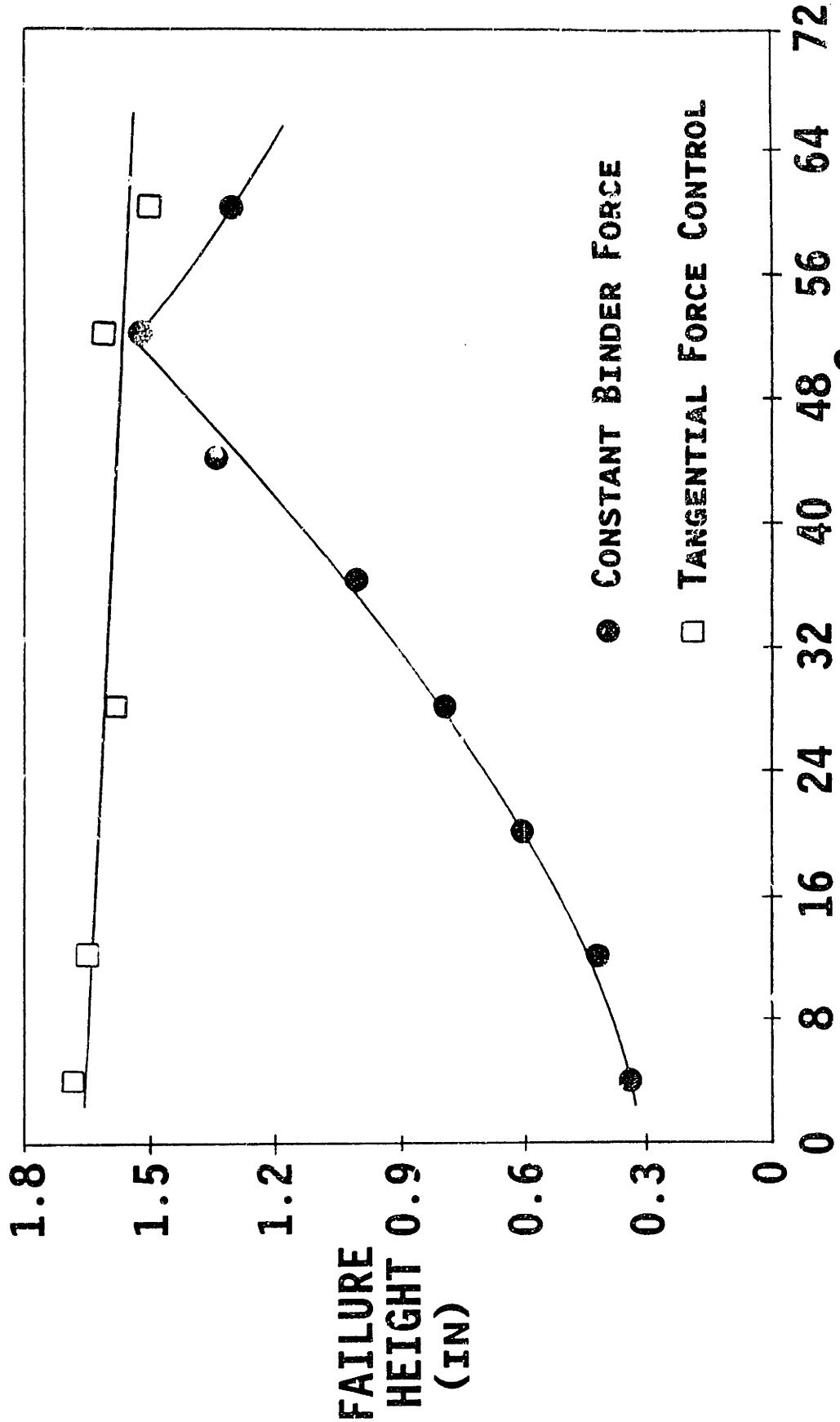

Fig. 4-26 Closed-Loop F_t Control: Change of Lubrication Condition to STP (equal radii, 0.025 in. material "A", 9.078 in. diameter)

Forming of a material with a different ultimate tensile strength (UTS) was done on this square die set. As explained in Appendix C, changes in thickness and UTS affect the maximum allowable force at the punch nose and require F_t target scaling. An "E" steel of the same 0.025 in. thickness was selected but this material was stronger. The standard target for this geometry was scaled by the ratio of the UTS values. The intercept became 15,000 x (64/47) = 20,400 lb. and the slope became 6,000 x (64/47) = 8,200 lb./in. This new target line is a close approximation to the optimum F_t trajectory shown in Fig. 4-27. Use of this new target for F_t control produces consistently high failure heights as expected (Fig. 4-28). This experiment shows that changes in material properties do not require a new set of tests to characterize the new target. Only simple information about the new UTS is required to continue use of F_t control.

The method of target determination used in this thesis relies on experiments to find the standard target for each new geometry. When geometries are similar, the target lines also bear similarities. The equal radii square die set described in this section has many features in common with the original cup geometry. The profile radii are the same, and the corner radii, where splitting occurs, are the same as the original circular punch radius. Conditions at the corner for both geometries are similar except that side wall effects occur in the square part. The F_t values at failure can be compared for the two geometries after scaling by their respective perimeters. Tests using STP lubrication and 0.025 in. thick "A" material were done for both geometries. During both tests the binder force was selected to give

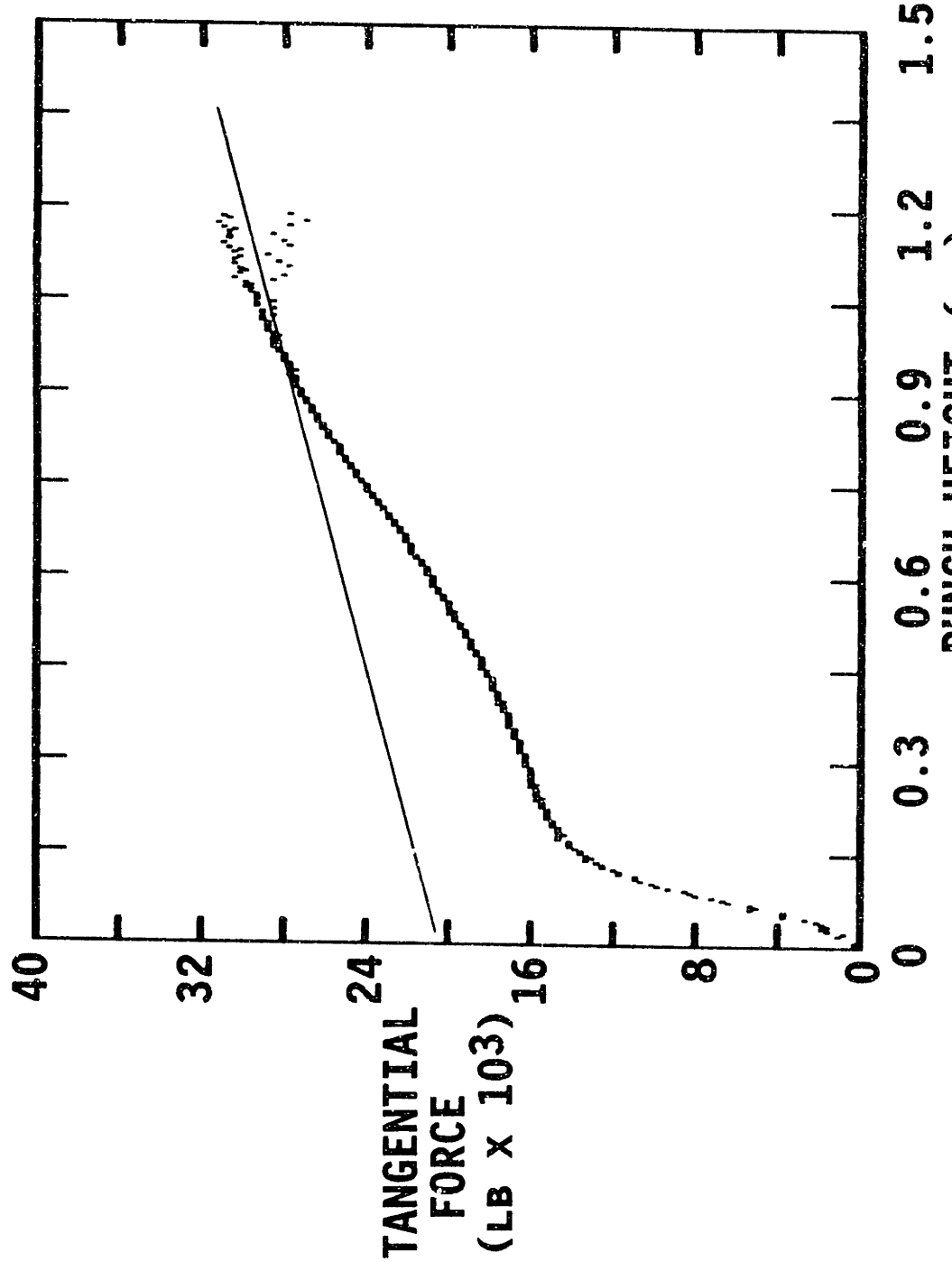

Fig. 4-27 Comparison of Theoretical Target to Experimentally Determined Optimum Target for New UTS (BF-24k, equal radii, 0.025 in. "E" (UTS 64ksi), dry, 9.078 in. dia.)

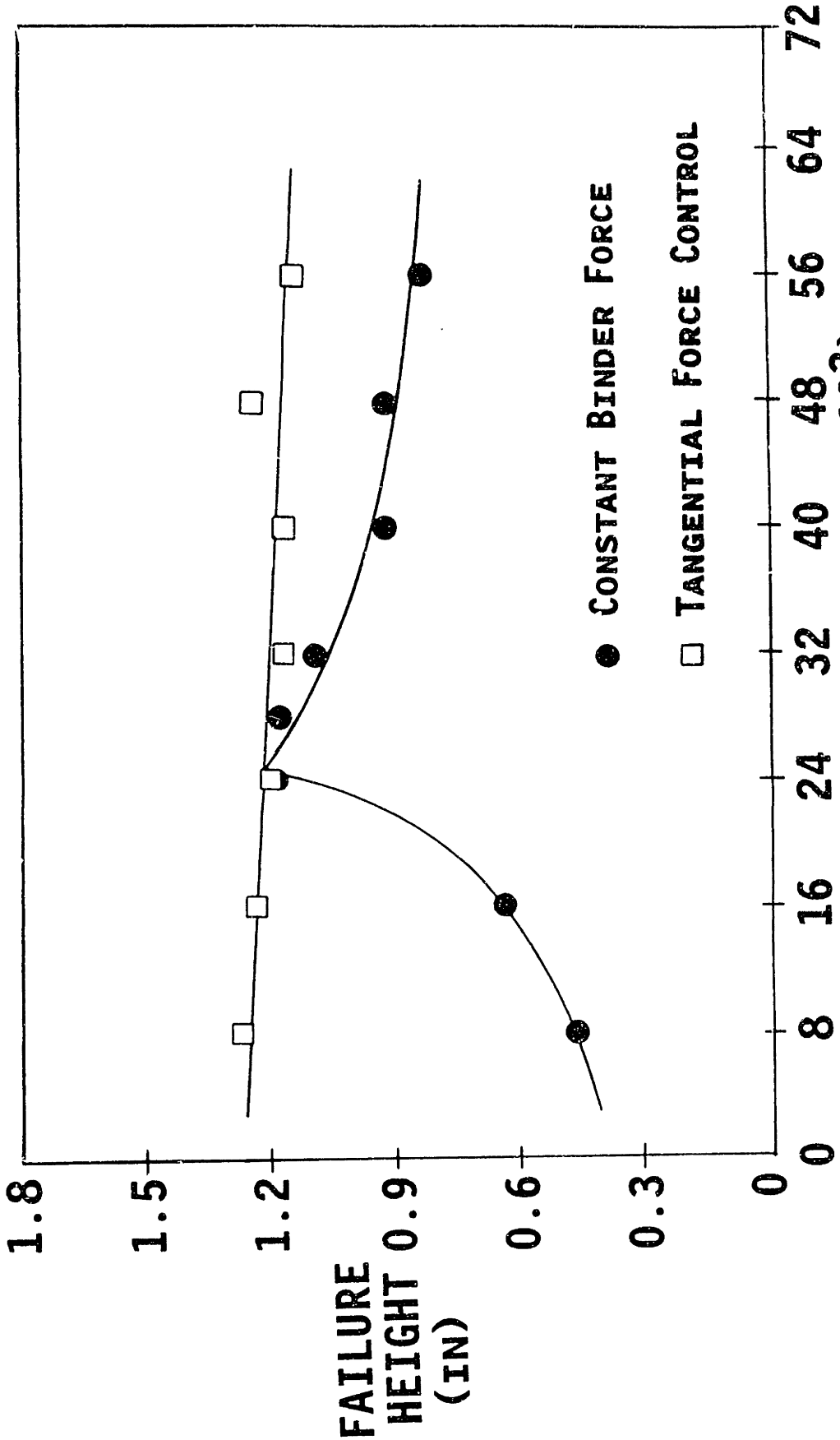

Fig. 4-28 Failure Height Using Proportional Target Scaling for New UTS Compared to Maximum Height (equal radii, 0.025 in. material "E" (UTS 64 ksi), dry, 9.078 in. diameter)

tearing and near optimal height. The cup geometry produced a maximum F_t = 12,000 lb. and F_t per unit of punch perimeter = 1600 lb. The square geometry produced a maximum F_t = 24,300 lb./in. and F_t per unit of punch perimeter = 1570 lb./in. The difference between the two values is only 2%, which approximates the required accuracy of F_t target selection. In this special case where the conical and square die sets shared many features, a nearly optimal F_t target could have been calculated using perimeter scaling rather than relying on tests. For generalized geometries such a simple relationship would probably not yield such close agreement and experiments would be required to find the optimum F_t target. Even though the method has drawbacks, the use of F_t scaling is superior to binder force or pressure scaling, which are sometimes used. F_t scaling would not depend on flange conditions, such as friction coefficient and hoop stress, that would require unknown changes to binder force. In the case of these two geometries, F_t scales proportionally with punch perimeter while the required binder forces and pressures are far from proportional to perimeter. The binder force per unit perimeter for the cup is 940 lb./in. while the value for the equal radii pan is more than three times higher, at 3,360 lb./in. Similar differences in optimal binder pressure for the two geometries would exist because the flange widths of the cups and pans are approximately equal

Tangential Force Control for Unequal Corner Radii

In the above section tangential force (F_t) control tests were extended from the original cup tests to a square geometry with equal corner radii. In this section F_t control is applied to a second square

geometry which has unequal corner radii. This die set has four different corner radii ranging from 0.5 to 1.5 in. This configuration has less symmetry than the previous two and is a closer approximation to typical automotive parts, which have complex three dimensional shapes.

The same 0.025 in. "A" material was used in these tests as for the equal radii geometry above. However DC200 silicone lubricant was used here rather than the previous dry conditions. The new lubricant was used for several reasons. The silicone oil eliminated the stick-slip induced noise which made standard target selection more difficult because of the difficulty in locating the "true" F_t trajectory. Use of a lubricant was required to prevent further surface damage to the binder and die surfaces during flange draw-in. The benefit of silicone oil over other lubricants such as STP and mineral oil is its unusually high friction coefficient, which is even higher than dry conditions. The high friction forces produced by silicone oil shifted the optimum binder force to lower values and allowed tests using initial binder forces much higher than the optimum.

The F_t trajectories for five widely spaced binder forces are shown in Fig. 4-29. A target line was selected that is parallel to the end of the optimum, 19,000 lb. binder force curve as was done for the axisymmetric geometry. The target line is shifted up by 5% of the final F_t value to ensure failure by tearing during control. At 0.3 in. punch displacement the target line is 3,000 lb. above the optimum F_t curve. This large difference from the optimum is not important because early F_t values have much less effect on failure height than later values.

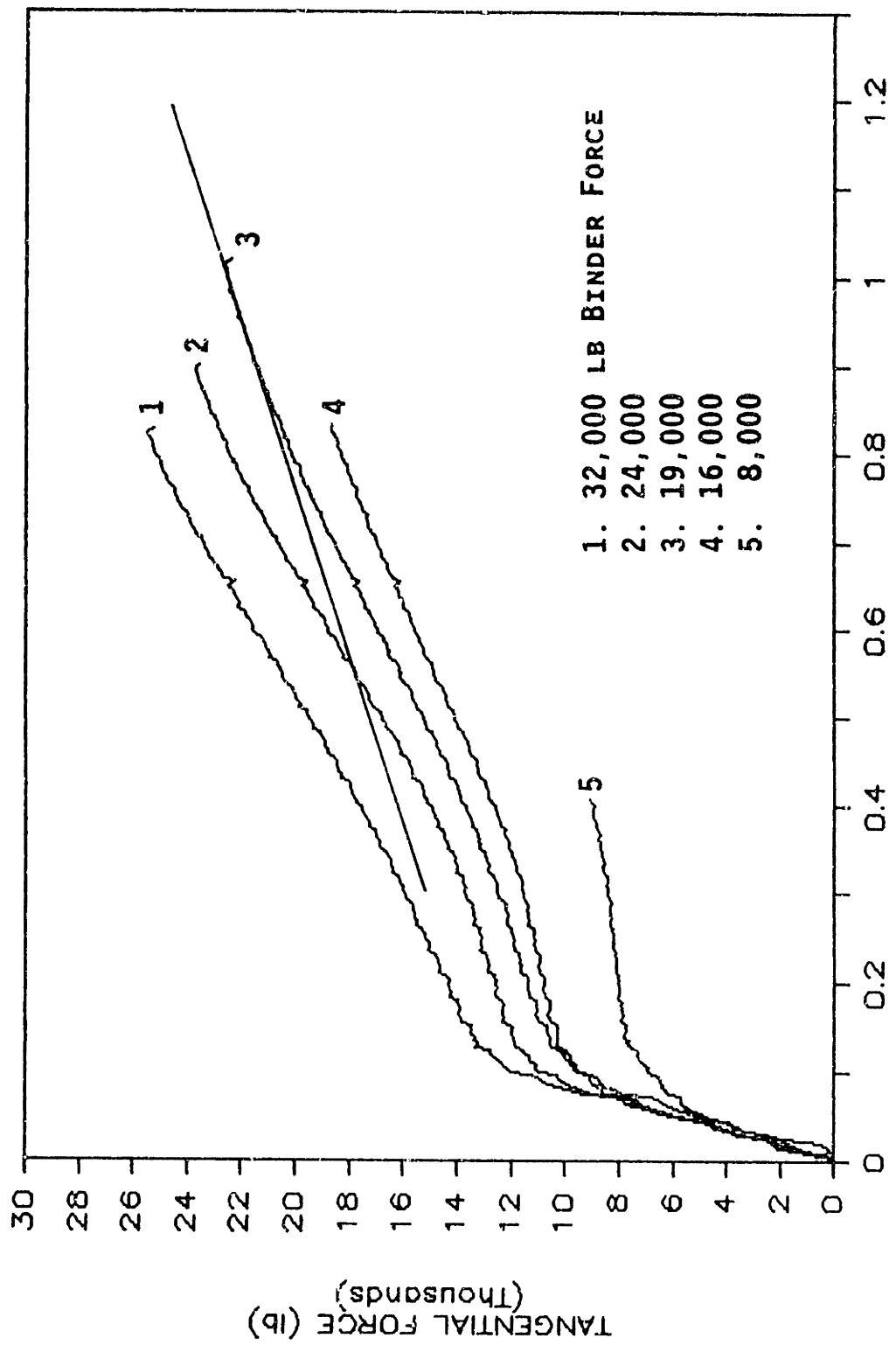

Fig. 4-29 Optimum F_t Trajectory and Target Selection for Unequal Corner Radii Square Geometry (0.025 in. material "A", silicone, 9.078 in. diameter).

The target determined by the experiments above was used in F_t tests. Near-optimal failure heights occurred for a wide range of initial binder forces (Fig. 4-30). One characteristic of the uncontrolled failure height is the relatively constant height achieved for any high binder force. At the highest binder forces no draw-in occurred and therefore variations in binder force had no effect, causing the flat slope of the curve. Buckling failure for this geometry usually occurred in one particular location; the side wall between the smallest and largest corner radii. As expected, tearing always occurred on the punch nose at the sharpest (0.5 in. radius) corner, since this was the region of highest radial stress.

The effect of lubrication change on the F_t target selected above is investigated in Fig. 4-31. Tangential force trajectories for three lubrication conditions is presented while using the respective optimum constant binder forces. This figure shows that these optimum trajectories are nearly congruent, particularly near the critical final stages of forming. This result implies that use of the above target in control tests of various lubricants would produce consistently high failure heights. Tests using STP lubrication were done using the original target that was derived from tests using silicone lubrication. Figure 4-32 shows that formed heights were nearly optimal for a wide range of initial binder forces. This result indicates that target changes are not required for good control performance even if lubrication changes.

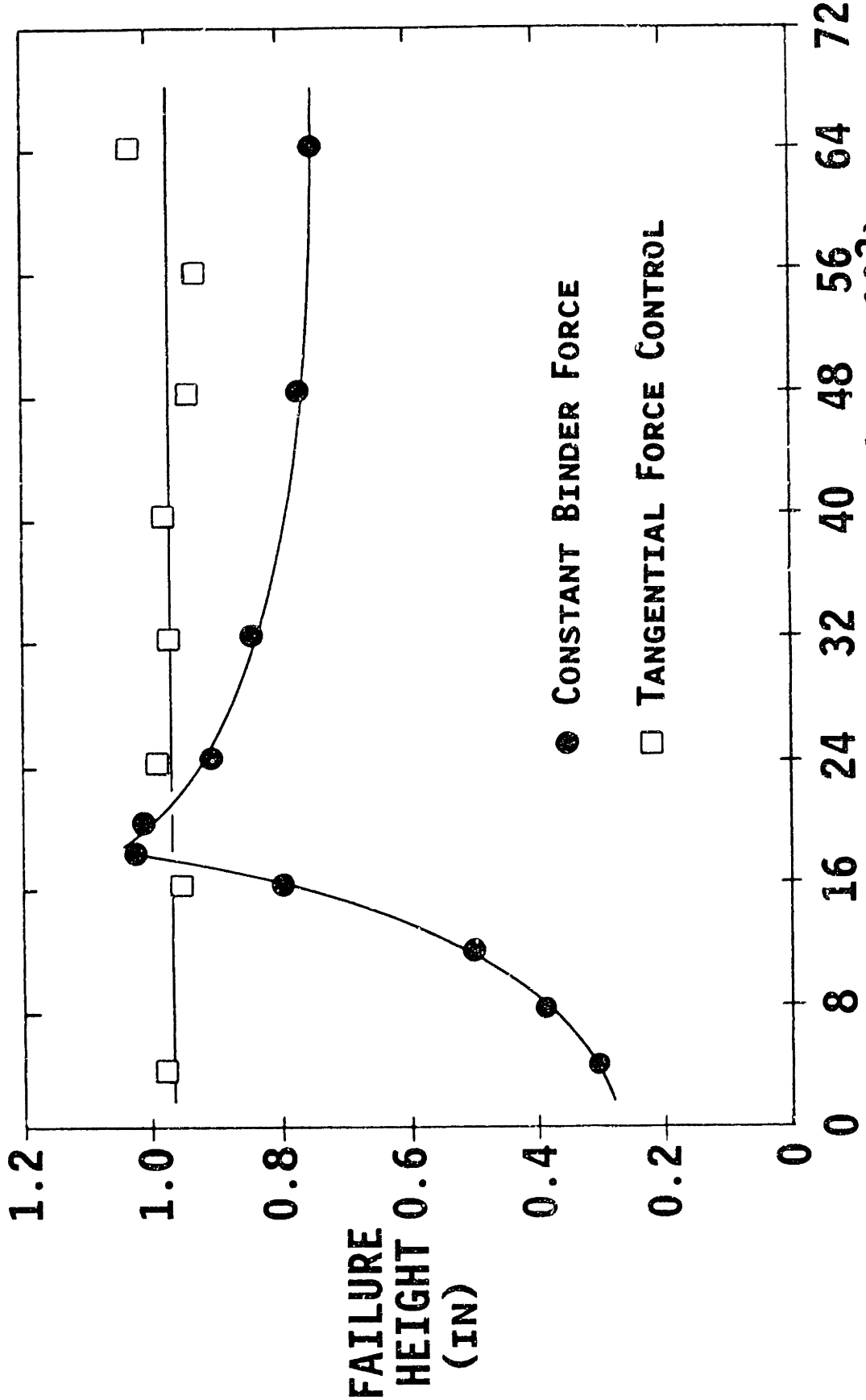

Fig. 4-30 Closed-Loop F_t Control: Unequal Radii Square Geometry Using Standard Conditions (0.025 in. material "A", silicone, 9.078 in. diameter).

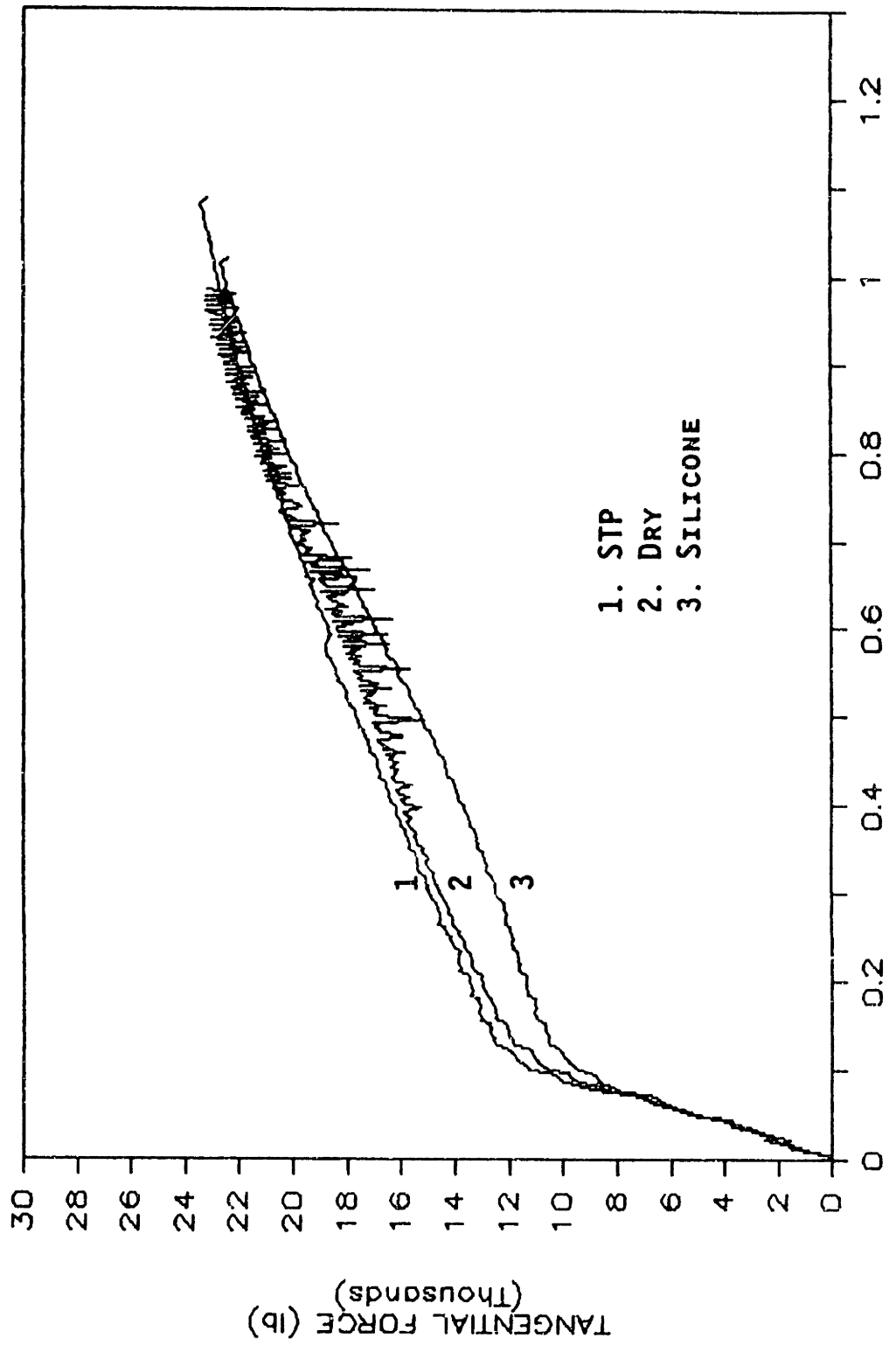

Fig. 4-31 Tangential Force for Three Lubrication Conditions Using the Respective Optimum Binder Forces (silicone:19k lb, dry:26k, STP:54k, unequal, 0.025 in. "A", 9.078 in.)

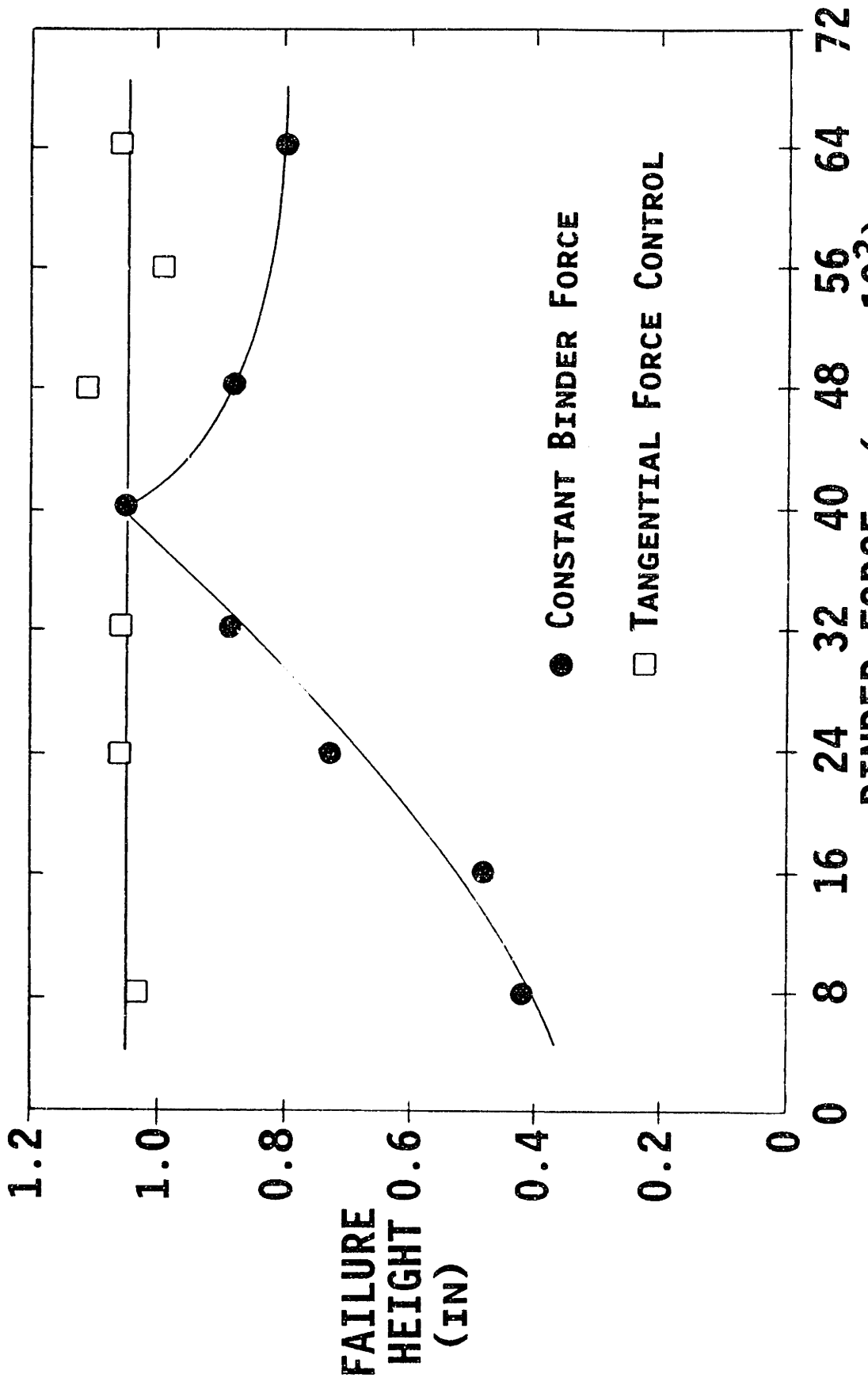

Fig. 4-32 Closed-Loop F_t Control: Change of Lubricant to STP (unequal radii, 0.025 in. material "A", 9.078 in. diameter)

The effect of blank diameter on F_t control performance was also tested. Blanks of 9.328 in. diameter, which is 0.250 in. larger than the standard, were formed using the standard unequal corner target developed above. The effect of diameter change was almost eliminated by the control action as illustrated in Fig. 4-33.

The next two tests investigated the effect of eccentric blank placement. The blanks were moved 0.188 in. toward the 0.5 in. radius punch corner. The standard, silicone lubricant was used in the first test and STP lubricant was used in the second test. The second test varies blank position and lubrication simultaneously, in order to determine control performance during perturbations of interacting variables. Figures 4-34 and 4-35 show how F_t control nearly eliminates the effects of eccentric blank placement, even during simultaneous lubrication changes.

The above perturbations of lubrication, blank diameter, and blank position did not require alteration of the standard F_t target of the unequal corner radii geometry. However, changes of the material thickness and UTS require corresponding target changes as discussed above and in Appendix C. The 0.030 in. "F" material was selected for this last test of the F_t control method. The first step in calculating the new F_t target for this material is scaling the standard target by the ratio of the new and standard UTS values. The result is an intercept of 12,000x(65/47) = 16,560 lb and a slope of 11.5x(65/47) = 15.87 lb/in. After scaling the target for the new UTS, it must be scaled for the new thickness. The intermediate target from above is

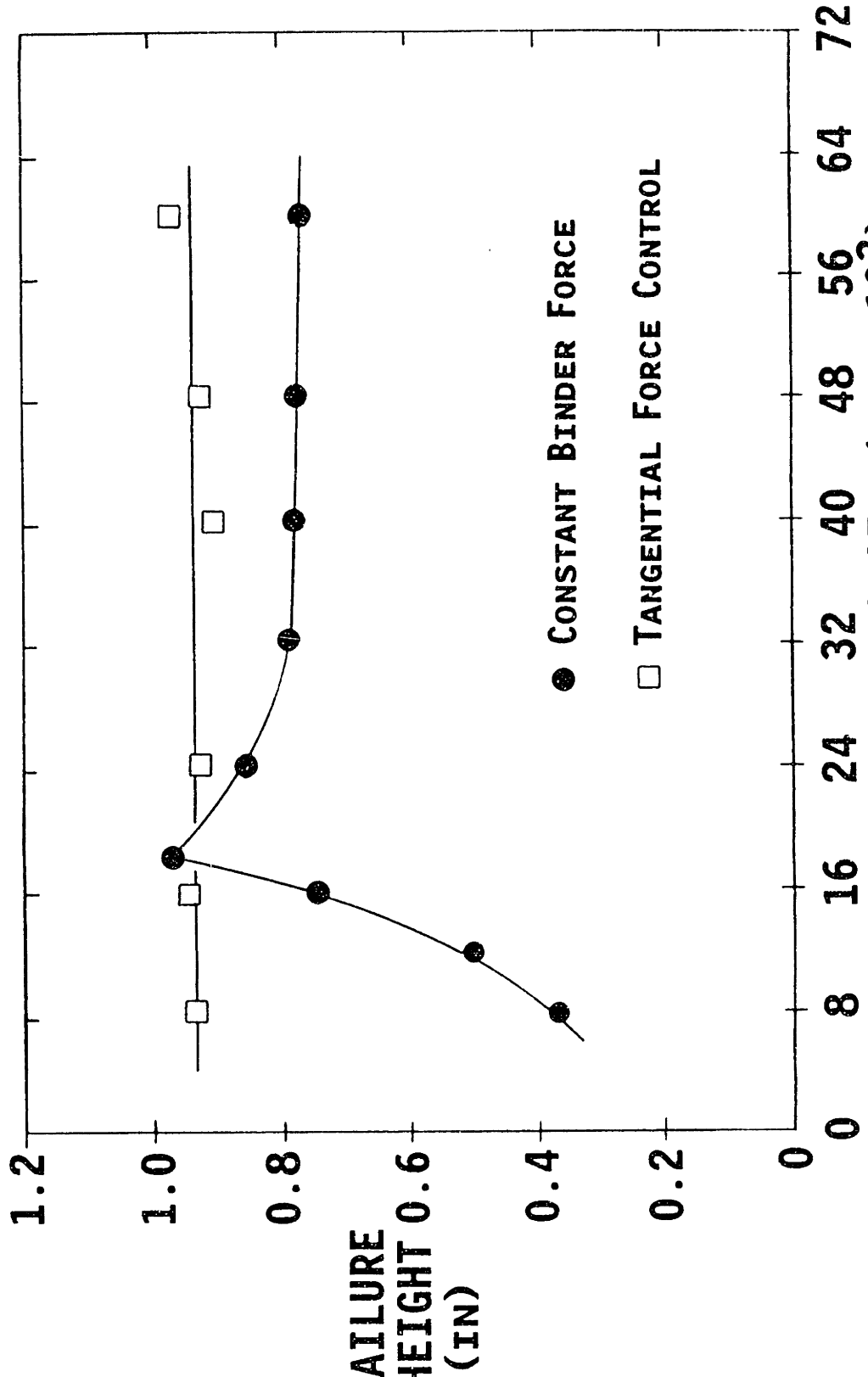

Fig. 4-33 Closed-Loop F_t Control: Change of Blank Diameter to 9.328 in. (unequal radii, 0.025 in. material "A", silicone)

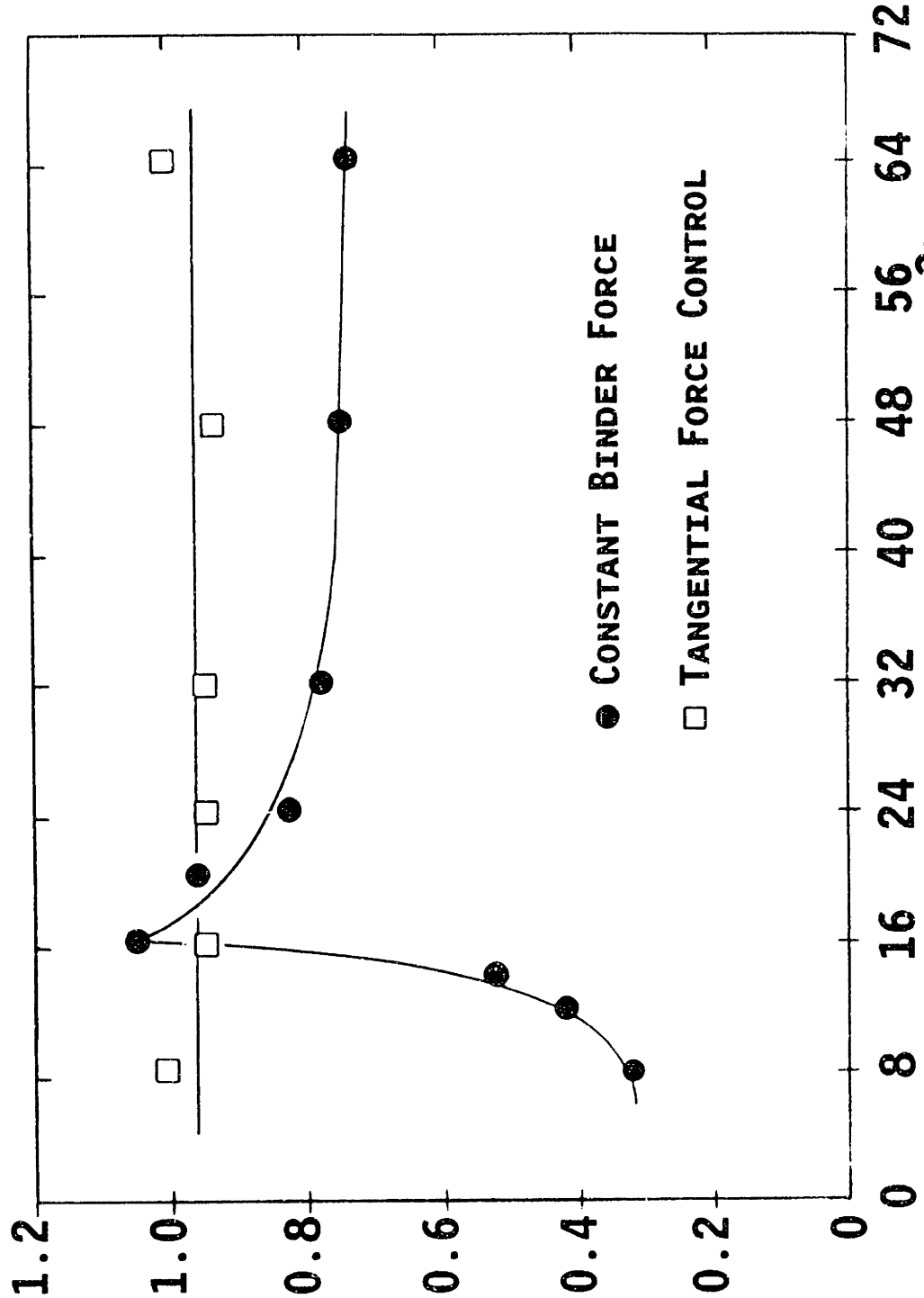

Fig. 4-34 Closed-Loop F_t Control: 0.188 in. Eccentric Blank Position (unequal radii, 0.025 in. material "A", silicone, 9.078 in. diameter)

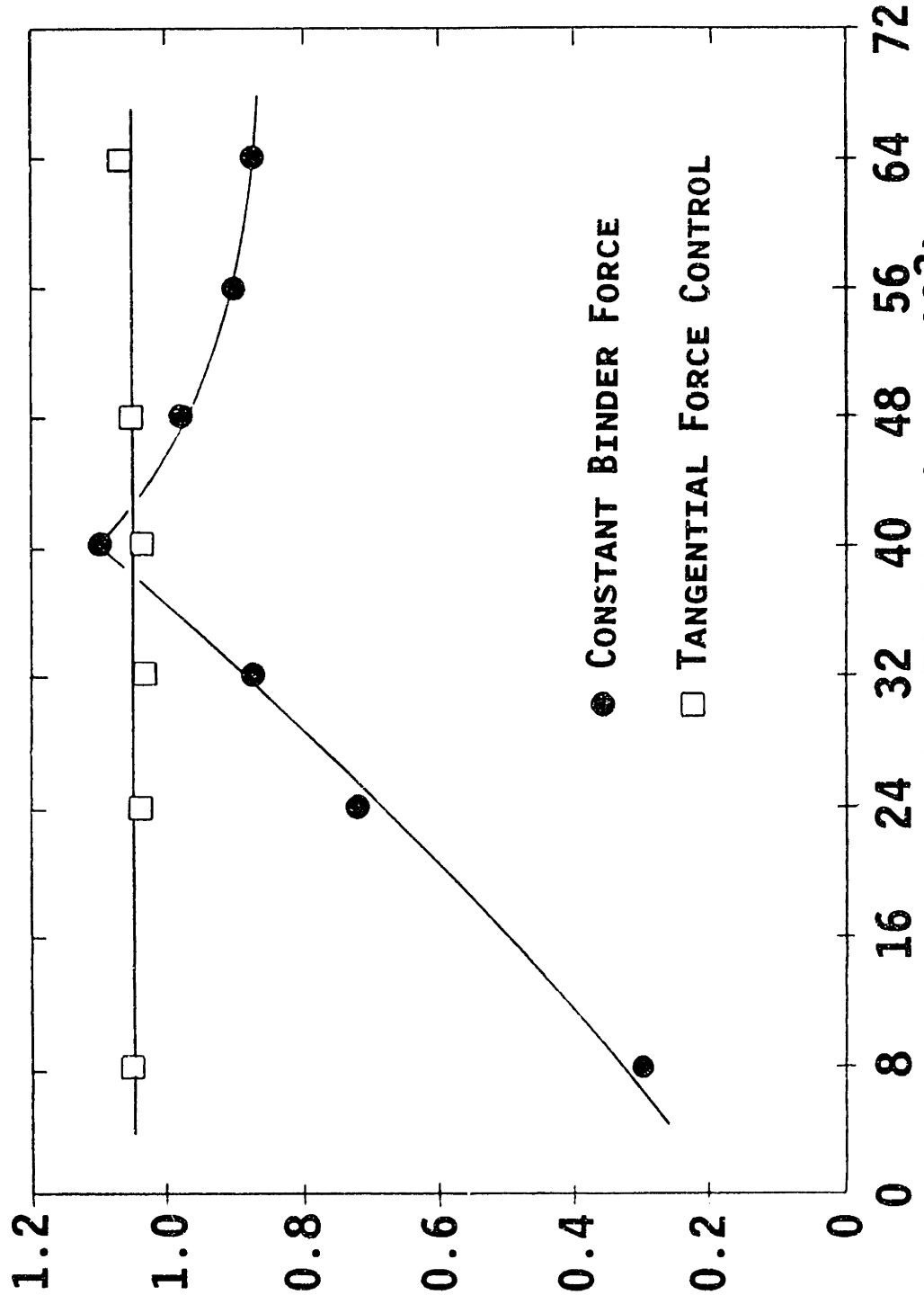

Fig. 4-35 Closed-Loop F_t Control: 0.188 in. Eccentric Blank Position with Lubrication Change to STP (unequal radii, 0.025 in. material "A", 9.078 in. diameter)

multiplied by 30/25 and then multiplied again by $(30/25)^{1.25}$. This final calculation produces a target line having an intercept of 19,900 lb and a slope of 15.2 lb/in. Tests were done using this calculated target and the results are presented in Fig. 4-36. The failure heights using the calculated target are essentially equal to the greatest height achieved using the optimum constant binder force. These results support the methods of UTS and thickness scaling developed in this thesis, which are important to the broad applicability of the F_t control method.

In the section above, the F_t per unit of punch perimeter was compared for the conical and equal radii square geometries. The values of this force were almost equal for these two geometries that share many features. The same calculation can be done for the unequal radii square geometry. A test using the optimum binder force with STP lubrication and 0.025 in. "A" material produced a F_t value at fracture of 23,400 lb. The corresponding force per unit perimeter is 1480 lb./in. This value is 8% lower than the conical value and 6% lower than the equal radii case. This variation is too large to allow off-line calculation of the new F_t target by perimeter scaling. However, the F_t force per inch values are strikingly similar considering the differences between the three geometries.

Tangential Force Control Summary

A method was developed above to estimate and control the average meridional stress at the punch nose of a forming part. For a particular blank thickness, the tangential force (F_t) is proportional to the meridional stress which has certain stability limits. Optimal F_t

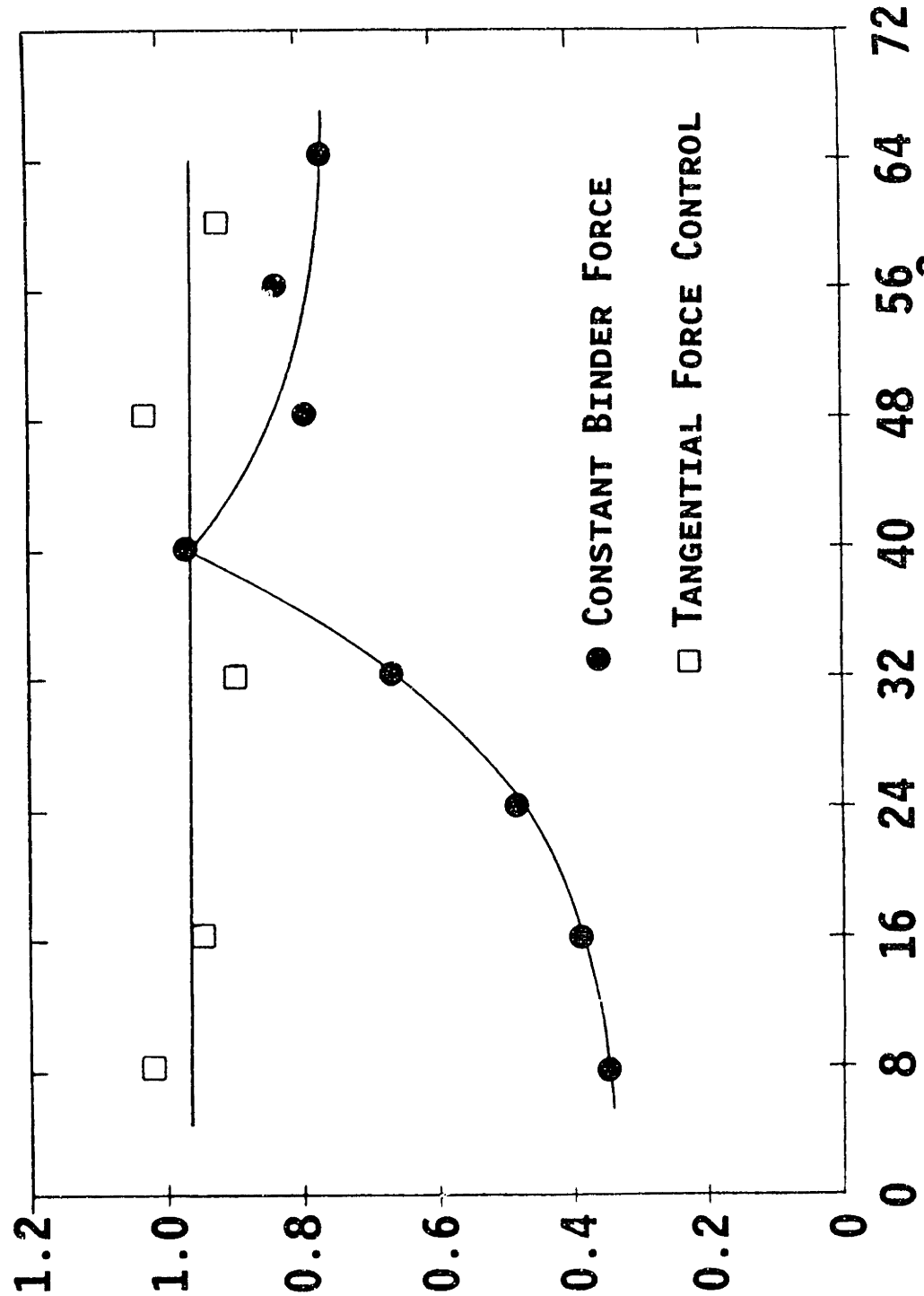

Fig. 4-36 Failure Height Using Vertical and Horizontal Target Scaling for UTS and Thickness Compared to Maximum Height (unequal, 0.030 in. "F" (UTS 65ksi), silicone, 9.078 in)

trajectories were determined experimentally for three die set geometries. Control of F_t to these standard trajectories eliminated premature failure during standard conditions and various initial binder forces. Failure heights were also near-optimal for lubrication, blank diameter, and blank alignment variations. These three standard targets were modified theoretically for two additional variations: blank thickness and material strength. Further tests using these modified targets also produced near-optimal failure heights because of a drastic reduction in sensitivity to thickness and strength variations.

THE NORMALIZED AVERAGE THICKNESS CONTROL METHOD

While F_t is an estimate of engineering stress, normalized average thickness (t_{avg}) is correlated with part strain. As discussed in Chapter 3, t_{avg} is the average part thickness in the unsupported area between the punch and die. Values of t_{avg} are calculated from on-line measurements of punch height and edge draw-in. A family of trajectories of t_{avg} for the first geometry, conical cups, is shown in Fig. 4-37 for standard conditions (STP, 0.020 in. "C" material, 6.25 in. diameter). This experimental data shows the t_{avg} curves for a low binder force (3,000 lb.), causing buckling, and a high binder force (15,000 lb.), causing tearing. The t_{avg} curve for the low binder force is higher because lower flange friction forces allow more draw-in and reduce part thinning. A higher binder force restricts draw-in and accelerates part thinning as seen in the lower curve. The t_{avg} curve for the optimum binder force discussed above (6,000 lb.) has an intermediate position and gives the highest failure height. If t_{avg} were controlled to this optimum "signature" trajectory regardless of process conditions, similar part strains would be expected. Duplication of optimum strain distributions would in turn produce optimum failure height.

Normalized Average Thickness Target Selection for Cups

The t_{avg} target curve shown in Fig. 4-37 is an exponential approximation of the optimum t_{avg} curve. The target curve intersects the t_{avg}=1 line at 0.2 in. and has an amplitude of 0.09 and a "time" constant of 0.4 in. (Because the independent variable in all of the tests is punch height which is measured in distance instead of time, the mathematical equivalent to the time constant is measured in

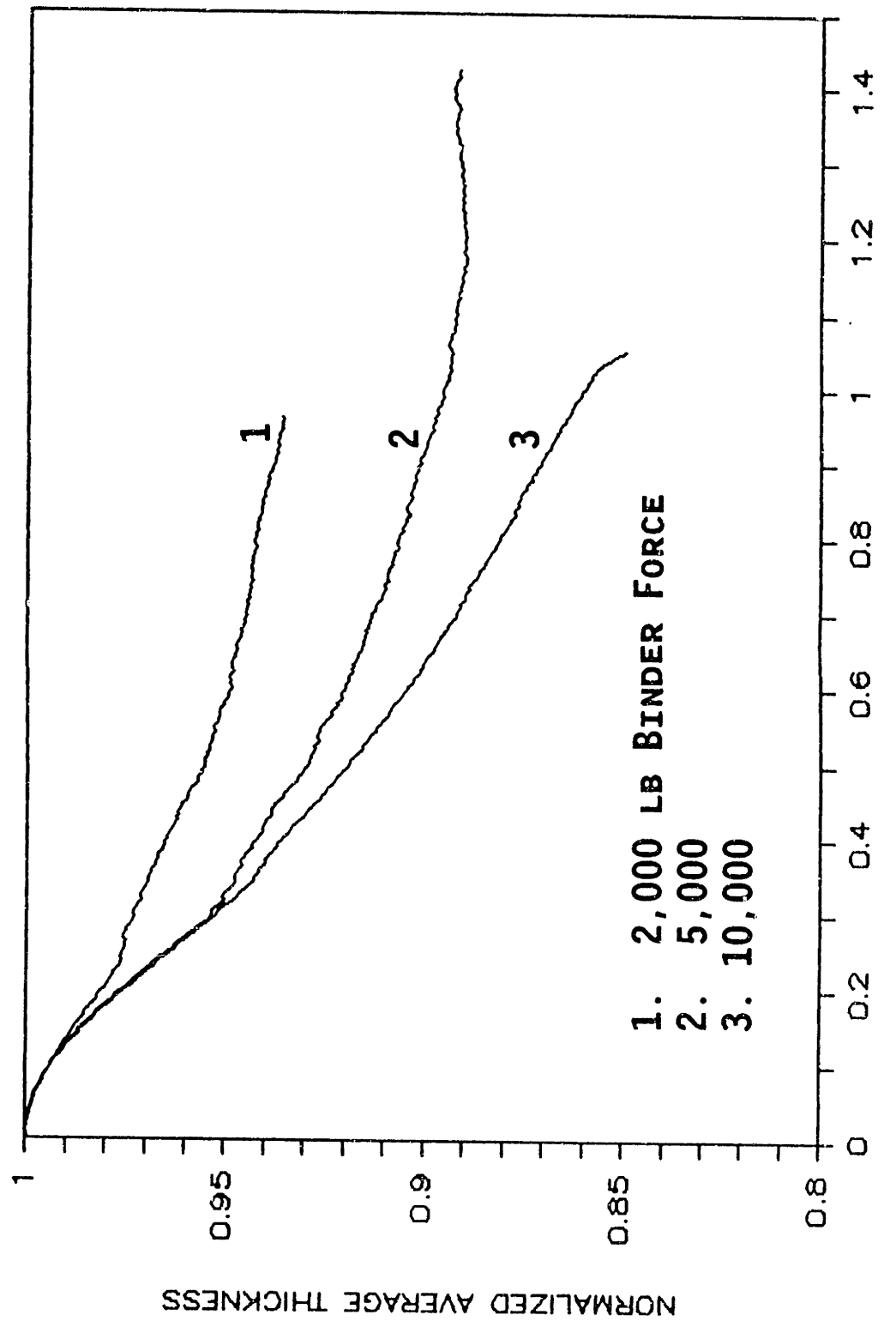

Fig. 4-37 Optimum Normalized Average Thickness Trajectory (t_{avg}) and Target Selection for the Cup Geometry (0.020 in. material "C", STP, 6.25 in. diameter).

displacement.)

The exponential model is not a good approximation of the t_{avg} response during the first 0.4 in. of forming. The characteristic shape of the t_{avg} trajectory changes after the initial deformation period. As with the F_t scheme, the t_{avg} control system is designed for the later stages of deformation. Therefore, the t_{avg} controller is activated only after the first 0.4 in. of punch motion.

Normalized Average Thickness Control of Cups for Standard Conditions

An optimum t_{avg} "signature" trajectory is used above as the basis for selecting the t_{avg} target for use during closed-loop control. The t_{avg} target drawn in Fig. 4-37 was used in tests of t_{avg} control to adjust the binder force as forming progressed. These initial tests used standard forming conditions like those used above during target selection. Figure 4-38 shows the resulting closed-loop failure heights along with the corresponding constant binder force, open-loop heights repeated from Fig. 4-1. Regardless of initial binder force, t_{avg} control resulted in failure heights near the best constant binder force height. The control system nearly eliminates the need for accurate predictions of optimum binder forces that are so important in the uncontrolled, constant binder force case.

To be effective, the t_{avg} controller must bring the t_{avg} trajectory rapidly to the target curve. Failure heights will be maximized by reducing deviations from the optimum t_{avg}, even early in the cycle, as demonstrated for the F_t controller (Fig 4-8). The t_{avg} trajectories

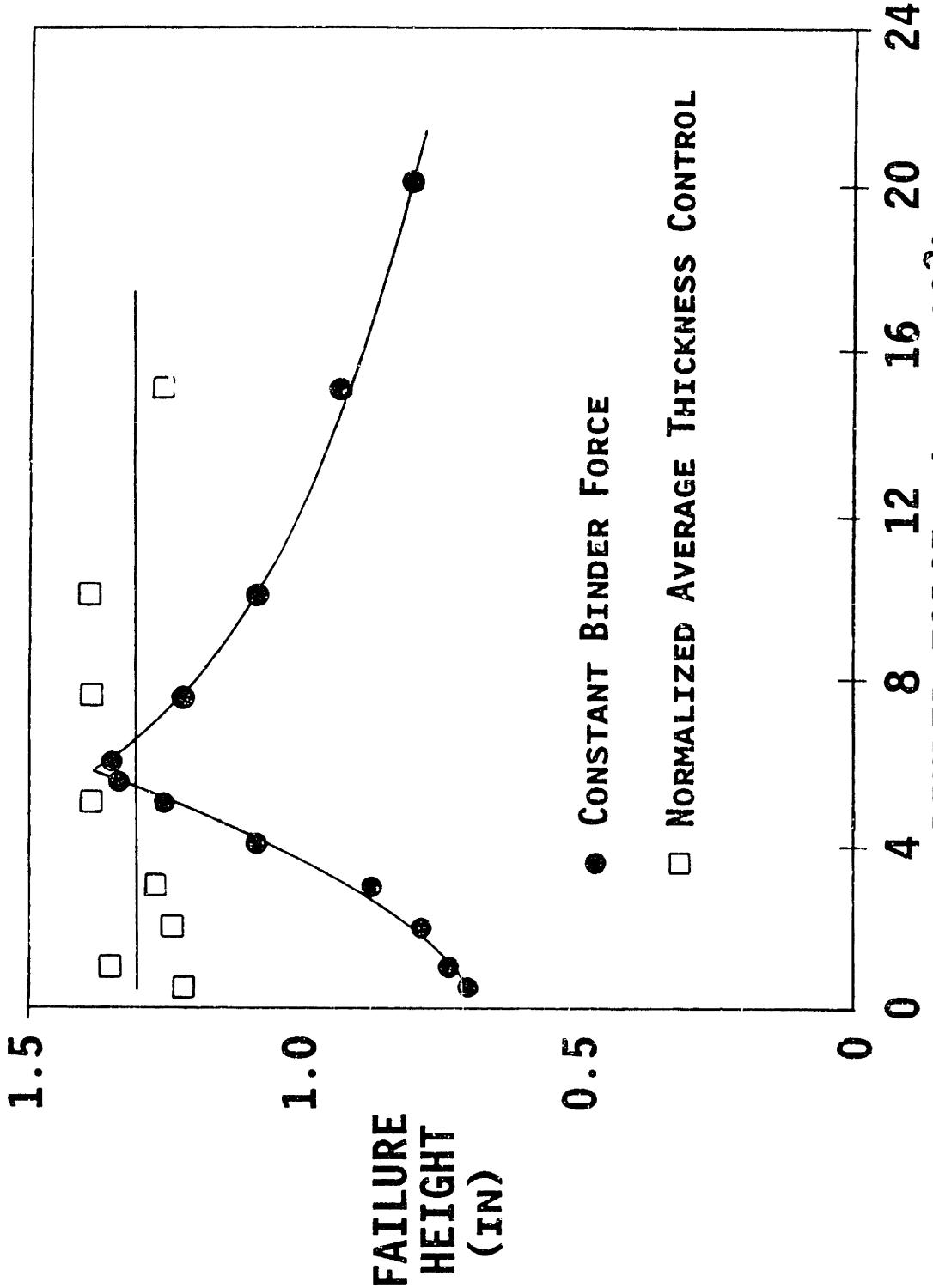

Fig. 4-38 Closed-Loop t_{avg} Control: Cup Geometry Using Standard Conditions (0.020 in. material "C", STP, 6.25 in. diameter).

during t_{avg} control for three initial binder forces are shown in Fig. 4-39. The paths of t_{avg} are diverging early in the forming cycle before control starts at 0.4 in. punch height. After t_{avg} control begins to adjust the binder force, the t_{avg} values converge quickly. Figure 4-39 illustrates how the three t_{avg} trajectories converge to the target at 0.75 in. punch height.

Control of t_{avg} to a particular target curve results in a typical strain distribution. For given conditions, the controller will also "find" a particular binder force value which will give a near-maximum failure height. Figure 4-40 displays the binder force trajectories during the tests above using 1,000 lb. and 15,000 lb. initial binder forces. The optimum binder force, derived from constant binder force tests, for the conditions of Fig. 4-40 was 7,500 lb. After the early constant binder force period, the binder force trajectories for both initial conditions converged rapidly. The final binder force value for both cases was near 7,000 lb., which is close to the optimal binder force of 7,500 lb. These binder force trajectories show the basis for failure height improvements resulting from t_{avg} control.

For particular conditions, there is an optimum binder force trajectory that produces particular F_t and t_{avg} trajectories. The F_t and t_{avg} values are not independent and controlling one trajectory to an optimum also controls the other to its corresponding optimum. Figure 4-41 shows the trajectories of F_t during the three t_{avg} control tests discussed above (Fig. 4-39). The three F_t paths converged to a line closely approximating the target line used for F_t control in the

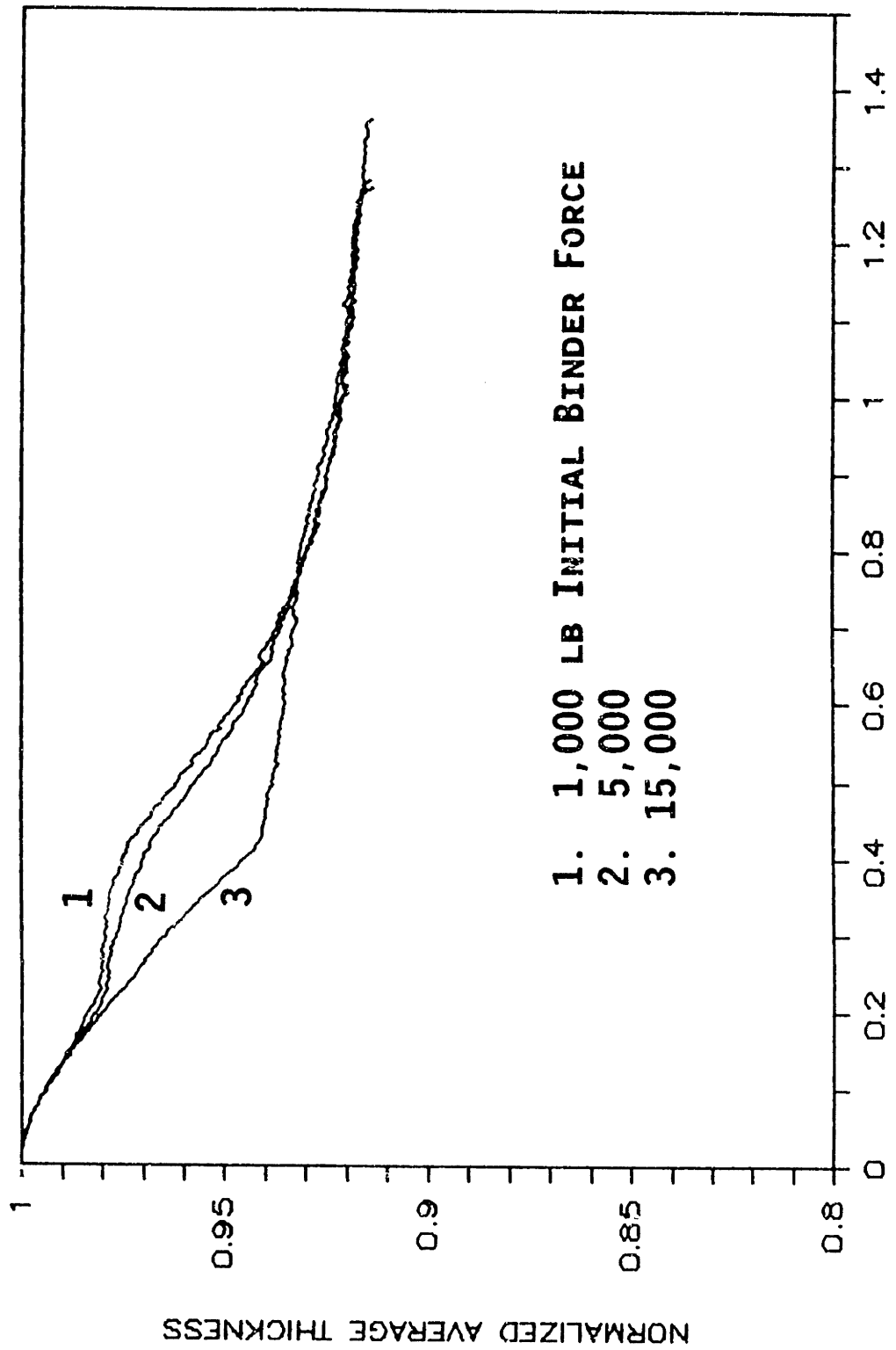

Fig. 4-39 Normalized Average Thickness Dynamic Trajectories during Control after different initial binder forces (cup geometry, 0.020 in. material "C", STP, 6.25 in. diameter)

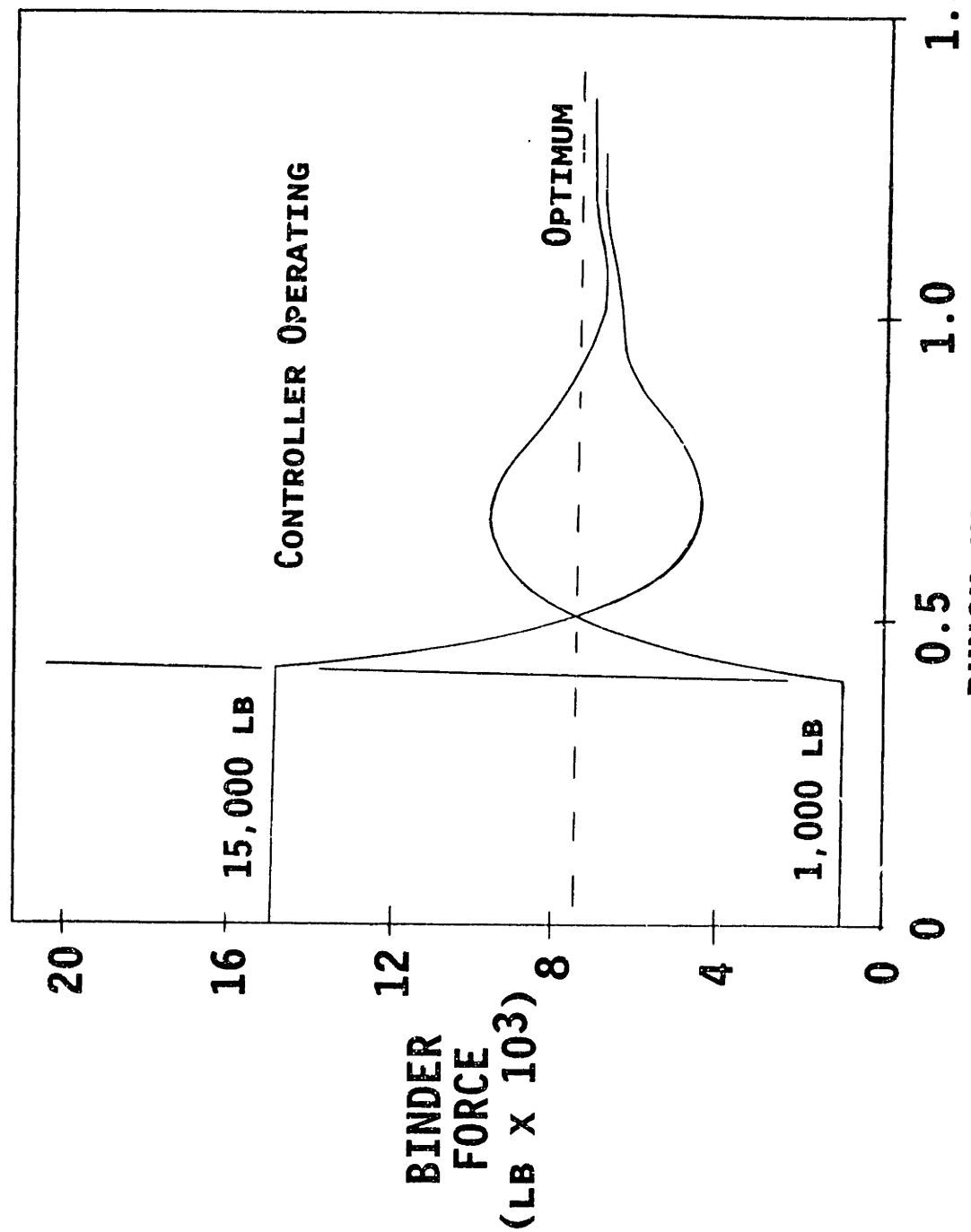

Fig. 4-40 Binder Force Dynamics during t_{avg} Control (cup geometry, 0.020 in. material "C", STP, 6.25 in. diameter)

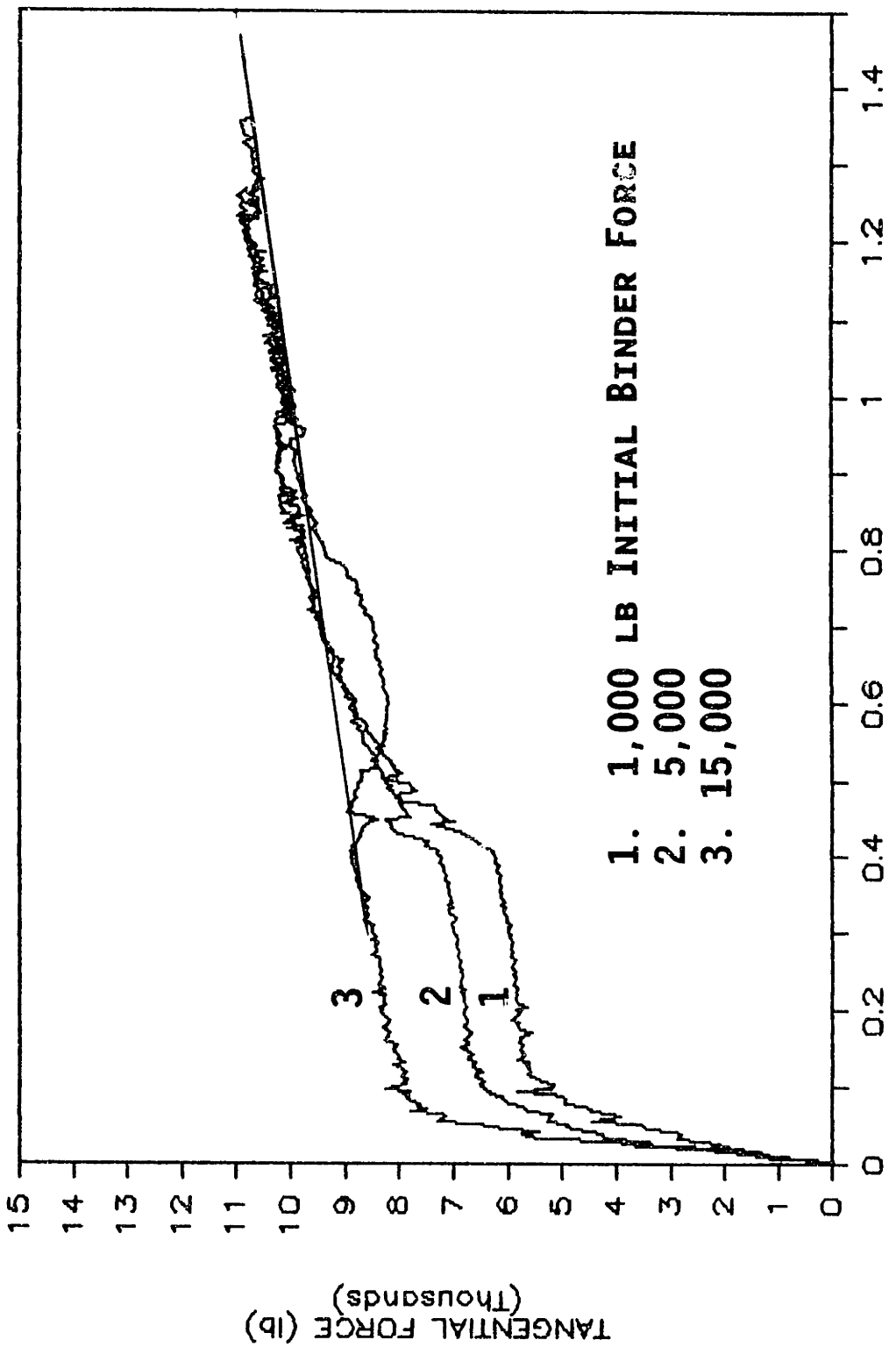

Fig. 4-41 Tangential Force Trajectory during t_{avg} Control (cup geometry, 0.020 in. material "C", STP, 6.25 in. diameter)

previous sections. These curves show that control of F_t or t_{avg} can result in very similar part conditions and similar failure heights. The selection of one type of control over the other depends most on implementation issues, such as instrumentation requirements, rather than inherent superiority of one concept over the other.

Normalized Average Thickness Control of Cups During Perturbations

Changes to initial binder force are a good test of the F_t and t_{avg} controllers because these changes simulate less than optimal initial flange restraining force. Another source of restraining force deviation is friction coefficient alteration due to lubrication change. To successfully eliminate the effect of lubrication variations on failure height, the proper t_{avg} target must be selected. The divergent t_{avg} trajectories shown in Figure 4-42 illustrate the strong effect of lubrication on t_{avg} and failure height. These curves show t_{avg} for a constant 5,000 lb. binder force. However, if the optimum binder force for each condition is used, the t_{avg} curves are much more similar to each other and to the standard target developed above (Fig. 4-43). This figure shows that changes in lubrication have minimal effect on the optimum target position. No target adjustment is required for lubrication changes, which are so difficult to predict and measure. Other process variations, such as material surface finish, that change flange friction forces should also have little effect on t_{avg} target position.

Tests during dry (unlubricated) and teflon particle spray lubrication were done using the standard t_{avg} target derived above.

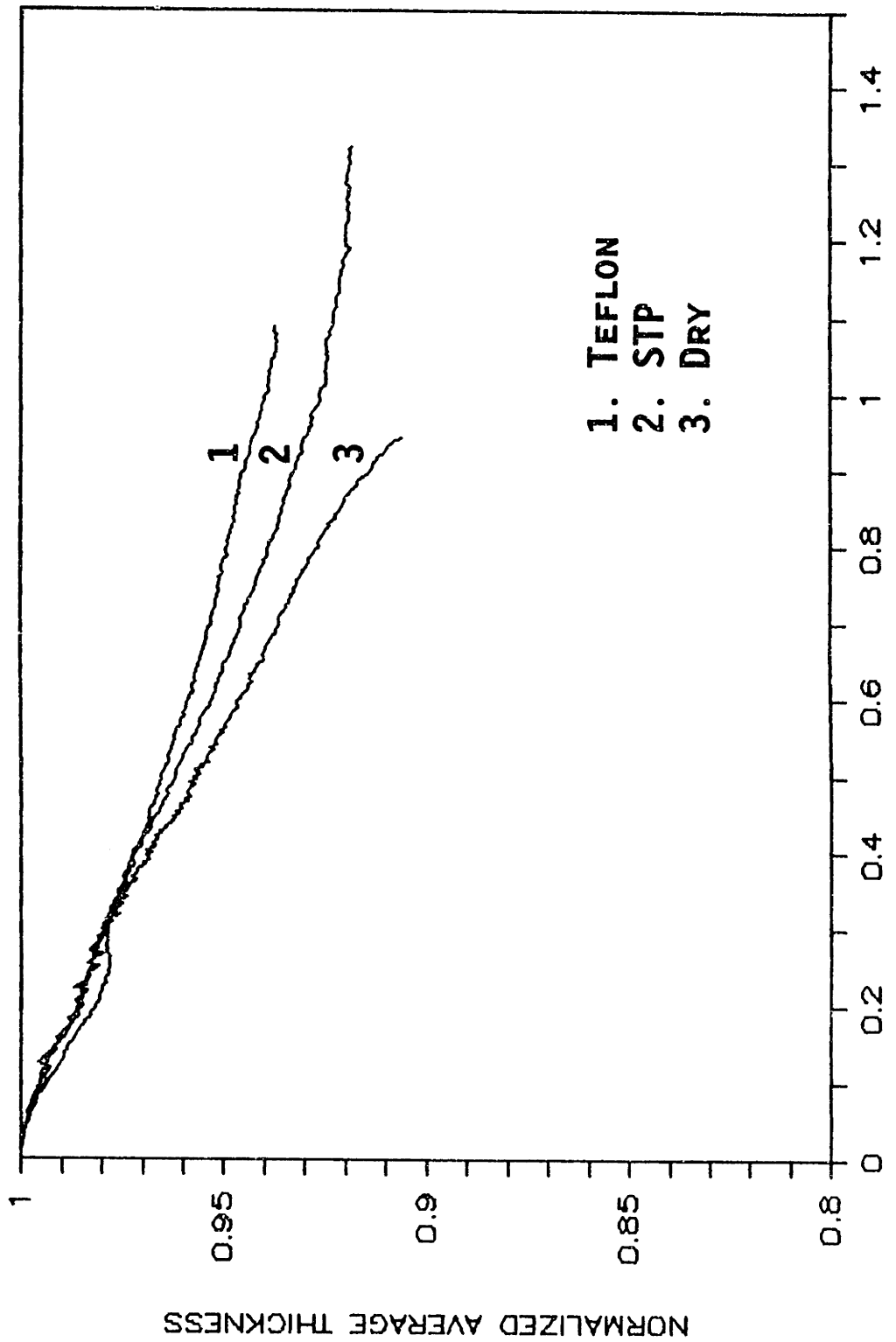

Fig. 4-42 Normalized Average Thickness Trajectories for Three Lubrication Conditions Using One Binder Force (BF = 5,000 lb, cup geometry, 0.020 in. "C", 6.25 in.)

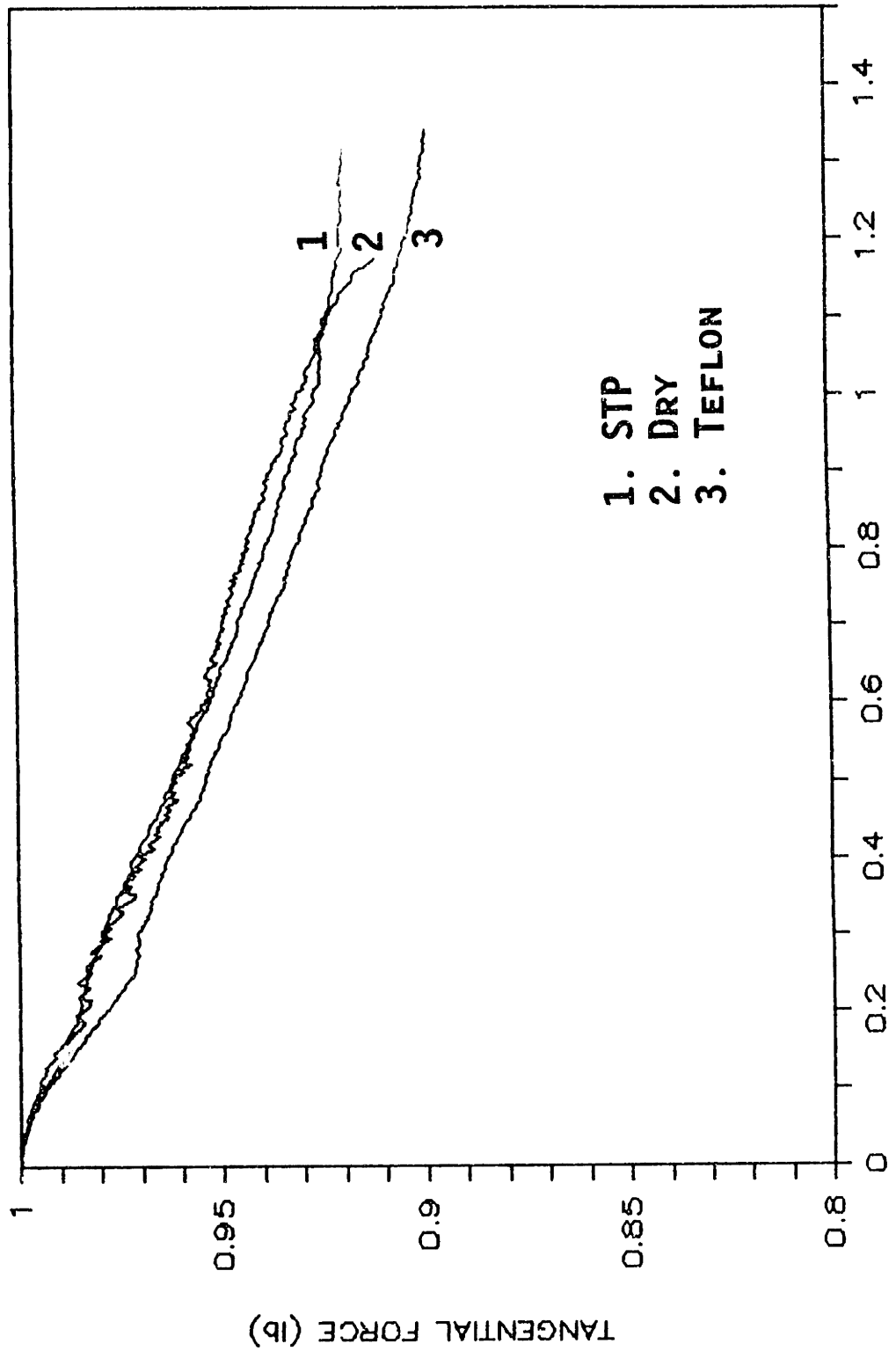

Fig. 4-43 Normalized Average Thickness for Three Lubrication Conditions Using Respective Optimum Binder Forces (dry:3k lb, STP:5k, teflon:10k, cup, 0.020 in. "C", 6.25 in.)

Figure 4-44 shows that t_{avg} control effectively eliminated the effect of initial binder force selection during dry tests. During tests using teflon lubrication, the closed-loop failure heights were even higher than the best constant binder force result (Fig. 4-45). These tests using dry and teflon lubrication illustrate that the use of the t_{avg} control effectively compensates for the effects of lubrication changes.

Another process parameter that affects flange restraint is blank diameter, which acts through hoop stress rather than frictional forces. Larger blanks form wider flanges that generate higher circumferential stress as the perimeter shortens during draw-in. The higher hoop stresses of a larger, 6.50 in. blank reduce draw-in and produce lower t_{avg} values for a given binder force (Fig. 4-46). However, when the lower optimal binder force is used for the larger blanks, the t_{avg} trajectories of the 6.50 in. and 6.25 in. blanks are almost congruent (Fig. 4-47). Tests using the standard target confirm that t_{avg} control of the larger blanks produces full formed heights without target alterations (Fig. 4-48). Under production conditions, dimensional variations during the blanking operation would have little effect on part forming success while using t_{avg} control.

Forming control of thicker blanks is more complex. While the optimum t_{avg} target does not shift during lubrication and diameter changes, the optimum trajectory is different for thickness changes. Figure 4-49 shows the optimum t_{avg} trajectories for the standard 0.020 in. blanks and thicker, 0.025 in. blanks, which were also used in the F_t tests above. These curves approximate the ideal target curves and the

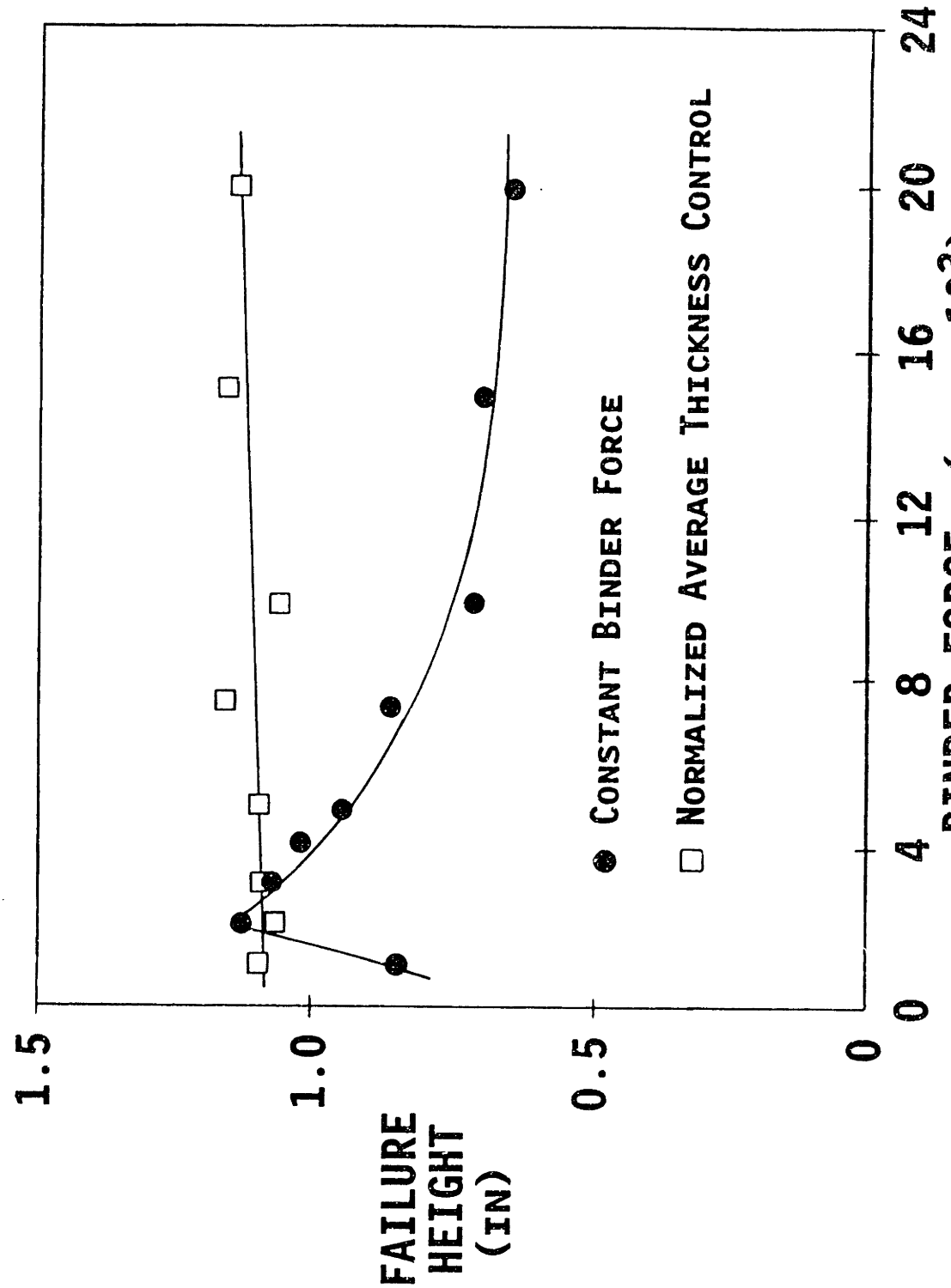

Fig. 4-44 Closed-Loop t_{avg} Control: Unlubricated Conditions (cup geometry, 0.020 in. material "C", 6.25 in. diameter)

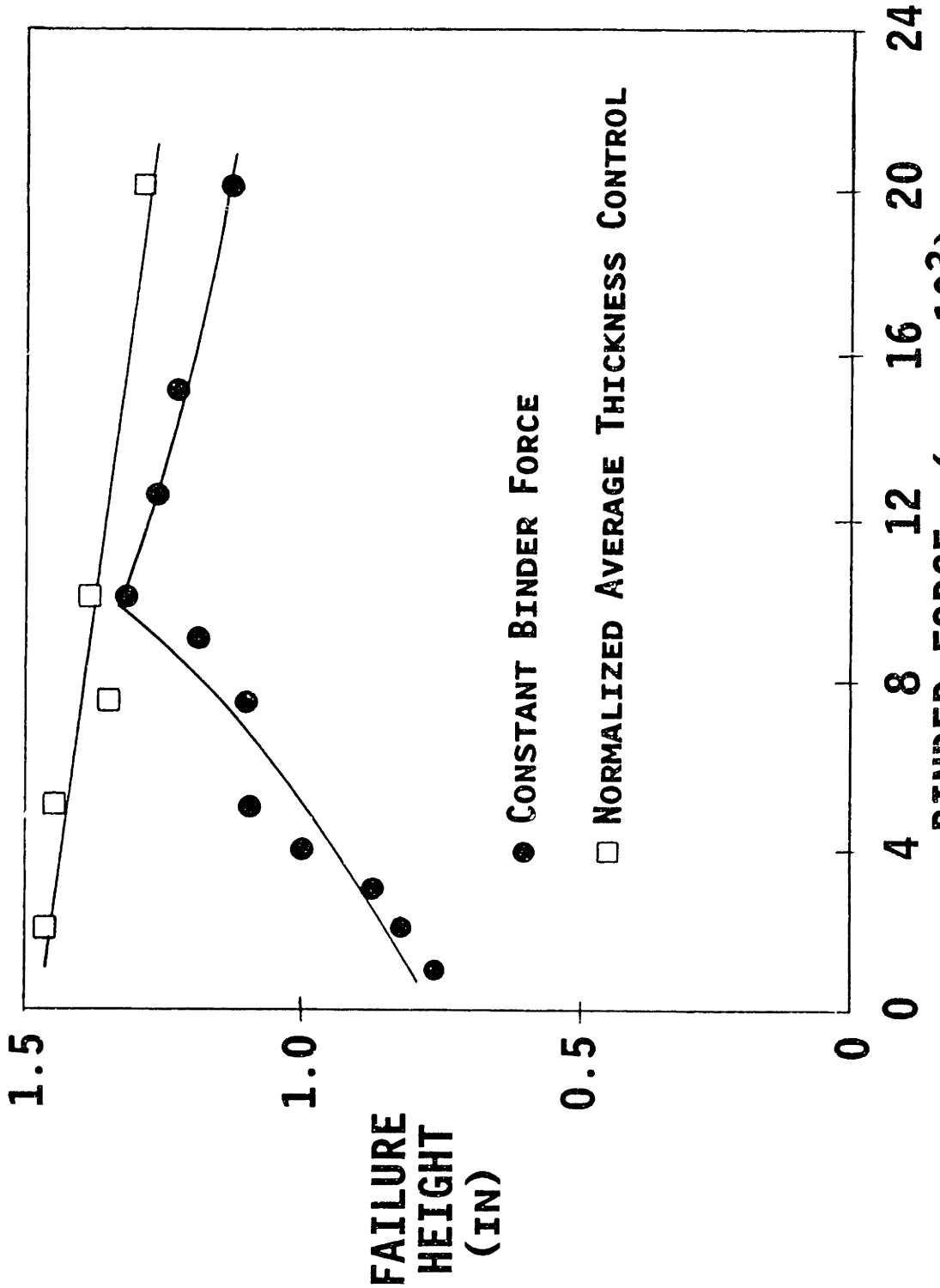

Fig. 4-45 Closed-Loop t_{avg} Control: Teflon Lubrication (cup geometry, 0.020 in. material "C", 6.25 in. diameter)

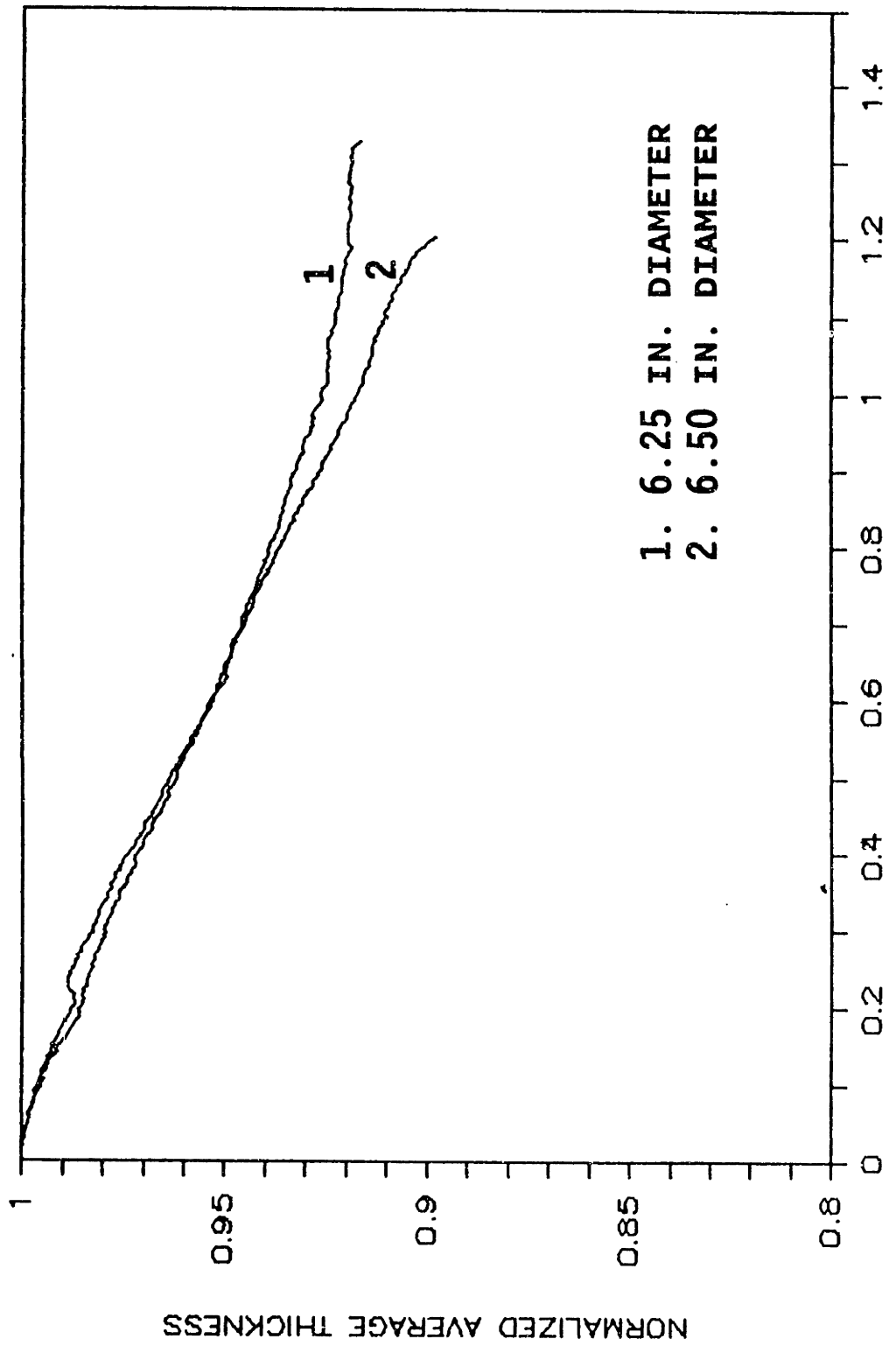

Fig. 4-46 Normalized Average Thickness Trajectories for Two Blank Diameters Using One Binder Force (binder force = 5,000 lb, cup geometry, 0.020 in. material "C", STP)

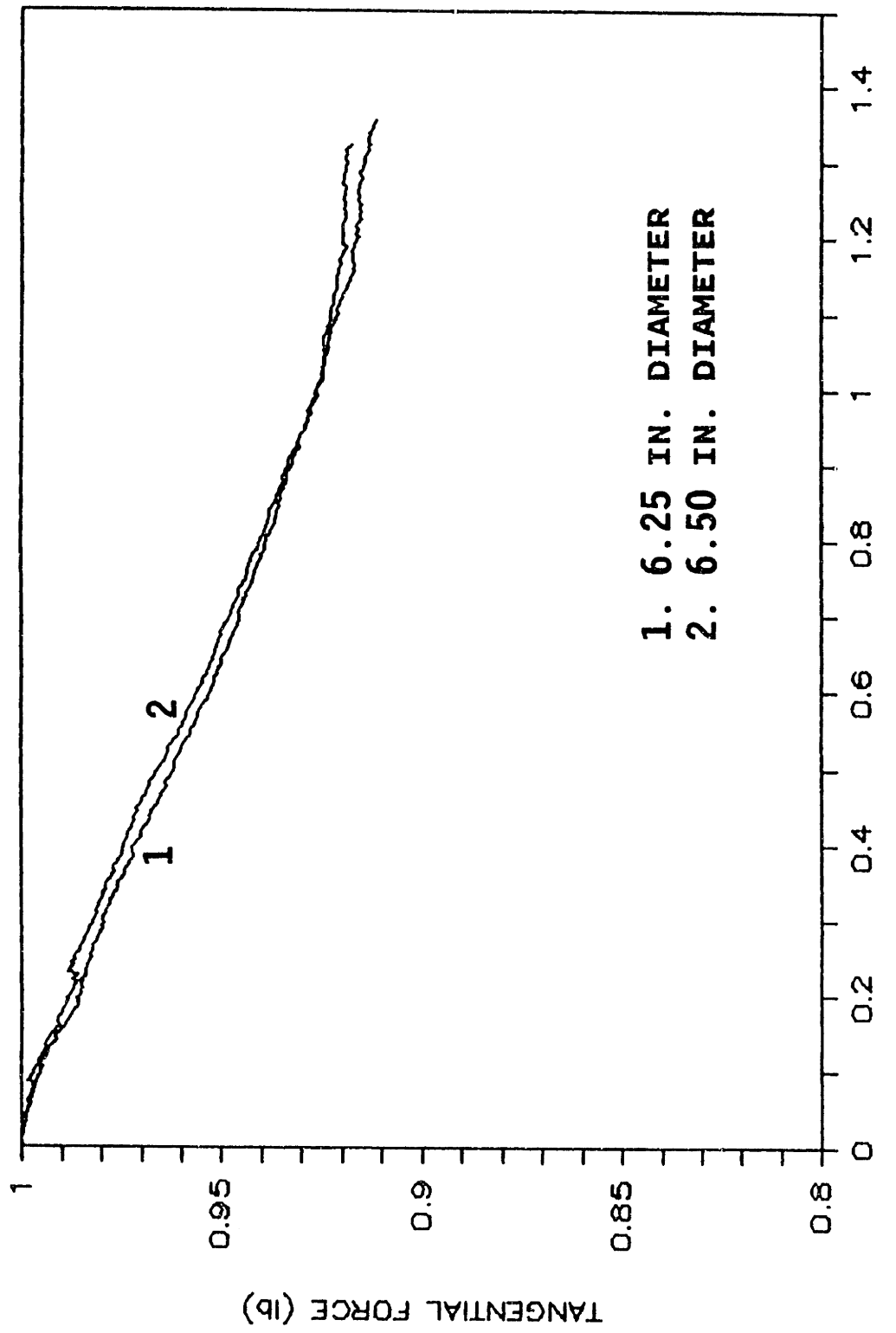

Fig. 4-47 Normalized Average Thickness Trajectories for Two Blank Diameters Using the Respective Optimum Binder Forces (6.25:5k lb, 6.50:2k, cup, 0.020 in. material "C", STP)

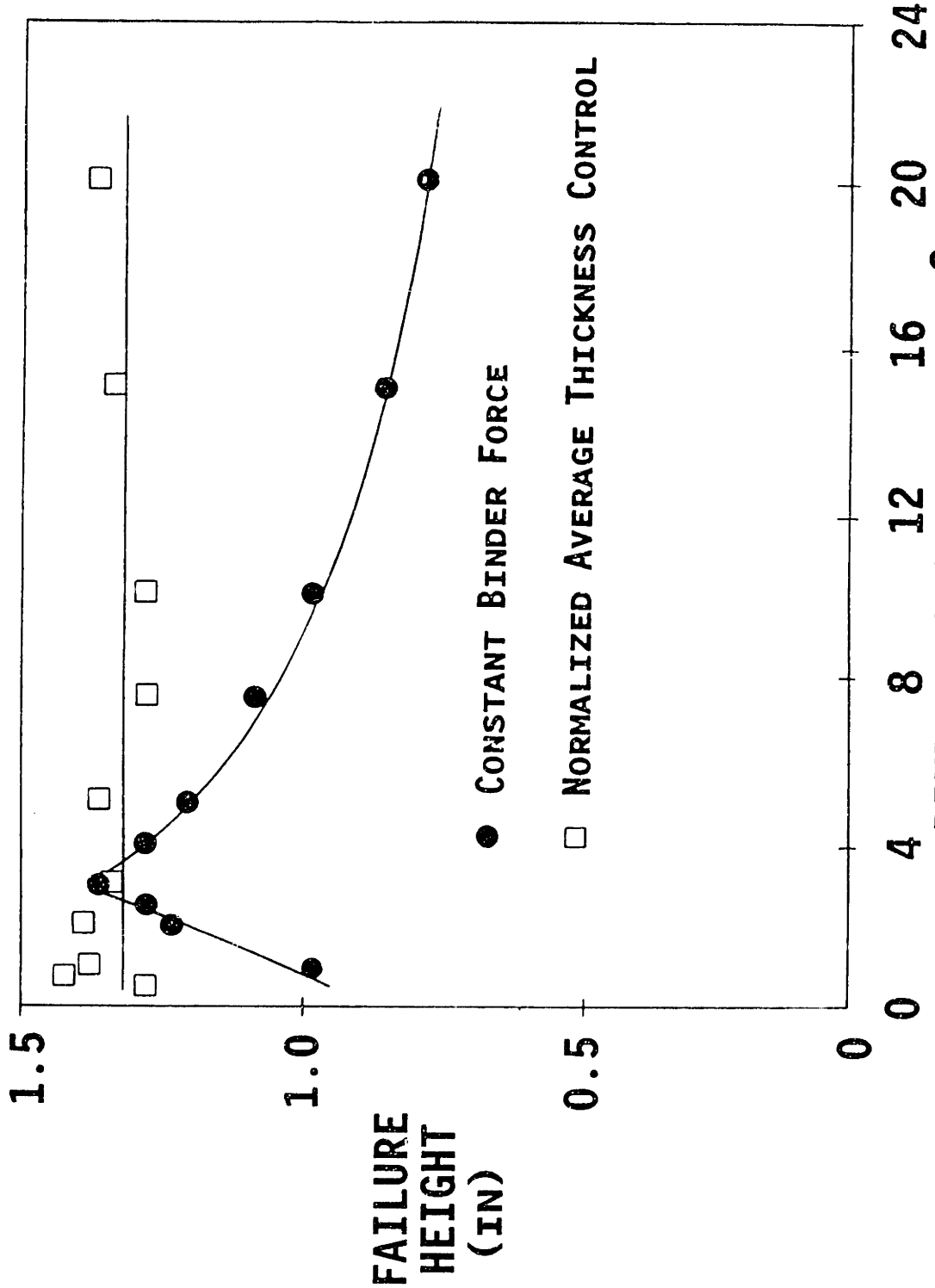

Fig. 4-48 Closed-Loop t_{avg} Control: Change of Blank Diameter to 6.50 in. (cup geometry, 0.020 in. material "C", STP)

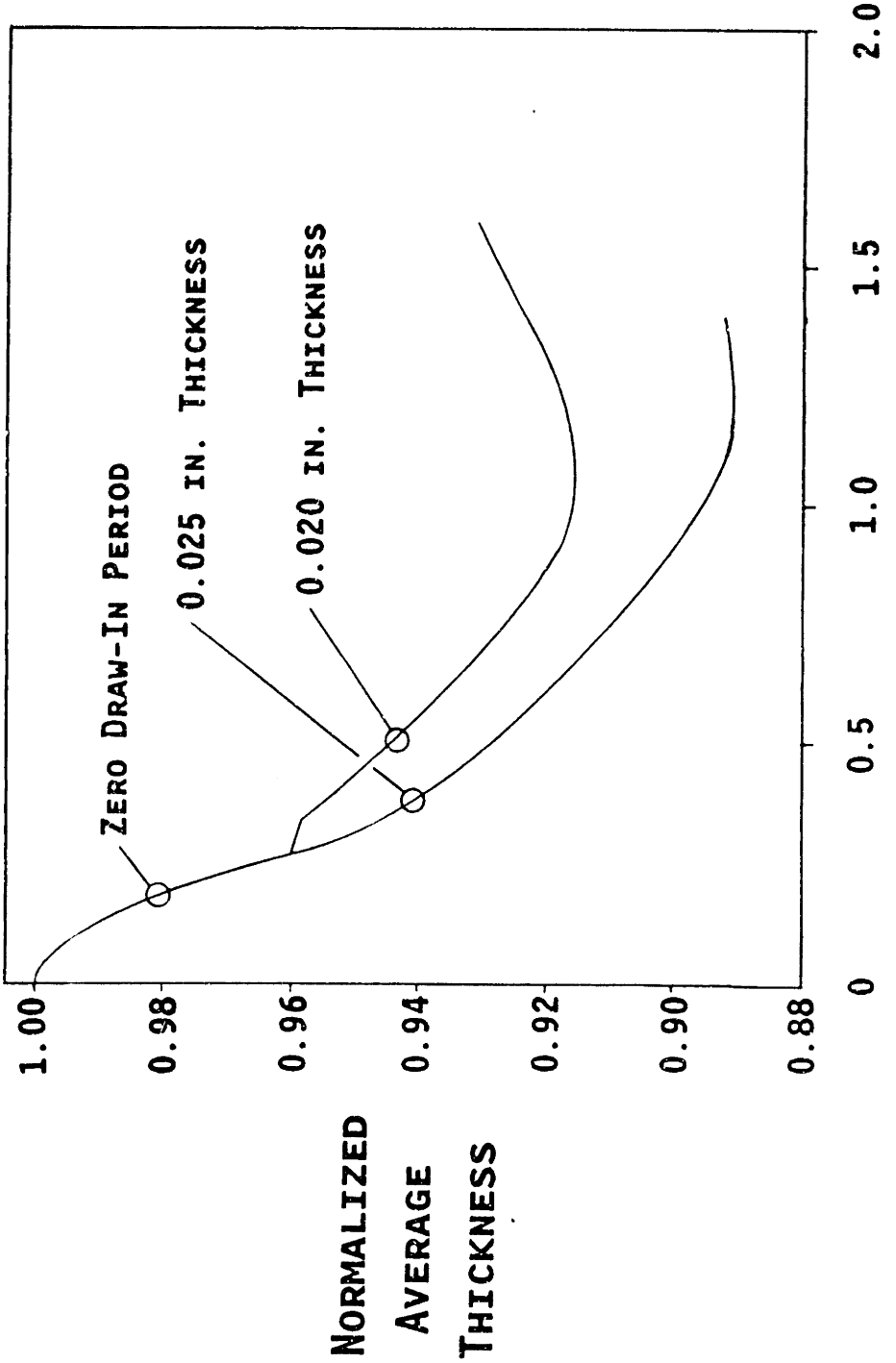

Fig. 4-49 Normalized Average Thickness Trajectories for Two Blank Thicknesses Using the Respective Optimum Binder Forces (cup, 0.020 in."C" (5k), 0.025 in."B"(6k), STP, 6.25 in)

0.025 in. path is significantly higher than the standard thickness path. The thicker material has a higher optimum trajectory because of its increased ability to withstand higher compressive hoop strains. More draw-in is possible for the thicker material, which results in the higher terminal value of t_{avg} at optimum cup height.

The standard t_{avg} target curve was used for t_{avg} control to assess the impact of the target shift on failure height during thickness changes. Figure 4-50 shows that the failure heights produced by the standard target increased during forming of 0.025 in. blanks. However, the controlled height did not increase as much as the uncontrolled peak, i.e. t_{avg} control did not fully utilize the increased formability of the thicker material. The t_{avg} controller produced cups with 92% of the optimal height by capturing 50% of the available height *increase*. This result was considered satisfactory and tests using target scaling were not attempted.

The use of the standard target for thicker material was much more successful for t_{avg} control than F_t control. As described above, use of the standard F_t target for 0.025 in. blanks gave failure heights 20% lower than for the 0.020 in standard material. If simple vertical scaling of the F_t target is done proportionate to thickness, failure heights are equal to the 0.020 in. thickness but not greater. In contrast, use of the standard 0.020 in. target for t_{avg} control increases the failure height by approximately 8%.

As for F_t control above, t_{avg} control tests were done using 0.020

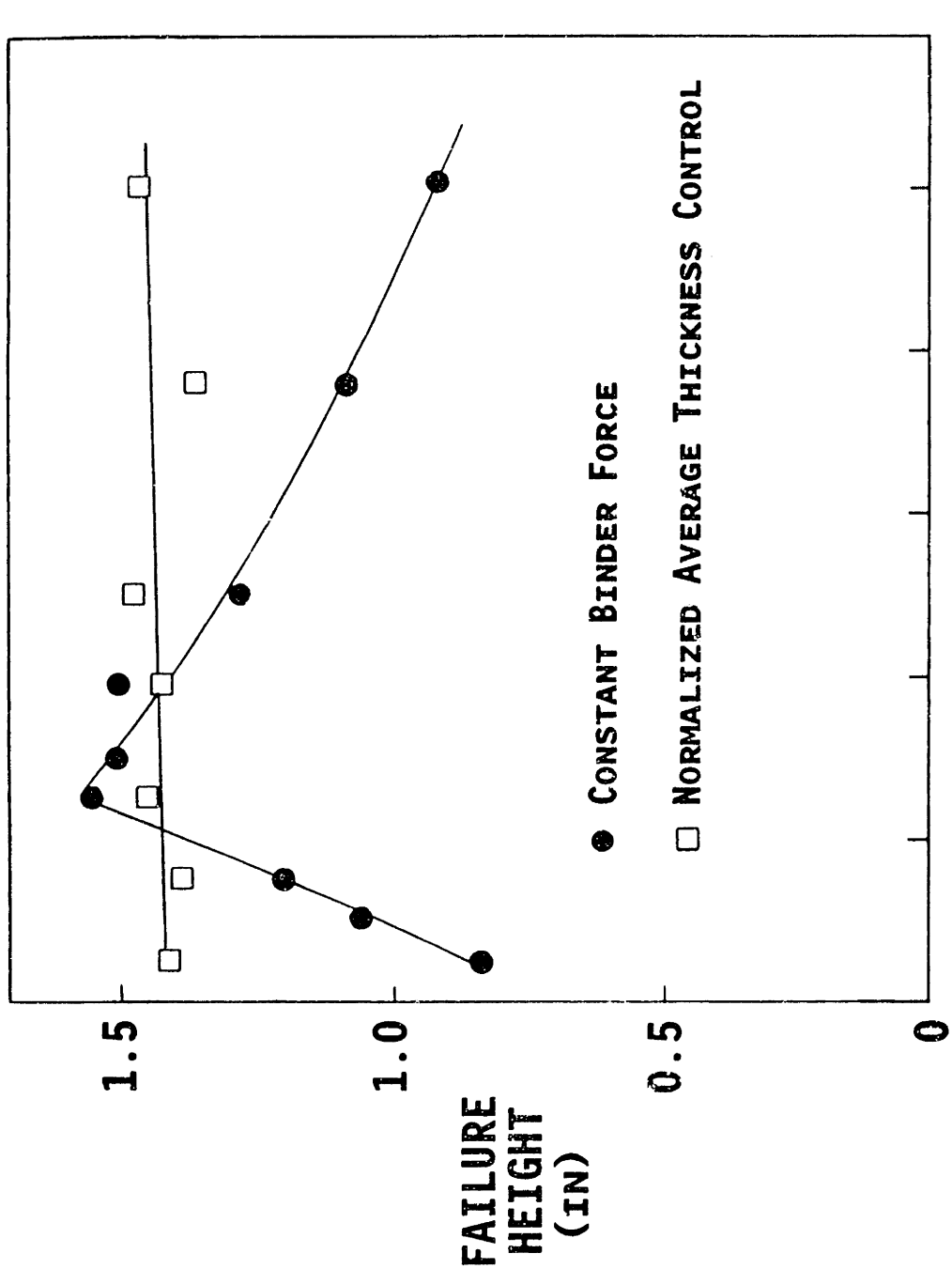

Fig. 4-50 Closed-Loop t_{avg} Control: Use of the Standard Target with a Non-Standard Blank Thickness (cup geometry, 0.025 in. material "B", STP, 6.25 in. diameter)

in. "D" material that has a 14% higher UTS than the standard material. The standard t_{avg} target was used and the resulting heights are shown in Fig. 4-51. This figure shows that controlled failure heights are high for low initial binder forces, but control effectiveness decreases at high initial binder forces. The premature failures at high initial binder forces are caused by slow speed of the process response relative to the generally low failure heights for this material. Binder force was adjusted downwards by the controller and did not recover to a higher equilibrium value before failure occurred.

The last t_{avg} control test series for cup forming used material with both UTS and thickness changes from the standard. The 0.025 "A" material blanks have a 9% lower UTS and 25% greater thickness. Use of the standard t_{avg} target during control produced the failure heights plotted in Fig. 4-52. The results are similar to the 0.025 in. tests above, which used the standard UTS. The t_{avg} controller produced cups with 90% of the optimal height by capturing 50% of the available height *increase*. In this case the 50% increase in height is more, because of the improved formability of the "A" material.

Normalized Average Thickness Control of Unequal Corner Radii Pans

A single t_{avg} test series was completed to assess the performance of the controller for the equal corner radii geometry. The standard conditions for this geometry were used, which include silicone lubrication and 0.025 in. "A" material. There was no significant loss in controller performance while using this asymmetric geometry (Fig. 4-53). This result suggests that forming of more complex geometries, which are more

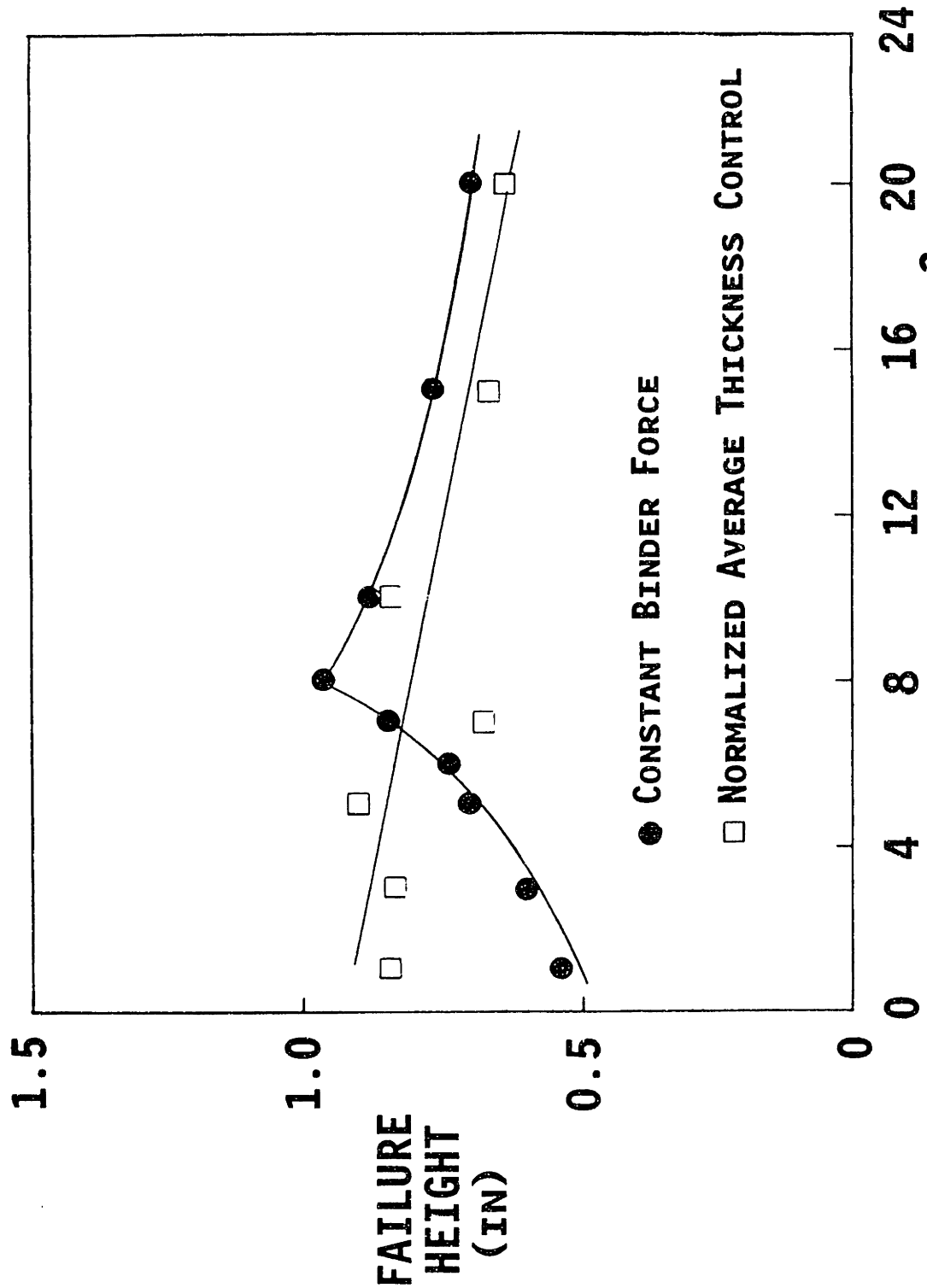

Fig. 4-51 Closed-Loop t_{avg} Control: Use of the Standard Target with a Non-Standard UTS (cup geometry, 0.020 in. material "D" (UTS 58ksi), STP, 6.25 in. diameter)

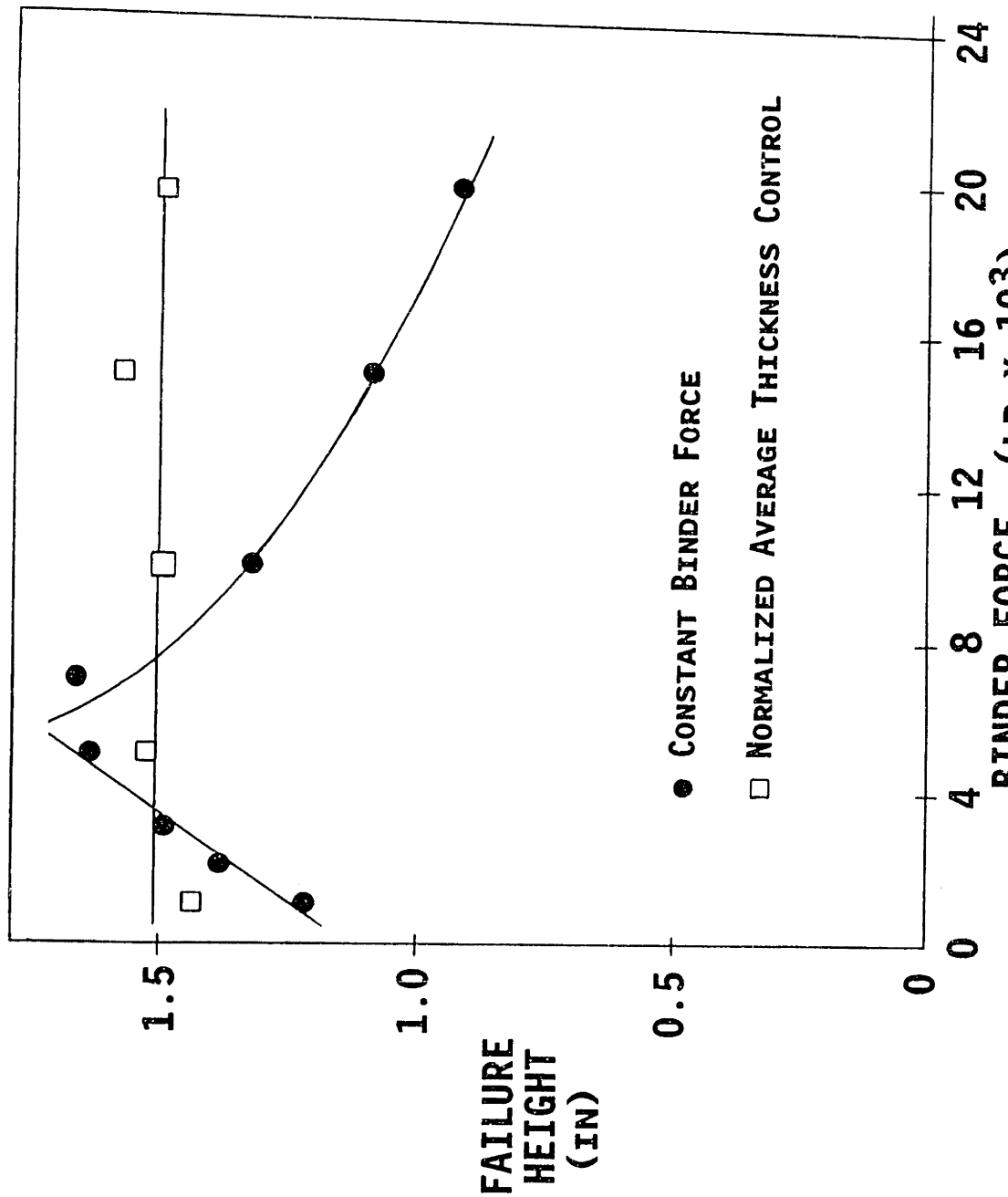

Fig. 4-52 Closed-Loop t_{avg} Control: Use of the Standard Target with a Non-Standard UTS and Thickness (cup geometry, 0.020 in. material "A" UTS (47ksi), STP, 6.25 in. dia.)

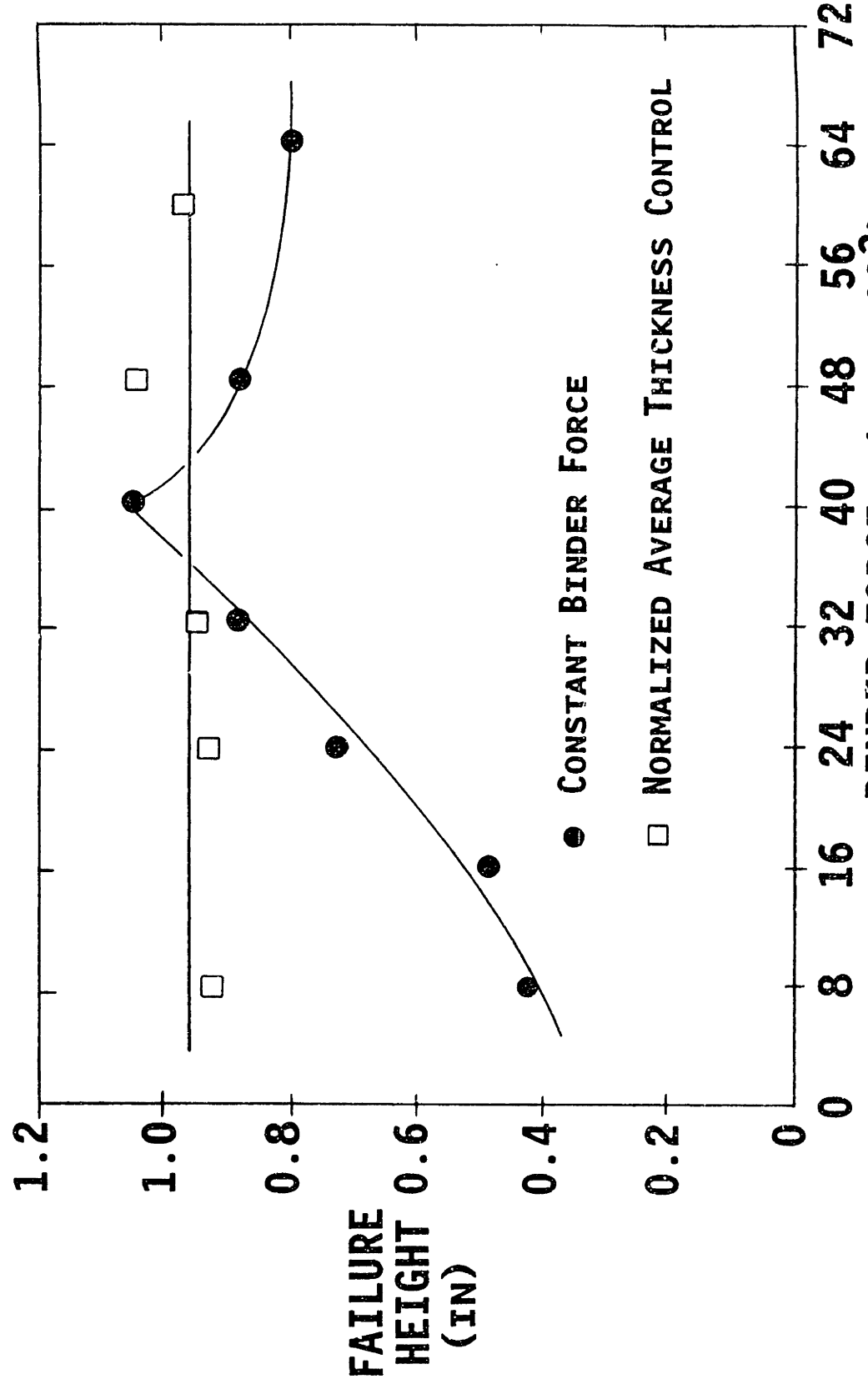

Fig. 4-53 Closed-Loop t_{avg} Control: Unequal Radii Square Geometry Using Standard Conditions (0.025 in. material "A", silicone, 9.078 in. diameter)

typical of industrial production, could be substantially improved by using the t_{avg} control method.

Chapter 5 CONCLUSIONS AND RECOMMENDATIONS

This thesis was motivated by the difficulty of consistently producing high quality drawn sheet metal parts. A large array of unpredictable factors affect the forming conditions and make correction of forming failures difficult. Much previous work on understanding practical sheet metal forming has concentrated on analysis of strain distributions of failed parts. Other work models binder force requirements based on assumed knowledge of forming conditions. Neither of these approaches, in and of themselves, can address the problems associated with frequent and unpredictable variations in forming conditions.

Methods are developed in this work that avoid the need for precise knowledge of initial forming conditions and unmeasurable, in-process boundary conditions. Two main estimates of part condition are defined that are based on forming parameters that are measurable as forming progresses. Tangential force (F_t) values estimate the average force and stress in the sheet at the punch nose. F_t is based on simple punch force and punch height measurements. The second method, normalized average thickness (t_{avg}), estimates the part thickness and is related to the in-plane strains. Calculation of t_{avg} requires edge draw-in or circumference measurements and punch height. Once real-time measurements of material condition are available, these values can be controlled to optimal trajectories by modulating binder force continuously during forming.

Selection of proper target trajectories for F_t and t_{avg} during forming is as important as real-time calculation of F_t and t_{avg}. This work proposes a two step procedure for F_t target identification. For each die geometry, a series of tests is performed to identify the optimum constant binder force and the associated optimum F_t trajectory. This optimum trajectory can be used as a target. The effect of variations of lubrication, blank diameter, and blank position on the failure height are much reduced by controlling in-process F_t values to this target. Variations in blank tensile strength require scaling this experimental F_t target proportionately with strength. The effect of blank thickness changes can be estimated through application of shell buckling theory, and the original F_t target modified in accord with this result. Thus, depending on the type of disturbance, F_t targets are developed from a combination of experimental and analytical techniques.

Each of the two control methods has particular strengths and weaknesses. Determination of the t_{avg} target is simpler than selection of the F_t target because only one target is required during any of the selected process disturbances. This target is simply the optimum t_{avg} trajectory from one standard test using the optimum constant binder force. However, the t_{avg} control method relies on an accurate measure of average edge draw-in which may be difficult to attain because of uneven local draw-in. Conversely, the F_t control method requires only punch force measurements, which are easier to supply. Tangential force target selection is more complicated than t_{avg} target selection if blank ultimate tensile strength or thickness vary. These variations require scaling the target using relationships discussed above. Both the F_t and

t_{avg} control algorithms used coefficients, or gains, that did not require modification for any of the test conditions.

Application of these two control techniques is simplified by the limited need for target readjustments and the use of constant control gains. Only limited knowledge of deviations in production conditions is required after initial target selection, which greatly facilitates the industrial use of these methods.

The performance of both F_t and t_{avg} control was determined in a comprehensive test program. Both cup and pan die geometries were used along with perturbations of lubrication, blank thickness and diameter, blank position, and material properties. In almost all cases, failure height during closed-loop control was nearly equal to the height for the ideal constant binder force. Regardless of the forming conditions, the control systems "find" the unknown optimum binder force which gives greatest failure height. The ability of the control systems to produce high failure heights in tests indicates that forming failures during production would be minimized by decreasing the sensitivity to process variations.

Recommendations

1. Analysis of the local stress-strain conditions that cause failure should lead to optimized targets which produce formed heights greater than under constant force conditions. Current work using the finite element method by Sim and Boyce [17] will use the new understanding of the stress-strain state to propose

improved targets for the F_t and t_{avg} control methods.

2. Trials using an industrial hydraulic press on typical production parts would prove the utility of the control methods.

3. Alterations of the binder force trajectory produced during F_t control may signal important changes in process conditions. For example, reductions in final binder force at punch bottoming may indicate a loss in lubrication effectiveness. Limits for normal binder force values could be computerized and in this way changes in process conditions could be detected automatically.

REFERENCES

1. Siekirk, J.F., "Process Variable Effects on Sheet Metal Quality," Journal of Applied Metalworking, Vol. 4, No. 3, July 1986, pp. 262-269.

2. Keeler, S.P., and Backofen, W.A., Trans. A.S.M., Vol. 56, 1963, p.251.

3. Goodwin, G.H., "Application of Strain Analysis to Sheet Metal Forming Problems in the Press Shop," SAE Automotive Engineering Congress, Detroit, January 1968.

4. Keeler, S.P., "Circular Grid Systems - a Valuable Aid for Evaluation of Sheet Metal Forming," Sheet Metal Industries, Vol. 45, 1969, p. 633.

5. Senior, B.W., "Flange Wrinkling in Deep-Drawing Operations," Journal of the Mechanics and Physics of Solids, Vol. 4, 1956, pp. 235-246.

6. Yu, T.X., and Johnson, W., "The Buckling of Annular Plates in Relation to the Deep-drawing Process," Int. J. Mech. Sci., Vol. 24, No. 3, 1982, pp. 175-188.

7. Yossifon, S., and Tirosh, J., "Buckling Prevention by Lateral Fluid Pressure in Deep-Drawing," Int. J. Mech Sci., Vol. 27, No. 3, 1985, pp. 177-185.

8. Havranek, J., "Wrinkling Limit of Tapered Pressings," Journal of the Australian Institute of Metals, Vol. 20, No. 2, June 1975, pp. 114-119.

9. Hobbs, R.M., "Use of Grid Strain Analysis for Die Development and Process Control in Australian Press Shops," Sheet Metal Industries, Vol. 55, April 1978, pp. 451-464.

10. Yoshida, K., and Hayashi, Y., "Developments in Research into Sheet Metal Forming Processes in Japan - Part 2," Sheet Metal Industries, Vol. 56, March 1979, pp. 261-270.

11. Havranek, J., "The Effect of Mechanical Properties of Sheet Steels on the Wrinkling Behaviour During Deep Drawing of Conical Shells," Journal of Mechanical Working Technology, Vol. 1, No. 2, November 1977, pp.115-129.

12. Swiatkowski, K., Muzykiewicz, W., and Sikora, S., "UnKonventionelles Tiefziehen erschliesst Umformreserven," Bander Bleche Rohre, October 1986, pp. 223-.

13. Romer, I., Fischer, F., and Breun, F., "Uber den Einfluss eines variablen Niederhalterdrucks auf das Grenzziehverhaltnis," Stahl und Eisen, Vol. 104, No. 21, 15 October 1984, pp. 1065-1072.

14. Doege, E., and Sommer, N., "Der Niederhalterdruck beim Tiefziehen nichtrotations-symmetrischer Ziehteile," Stahl und Eisen, Vol. 107, No. 8, 20 April 1987, pp. 345-350.

15. Manabe, K., Nishimura, H., and Hamano, H., "An Improvement in Deep Drawability of Steel/Plastic Laminate Sheets by Control of Blank Holding Force" in Advanced Technology of Plasticity, edited by K. Lange, Springer-Verlag, 1987, pp. 1297-1304.

16. Logan, R.W., "Sheet Metal Formability Simulation and Experiment," Ph.D. Thesis, University of Michigan, 1985.

17. Sim, H.B., and Boyce, M.C,, "A Finite Element Analysis of Real-Time Sheet Forming Stability Control in Cup-Forming," to be submitted to the Journal of Engineering for Industry, 1989.

18. Lee, C. and Hardt, D.E., "Closed-Loop Control of Sheet Metal Stability During Stamping", 1986 North American Manufacturing

Research Conference, May 28-30, 1986.

19. Lee, C.Y., "Closed-Loop Control of Sheet Metal Stability during Forming," S.M. Thesis, Massachusetts Institute of Technology, Feb. 1986.

20. Hutchinson, J.W., and Neale, K.W., "Wrinkling of Curved Thin Sheet Metal," Plastic Instability, Considere Memorial Symposium, Paris, 1985.

21. Tesawa, K., and Nishimura, G., J. Soc. Naval Arch., Vol. 47, 1931, p.129.

22. Timoshenko, S.P., Theory of Elastic Stability, McGraw Hill, 1961, pp. 349-350.

Appendix A CALCULATION OF NORMALIZED AVERAGE THICKNESS

Normalized average thickness is the average thickness of the unsupported material in the die cavity divided by the initial blank thickness. The average sheet thickness is calculated by dividing the volume of material in the die cavity by the surface area of this same material. This can be expressed as:

$$t_{avg} = V_f / (A_f t_i) \tag{A-1}$$

Where:

$$V_f = (\Pi/4)(D_d^2 - D_p^2)t_i + [(\Pi/4)D^2 t_i - \Pi r^2 t_i] \tag{A-2}$$

and if the draw-in $x = D/2 - r$

$$V_f = \Pi t_i[(D_d^2 - D_p^2)/4 + (D-x)x] \tag{A-3}$$

$$A = (D_p + D_d)s/2 \tag{A-4}$$

$$s = [\,(D_d/2 - D_p/2)^2 + (Y_p)^2\,]^{1/2}$$

and

V_f, A_f = volume and surface area of the material in the unsupported region (frustum)
D = initial diameter of the blank,
D_d = die diameter,
D_p = the punch diameter,
r = the current radius of the blank,
s = the length of the frustum along a meridian,
t_i = the initial thickness of the blank,
x = the "draw-in" or displacement of the edge of the blank,
Y_p = the punch travel.

Combining Eqs. A-2, A-3 and A-4, the non-dimensional normalized average thickness model is

$$t_{avg} = \frac{V_f}{A_f t_i} = \frac{[(D_d^2 - D_p^2)/4 + (D-x)x]}{(D_p + D_d)s/2} \qquad \text{(A-5)}$$

Note that Eq. A-5 was derived assuming sharp edges on the die and punch. Although the finite radius on these tools will change the expression for t_{avg}, this simplified form was retained to permit its use in a real-time control scheme.

Appendix B CONTROL ALGORITHM FORMULATION AND GAIN CALCULATIONS

During closed-loop control, the calculated value of F_t or t_{avg} is compared to the desired target value and an appropriate change to binder force is made based on the error. A "proportional plus integral" (PI) control algorithm (Eq. B-1) is executed approximately each 0.004 in. of punch displacement.

$$BF_d = BF_n + (K_p * (E_n - E_{n-1})) + (K_i * E_n) \qquad \text{(B-1)}$$

$$E_n = T_{f\ target} - T_{f\ current} \quad \text{or} \quad = t_{avg\ target} - t_{avg\ current}$$

$$E_{n-1} = T_{f\ target} - T_{f\ previous} \quad \text{or} \quad = t_{avg\ target} - t_{avg\ previous}$$

where BF_d = Desired Binder Force
BF_n = Current Binder Force
E_n = Current Error
E_{n-1} = Previous Error
K_p = Proportional Control Gain
K_i = Integral Control Gain

This PI controller provides a combination of rapid adjustment of the controlled variable and convergence of the error to zero, i.e. no steady-state error. However, to achieve satisfactory tracking of the target the control gains, K_p and K_i, must be chosen carefully for each control type.

Selection of the Proportional and Integral Control Gains for F_t Control

To calculate the required control gains from control theory, the process gains must first be characterized. These process gains are the response of the controlled variable, e.g. F_t, to a unit change in binder force. A series of step changes to binder force was completed and the

response of F_t was modelled as a first order process. Standard cup forming conditions were used for these tests as described in Chapter 4. The process gain at different punch heights varied from 0.20 to 0.14 lb. F_t per lb. binder force. The "time" constant was 0.015 in. (Because the independent variable in these tests is punch displacement rather than time, the time constant has units of length.) The resulting process transfer function is:

$$H(s) = \frac{0.17}{(0.015s + 1)}$$

The control gains can be selected to give the same closed-loop time constant as the open-loop process while providing the advantage of zero steady-state error. Because the controller and process are linked serially, the individual transfer functions for the process and controller are multiplied to find the overall transfer function representing the closed-loop characteristics. The required controller transfer function G(s), and the gains K_p and K_I, are found from H(s) and the desired closed-loop response. The desired closed-loop transfer function with time constant = 0.015 in. is:

$$G(s)H(s) = \frac{67}{s} \qquad \text{(B-2)}$$

The required controller transfer function is:

$$G(s) = \frac{394\ (0.015s + 1)}{s} \qquad \text{(B-3)}$$

The control gains K_p and K_i can be found from the transfer function form of Eq. B-1:

$$G(s) = \frac{K_i\ ((K_p/K_i)s + 1)}{s} \qquad \text{(B-4)}$$

Solving for K_p using Eq. B-3 and B-4 gives K_p = 5.9 lb/lb. These equations give a continuous K_i = 394 lb/lb in. and a K_i for the discrete control algorithm of K_i = 1.48 lb/lb based on 267 calculations per inch.

The control gains derived above would give a extremely fast F_t response of 63% correction in 0.015 inches of punch travel. These gains could not be used however, because of process nonlinearities. The most severe of these problems was saturation of the binder force. Saturation due to the press capacity limit occurred, but more problematic were tendencies to drive the binder force to zero. This resulted in rapid and uncontrolled flange and frustum buckling. To maintain binder force within the safe operating region, K_p and K_i were reduced by 48% and 83% respectively avoid saturation problems. The resulting gains, K_p = 2.5 and K_i = 0.25, are used for all reported standard tests (Table B-1). The resulting closed-loop time constant for the equivalent first order system is 0.25 in., which is 17 times slower than attempted above. However, relative to a typical punch stroke of 1.30 in. this time constant is still short and gives rapid convergence of F_t to the target line.

Selection of Proportional and Integral Control Gains for t_{avg} Control

The control gains for t_{avg} control can be derived in the same way as for F_t control. The t_{avg} response to binder force steps has the same 0.015 in. "time" constant as the F_t response and but the process gain varies from 0.5×10^{-6} to 2×10^{-6} lb.$^{-1}$. Equation B-5 is the desired control transfer function using the average process gain value of 1.2×10^{-6} and the same desired closed-loop transfer function as above (Eq. B-2).

$$G(s) = \frac{5.6 \times 10^6 \ (0.015s + 1)}{s}$$

Solving for K_p and K_i using Eq. B-4 and converting into values for the discrete control equation gives K_p = 840,000 lb. and K_i = 210,000 lb. These values cause saturation of the binder force values just as the theoretically derived values for the F_t controller. The above K_p and K_i values were reduced 52% and 90% respectively to produce the t_{avg} gains used in all t_{avg} tests discussed in this thesis (Table B-1).

	K_p	K_i
Tangential Force (F_t)	2.5 lb/lb	0.25 lb/lb
Normalized Avg. Thick. (t_{avg})	400,000 lb	20,000 lb

Table B-1 The Control Gains Used in the Experiments

Appendix C A THEORETICAL ANALYSIS OF TARGET SCALING FOR THICKNESS

When thicker blank material is formed using tangential force control, the tangential force target could simply be scaled proportionally with the blank thickness change. While this technique maintains similar heights at failure as shown by experiments, it does not optimize failure height. Because thicker blanks can withstand greater compressive forces before buckling, a less than proportional increase in the target is optimal. The analysis below attempts to find the optimal tangential force scaling for thickness changes by considering buckling failure.

The tangential force target line can be scaled either by tangential force (vertically) or punch displacement (horizontally). Vertical scaling by tangential force would scale the radially directed stress which has only a weak effect on buckling in the frustum. Therefore, scaling is attempted by relating thickness change to critical strain change and then to the punch displacement.

A study of buckling in sheet metal shells was done by Hutchinson and Neale [20]. This work does not apply to the current geometry because the meridians of the frustum are not curved. The buckling in this work is not axisymmetric as produced by axial compression, and so the use of plate buckling theory is appropriate as used by Tesawa and Nishimura [21] and Havranek [8].

In Timoshenko's Theory of Elastic Stability [22] the theory of

buckling for thin plates is investigated. Starting with a general case using the energy method, it is shown below that the critical stress is directly proportional to Young's Modulus and to the thickness squared. This is the first step towards finding how critical punch displacement varies with thickness.

The equation which describes the requirement for buckling initiation is

$$\Delta W = \Delta U$$

where

W = work done by external force
U = strain energy for the same deflection

For a thin plate subject to forces along all edges the incremental work and strain energy are

$$\Delta W = -\frac{1}{2}\int\int\left(N_x\left(\frac{\partial\omega}{\partial x}\right)^2 + N_y\left(\frac{\partial\omega}{\partial y}\right)^2 + 2N_{xy}\frac{\partial\omega}{\partial x}\frac{\partial\omega}{\partial y}\right)dxdy$$

$$\Delta U = \frac{Et^3}{24(1-\nu^2)}\int\int\left(\left(\frac{\partial^2\omega}{\partial x^2}+\frac{\partial^2\omega}{\partial y^2}\right)^2 - 2(1-\nu)\left(\frac{\partial^2\omega}{\partial x^2}\frac{\partial^2\omega}{\partial y^2} - \left(\frac{\partial^2\omega}{\partial x\partial y}\right)^2\right)\right)dxdy$$

where

N_x = normal force per unit length in x direction
N_y = normal force per unit length in y direction
N_{xy} = shear force per unit length
ω = lateral displacement
E = Young's Modulus
t = thickness
ν = Poisson's ratio

If one assumes that forces N_x, N_y, and N_{xy} vary at the same rate near failure then

$$N_x = \alpha N_x'$$
$$N_y = \alpha N_y'$$
$$N_{xy} = \alpha N_{xy}'$$

where N_x', N_y', and N_{xy}' are constants.

By equating the expressions for δW and δU and then substituting for N_x, N_y, and N_{xy} one can solve for the force scaling factor α which gives the critical forces:

$$\alpha = \frac{\dfrac{Et^3}{12(1-\nu^2)} \iint \left(\left(\dfrac{\partial^2 \omega}{\partial x^2} + \dfrac{\partial^2 \omega}{\partial y^2} \right)^2 - 2(1-\nu) \left(\dfrac{\partial^2 \omega}{\partial x^2} \dfrac{\partial^2 \omega}{\partial y^2} - \left(\dfrac{\partial^2 \omega}{\partial x \partial y} \right)^2 \right) \right) dxdy}{- \iint \left(N_x' \left(\dfrac{\partial \omega}{\partial x} \right)^2 + N_y' \left(\dfrac{\partial \omega}{\partial y} \right)^2 + 2N_{xy}' \dfrac{\partial \omega}{\partial x} \dfrac{\partial \omega}{\partial y} \right) dxdy} \qquad \text{(B-1)}$$

For a plate of thickness t the forces N_x', N_y', and N_{xy}' can be related to the corresponding stresses:

$$N_x' = \sigma_x' t$$
$$N_y' = \sigma_y' t$$
$$N_{xy}' = \sigma_{xy}' t$$

Substituting the above three equations for force into Eq. C-1 gives

$$\alpha = \frac{\dfrac{Et^2}{12(1-\nu^2)} \iint \left(\left(\dfrac{\partial^2\omega}{\partial x^2} + \dfrac{\partial^2\omega}{\partial y^2} \right)^2 - 2(1-\nu) \left(\dfrac{\partial^2\omega}{\partial x^2}\dfrac{\partial^2\omega}{\partial y^2} - \left(\dfrac{\partial^2\omega}{\partial x \partial y} \right)^2 \right) \right) dxdy}{- \iint \left(N_x' \left(\dfrac{\partial\omega}{\partial x} \right)^2 + N_y' \left(\dfrac{\partial\omega}{\partial y} \right)^2 + 2N_{xy}' \dfrac{\partial\omega}{\partial x}\dfrac{\partial\omega}{\partial y} \right) dxdy}$$

For a fixed set of boundary conditions the values of the double integrations are constant, which gives

$$\alpha = \frac{Et^2}{12(1-\nu^2)} C \qquad \text{(C-2)}$$

The critical value of factor α can be related to the buckling stress; $N_x = \alpha N_x'$ gives $\sigma_x t = \alpha \sigma_x' t$.

Solving for α:

$$\alpha = \frac{\sigma_x}{\sigma_x'} = \text{Constant} * \sigma_x$$

Substituting into Eq. C-2 and combining constant terms gives the critical stress combination:

$$\sigma_x = Et^2C' \qquad \text{(C-3(a))}$$
$$\sigma_y = Et^2C' \qquad \text{(C-3(b))}$$
$$\sigma_{xy} = Et^2C' \qquad \text{(C-3(c))}$$

Equations C-3(a), C-3(b), and C-3(c) give the desired relationship between stress, elastic modulus and thickness. Note that no assumptions

about the boundary conditions were made except that they do not change. The relationship can be used even if stresses are applied in any direction in the plane of the material, as long as the three stresses have the same ratios to each other under the various critical conditions. This last assumption concerning constant stress ratios near failure is supported by Logan [16].

Timoshenko introduces the concept of "tangential modulus" E_t to extend the buckling theory to fully inelastic material in the case of beams. E_t is the slope of the stress-strain curve after passing the yield point. For a material with strain hardening

$$\text{stress} = \sigma = K\epsilon^n \tag{C-4}$$

and

$$E_t = \frac{d\sigma}{d\epsilon} = nK\epsilon^{n-1}$$

where ϵ = strain

Using Timoshenko's concept, E_t can be used to extend his formula for cylindrical shell buckling by replacing E by E_t (Eqs. C-3(a), C-3(b), C-3(c))

$$\sigma_{cr} = \frac{K\epsilon^{n-1}t^2}{4(1-\nu^2)R^2} \tag{C-5}$$

To find the change in critical strain for a change in material thickness, eliminate stress from Eq. C-5 by using Eq. C-4

$$\epsilon = \frac{nt^2}{4(1-\nu^2)R^2} = \text{Constant} * t^2 \qquad \text{(C-6)}$$

While the critical strain is proportional to $t^{2/n}$ for an elastic material, for an inelastic material such as exists in deep drawing, Eq. C-6 shows that the critical strain is simply proportional to t^2.

The ultimate goal is to relate the change in critical strain to the change in punch displacement which will be used to scale the tangential force target. Relationships between strain, draw-in, and punch displacement are required.

It can be assumed that movement of the material into the die cavity is directly proportional to the edge movement. Therefore the circumferential strain at the edge of the frustum, which causes buckling, is proportional to draw-in:

$$\epsilon = \text{Constant} * \text{Draw-in}$$

The final relationship between draw-in and punch height must be found. Third relationship can be broken into two simpler relationships between draw-in and meridional length, and between meridional length and punch height. The relationship between draw-in and meridional length depends on the amount of straining of material in the frustum. Test data plotted in Fig. C-1 shows the linear relationship between draw-in and meridional length. Tests of both standard blanks and 25% thicker blanks are plotted. The linear relationship holds for various

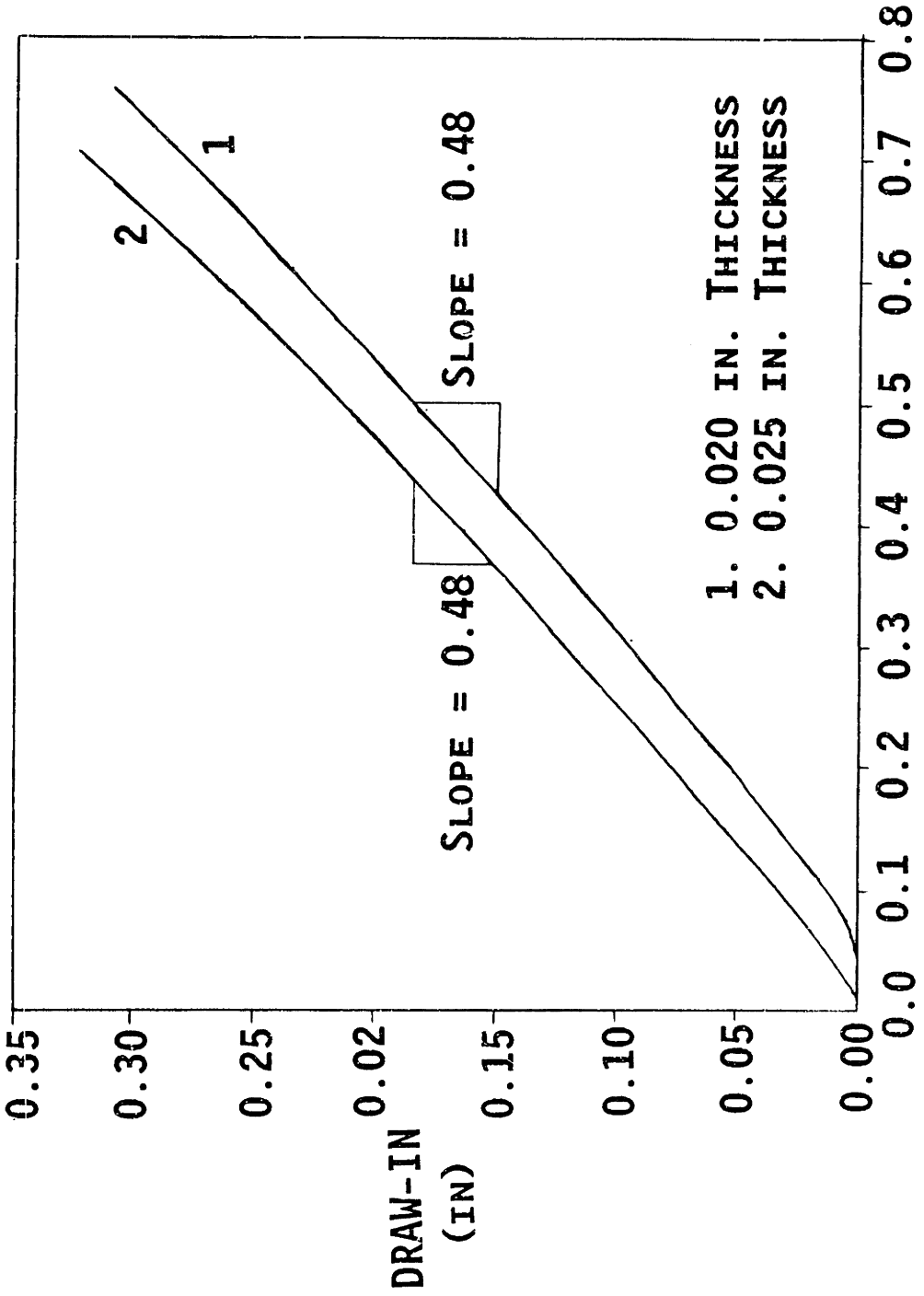

Fig. C-1 Typical Draw-in and Corresponding Meridional Length Change for two Blank Diameters (cup geometry, 0.020 in. material "C", STP, 6.25 in. diameter)

thicknesses which is important for use in target scaling for thickness. A second relationship between meridional length and punch height can be found from the die set geometry using trigonometry. Combining the above relationships between draw-in, meridional length, and punch height gives:

$$\text{Draw-in} = C\ [((R_d-R_p)^2 + H_i^2)^{0.5}) - (R_d-R_p)] \qquad (C\text{-}7)$$

where
C = constant
R_d = radius of the die (in.)
R_p = radius of the punch (in.)
H = punch height (in.)

If no straining occurred along the meridian, the constant C would equal 1. Comparison to data gives a value of C = 0.48 which indicates that half of the potential edge draw-in is lost because of straining.

A simpler model of the relationship between draw-in and punch displacement can be found by fitting a power law curve to Eq. C-7. The equation of a curve which matches the value and slope of Eq. C-7, with R_d-R_p=0.89 in. at punch height = 1.3 in., is

$$\text{Draw-in} = 0.21\ H^{1.6}$$

Other parameters may affect draw-in but are relatively minor. This equation provides the final relationship which allows calculation of tangential force changes from thickness changes.

The equations above relate strain to draw-in and draw-in to punch displacement. When combined, the equations show that strain is proportional to the 1.6 power of the punch displacement.

$$\epsilon = \text{Constant} * \text{draw-in} = \text{Constant} * H^{1.6}$$

Because the strain "ϵ" is also proportional to the square of the thickness (Eq. C-6), punch displacement change must be proportional to the 2.0/1.6 = 1.25 power of thickness. This scaling produces critical hoop strain simultaneously with critical meridional stress. Optimal formed height occurs when the critical tearing stress and critical wrinkling stress are simultaneously achieved. Scaling vertically in proportion to thickness change would produce tearing failure while the hoop stress remained well below the maximum. By scaling horizontally by thickness raised to the power 1.25, meridional stress ramp-up is delayed until simultaneous failure by buckling occurs.

The intent of the analysis above is to develop a method of target scaling that will alter a known optimal target rather than attempting the more difficult task of calculating the targets from theory alone. The example below assumes that a optimal target is known for the standard 0.020 in. material.

As a starting point for target alterations based on theory, the standard target is multiplied by the proportional change in thickness. This intermediate solution has the important effect of producing the

same stresses and strains in the thicker blanks as occurred in the standard tests using thin material. When the material conditions are the same as in the standard test, adjustments can be made for buckling propensity changes.

Application to Tangential Force Target Scaling

The optimal tangential force target line for 0.020 in. material is F_t(lb.) = 8000 + 2,000(lb./in.) * h(in.). The equation becomes F_t = 10,000 + 2,500 * h when scaled vertically for 25% thicker material. Both the y intercept and the slope are increased by 25% to give this intermediate target line. Finally the target line is scaled horizontally by $1.25^{1.25}$=1.32 because punch displacement should be proportional to the 1.25 power of thickness (Fig. 4-18). For any tangential force on the target line, the new corresponding punch displacement is 32% higher. This scaling requires that the slope of the equation is multiplied by 1/1.32 = 0.76 while the intercept is left unchanged. The resulting equation is

$$F_t = 10000 + 1,890 * h \qquad \text{(C-8)}$$

After final scaling the equation has the intercept of the +25% target line which was scaled for constant strain while the final slope is slightly flatter than the slope of the standard target line of the thin material.

The empirically verified optimal target equation for the thicker material is scaled to 15% above the standard target rather than 25%

above. The resulting optimal equation for the 25% thicker material is

$$F_t = 9200 + 2,300 * h \qquad \text{(C-9)}$$

Comparison to Experimental Data:

The validity of the theoretical target prediction is assessed by comparing the tangential force at failure as given by Eq. C-8 to the optimal empirical value from Eq. C-9. The theoretical optimal F_t at the failure height of 1.570 in. is 12,970 lb. while the empirical optimum F_t is 12,810 lb. For a 25% thicker material, the analysis above provides a final F_t increase of 16.4% over the original target for the thin material, while the optimal target increase from tests is 15%. This theoretically based target produces 86% of required target correction for thickness change, and so realizes 98% of the maximum formed height.

Application to Normalized Average Thickness Target Scaling

The target curve used for normalized average thickness (t_{avg}) control can be scaled in the same way as the tangential force target. Each value of the target will occur at a new punch displacement that is 1.32 times the original displacement. No vertical scaling is required because t_{avg} corresponds to a particular average strains and does not depend on thickness.

The scaling described above must be applied to an existing t_{avg} curve which produces the optimum failure height for the original blank thickness. The optimal target equation below is a power law fit to an empirically produced equation.

$$t_{avg} = 1 - A + A^{-(h-h0)/T} \qquad (C\text{-}10)$$

where
A = 0.11 = maximum deviation of t_{avg} below 1.0
h = punch height (in.)
h0 = 0.10 in. = target offset
T = 0.40 in. = target time constant

The equation resulting from scaling the t_{avg} target horizontally by a factor of 1.32 is

$$t_{avg} = 1 - A + A^{-(h-h0)/1.32T} \qquad (C\text{-}11)$$

Control tests of the 0.025 material were not done using a theoretically scaled target because the original target captured much of the possible height gain. Use of the unaltered target produced failure heights approximately midway between the 0.020 and the 0.025 optimum heights. The benefits of target scaling could not be as great for t_{avg} control as for F_t control where total lack of scaling produced heights 20% lower for the thicker material. The shallow slope of the t_{avg} target curve near failure heights shows that the effect of horizontal scaling by punch displacement will have only a small effect on the corresponding t_{avg} values.